3D Freeform Surface Measurement on Coordinate Measuring Machine Using Photometric Stereo Method

A thesis submitted in partial fulfilment of the requirements of Brunel University London for the degree of Doctor of Philosophy

by

Thammarat Somthong

College of Engineering, Design and Physical Sciences
Department of Mechanical, Aerospace and Civil Engineering, Brunel University London

June 2017

Abstract

Surface metrology has been widely used in manufacturing for many years. There has been a wide range of techniques applied for measuring surface topography. A photometric stereo technique is one of the best ways for the analysis of three-dimensional (3D) surface textural patterns. Many published works are concerned the developed approach for recovering the 3D profiles from surface normal. This research not only presents a methodology used to retrieve the profiles of surface roughness standards but also investigates the uncertainty estimation of textural measurement determined by the photometric stereo method. Various input quantities have been studied such as pixel error from recovered 3D surface textural patterns, the power of light source which involved with surface roughness average (Ra) value and the effect of room temperature. The surface roughness standards were utilized as the reference value. In term of increasing accuracy of the reference value, a contact method (stylus instrument) was used to calibrate them. Illumination angles of light source had some influence on the measurement results. A coordinate measuring machine (CMM) was used for holding the light source in order to study the effects of tilt and slant angles. The effect of tilt and slant angles were investigated. The results of these experiments successfully indicated that the angle used in photometric stereo method played an important role to the accuracy level of the roughness measurement results. The surface roughness specimen manufactured by a Computer Numerical Control (CNC) was applied to validate the capability of the photometric stereo system.

Acknowledgements

This research work could not have been achievable without the support of many people. First and foremost, I would like to express my gratitude to my supervisor, Dr. OingPing Yang for his valuable recommendations, guidance, motivations, encourages, and support throughout this research process.

I am grateful to the Royal Thai Government, Ministry of Sciences and Technology and National Institute of Metrology Thailand (NIMT) for sponsorship to my Ph.D. study. The thanks are also extended to Brunel University London for all the support for my Ph.D. research.

The special thanks are due to my colleagues, Dr. Monludee Ranusawud, Dr. Jariya Buajarern, and Dr. Wiroj Sudatum, for their valuable discussions in many regards on my research work. Special thanks are also to the Brunel technician staff, particularly Mr. Paul Yates for his always helpful assistance.

I am also thankful to my beloved family, my father, and mother who always support and encourage me until submitting this research study. I have also to say many thanks, my wife, to look after our daughter during this research study alone.

Table of Contents

Abbreviations

BIPM	Bureau International des Poids et Mesures
BS	The British Standard Institution
ISO	International Organisation for Standardization
ASME	American Society of Mechanical Engineers
CAD	Computer Aided Design
CAM	Computer Aided Manufacturing
CMM	Coordinate Measuring Machine
CNC	Computer Numerical Control
NPL	the National Physical Laboratory
NIMT	the National Institute of Metrology Thailand
PS	Photometric Stereo
3D	Three-dimensional
LED	Light emitting diode
SI	International System of Units

Nomenclature

p_n	The slope of the surface are calculated by the first partial derivative of z which relates with x axis
q_n	The slope of the surface are calculated by the first partial derivative of z which relates with y axis
R_a	Arithmetic average height
R_z	Maximum peak to valley height
R_p	Maximum peak height
R_v	Maximum valley height
R_q	Root mean square height
R_{sk}	Skewness
R_{ku}	Kurtosis
$\bar{x}$	Arithmetic mean
S	Estimated standard deviation
λ_{co}	Cut-off wavelength
l_r	Roughness sampling length
l_n	Roughness evaluation length
Ra_{PS}	Arithmetic of the photometric stereo method
Ra_{PSm}	Mean of the all pixel values of a surface image along one line
Ra_{PSmi}	Individual value in each pixel of a surface image along one line
R^2	Coefficient of determination
u_A	Type A evaluation of standard uncertainty

u_B	Type B evaluation of standard uncertainty
$s(\bar{q})$	Termed experimental standard deviation of mean
$u(x_i)$	Standard uncertainty
$u_c(y)$	Combine standard uncertainty
c_i	Sensitivity coefficient
k	Coverage factor
Z_p	Uncertainty of width of pixel of camera in mm
$u(Z_{ind})$	Uncertainty of measured value of the surface roughness standard under calibration
$u(Z_l)$	Uncertainty of the intensity of light source
$u(Z_{ix})$	Uncertainty of the resolution of the PS system
$u(Z_{mc})$	Uncertainty of the correction due to mechanical effect of CMM's movement correlating with roughness average variation
$u(Z_g)$	Uncertainty of the length of actual working standard scale from calibration certificate.
$u(Z_n)$	Uncertainty of the nominal value of surface roughness standard
$u(\bar{\alpha})$	Uncertainty of the thermal expansion coefficient between the materials of measurand and standard
$u(\Delta\bar{t})$	Uncertainty of the difference in room temperature during the measurement period.
En	Degree of equivalence ratio

List of Figures

List of Tables

Chapter 1 Introduction

1.1 Research background

Surface texture and form measurements are essential things in industrial manufacturing. When objects are built, they have to be measured and verified by commercial instruments with their drawing. The instrument applied for measuring the values of surface texture or form is created to have the best ability only one aspect. An instrument that has been widely used to measure shape and form rapidly with high accuracy in manufacturing is a Coordinate Measuring Machine (CMM).

As one of the most vital metrological instrumentations, Coordinate Measuring Machines (CMMs) are commonly used for measuring form in most industrial manufacturing. They are created for measuring surfaces' physical geometrical characteristics on workpieces. The basic function of coordinate metrology is the comparison of actual measurement from a surface shape, including all dimension measurements, with the desired shape on a drawing. The actual measurement of a workpiece shape is acquired by collecting data at certain points or an area on its surface. The methods for collecting data can be done by both contact and non-contact methods. All measuring points are shown in term of their measured coordinates, and it is possible to evaluate size, form, location and orientation from geometric elements on CMM's software. The probe system is one of the key elements of the CMMs. The probe system can be mainly separated by two techniques for data collection. The first technique requires the stylus probe being to contact with a surface object and the second technique is an optical technique in which morphological information is acquired without any contact between the sensor and a surface object. The contact method actually relates to a touch-trigger probe. A ruby ball has widely been used as a stylus probe on CMMs. When the stylus probes touch or trace on the object, it sometimes makes a scratch on a surface object. In the case non-contact probes, especially laser scanning and video techniques, it is a useful technique for measuring a surface object as the surface is not damaged and distorted. Non-contact probes are suitable techniques for measuring soft materials such as a polymer, plastic, and soft metal (Mears, et al., 2009). Non-contact probes for measuring surface, based on CMMs, is a more efficient method which is able to determine various surface characteristics.

In the other hand, an instrument that has been widely used to measure quickly surface finish with high accuracy in manufacturing is a surface texture measuring instrument. The method for measuring surface finish can be separated into two ways: stylus-based and non-contact methods. Stylus-based is a contact instrument that applies the stylus and skid to measure with the surface under test. Hence, the shape of stylus and skid will directly influence with data acquired from the surface (Smith, 2002). In the case of the non-contact method, there are many optical techniques: optical follower, interferometry, confocal microscopy, diffraction, focus variation. They are applied for the measurement of surfaces. Each technique has a certain working range which depends on the limitation of the method being used. In example, a specimen having a shiny surface is suitable for the measurement method that is able to evaluate reflection of the surface normal to the general plane. On the other hand, it is not suitable for the optical technique based on diffraction methods. Hence, the surface characteristics have to be studied before doing a measurement, being a good idea for choosing a right instrument. The surface features and working ranges are both factors to decide for choosing the type of the measurement instrument (Whitehouse, 2002).

Recently, many researchers effort to develop unique probes which can measure complex geometrical features and surface roughness in the micrometre range. The probes can be directly connected with CMMs. They have become multipurpose tools for measuring challenging dimensional tasks, increasing the performance of CMMs. Measurement range is focused on a micro level to support the industrial manufacturing such as automotive industry and ear implants and hearing aids.

In the research, the advantages of the CMM and surface texture measuring instrument are combined for measuring surface objects. The measurement system enables to determine the values of surface finish and form measurements by using the Photometric Stereo (PS) method, performed on the CMM's base. Moreover, measurement uncertainty is assessed to identify the performance of the PS system.

As previously mentioned, the surface roughness and form of specimens are performed by the CMM probe using the photometric stereo method. The light source is used instead of the touch-trigger probe by using the high accuracy movement of CMM's axes for illuminating a surface object. The object is placed on the CMM measuring table, with the centre aligned with the image axis. The camera is positioned perpendicular to the measuring object as shown in Figure 1.1. The PS is a method for evaluating shape and

reflectance of an object using three or more images under different lighting positions. The method uses different lighting conditions to measure the gradient field of the surface, which is calculated from an array of surface normals.

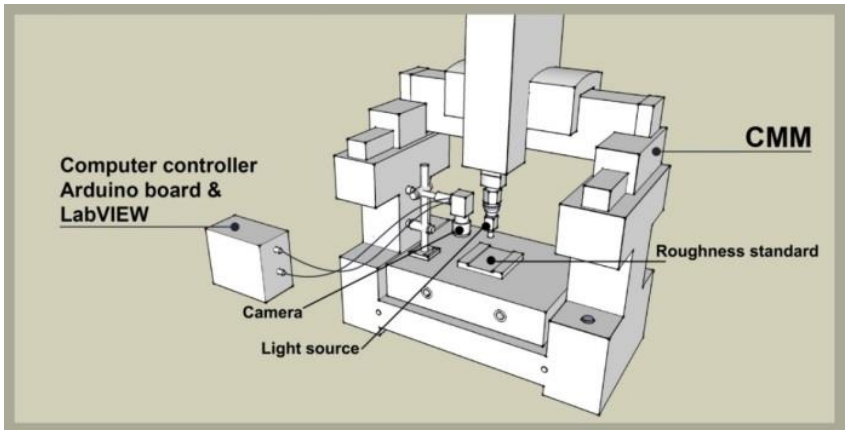

Figure 1.1 Using PS method with CMM for measuring an object

1.2 Aim and objectives of the research

The aim of this research is to achieve the 3D freeform surface and average surface roughness measurements using the PS method on the CMM and then investigate mathematical understandings of the measurement uncertainty. The objectives of the research are as follows:

1) To investigate the efficiency of the PS method for surface roughness measurement.
2) To carry out on-line measurement and real-time assessment of a component.
3) To develop reversal engineering based on 3D surface reconstruction.
4) To understand the effects of different slant angles on the measuring results of the surface roughness measurement.
5) To establish the calibration traceability and a mathematical model of measurement uncertainty of surface roughness measured by the PS method.
6) To validate and evaluate the performance of the PS system for measuring surface roughness.
7) To investigate the multi-source PS technique for measuring shape and form measurements.

1.3 Contributions and Novelties

The major contributions and novelties presented in this thesis are:

1) Extending the practicality of photometric stereo especially for roughness and form measurements
2) A novel method of evaluation surface roughness measurement from the photometric stereo method is developed by using the least square technique with measurement results from surface roughness standards which are calibrated by a stylus instrument.
3) The effects of tilt and slant angles are investigated by using the benefit of a coordinate measuring machine (CMM).
4) Roughness component can be separated from form and waviness components by using Gaussian density function.
5) Measurement uncertainty of the traditional photometric stereo method for measuring surface roughness has been built.
6) The validation method is used to confirm measurement efficiency of the photometric stereo method for surface roughness evaluation.
7) The one light source attached to CMM's probe system is applied for shape and form measurement based on multi-source photometric stereo technique. In this technique, the effects of shadows and specularities for form measurement can be eliminated.

1.4 Thesis outline

Chapter 1 introduces the research background and importance of the research including CMM and surface texture measuring instrument, contribution and novelties, aims and objectives, and structure of the thesis.

Chapter 2 reviews of all methods for recovering surface characteristics, the state of the art of surface texture and form measurements, and CMM error sources. Later, discussion of advantages and disadvantages for using contact and non-contact methods are for surface texture and form measurements being the motivation for the development of the PS technique based on surface roughness measurement.

Chapter 3 explains the contact measurement (stylus measurement) and the method to calibrate surface roughness standards. The aim of this chapter is to identify and realize

the method for setting-up stylus instrument and its functionality for surface roughness measurement. These systems are studied in detail, and the significant issues are discussed.

Chapter 4 describes the PS technique for 3D surface reconstruction to analyse average roughness profiles and then discusses the filtering in the process of partitioning profiles into roughness, waviness, and form. Validation of the data obtained from the PS method and contact based standard stylus instrument is performed to verify the capability of the PS for the proposed task. This chapter also discusses in detail the software and hardware development for data acquisition, and then calibration of the camera sensor and lens is discussed.

Chapter 5 discusses the uncertainty calibration procedure for the surface roughness measurement based on the PS method and also describes the method to validate the surface roughness measurement obtained from the PS method.

Chapter 6 explains a multi-source PS technique using the advantages of a CMM to move the light source around an object precisely. This method is used for measuring an object, which we call an arc shape, created from the 3D printing machine. The aim of this chapter is to compare the surface characteristics after surface recovery using the proposed method and using a traditional PS method. In addition, the width of arc shape profile is measured from proposed method for comparison with data obtained from the CMM. These systems are studied in detail, and some of the issues are discussed.

Chapter 7 draws conclusions arising from this research investigation. Further recommendations for future work are also provided.

Chapter 2 Literature Review

2.1 Introduction

The capability to acquire surface measurement has been improved and developed continuously for many years. Previously, surface measurements were primarily evaluated and measured by the basic operating principle of the pick-up, that is, a stylus instrument. Stylus instruments are most widely used for 2D surface texture measurement, with the specimen measured using x and z axes. When full details of a 3D surface texture are required, we have to measure more regular lines in the y axis, which is parallel with this line. This process is much more time consuming, and it takes much longer to finish one measurement area.

In industrial manufacturing processes, the system for surface measurement is an essential task of quality control. Recently, the part measuring technique has been carried out after the manufacturing processes have been completed. Moreover, the object must be removed from the on-line production, and the results can only be shown on 2D surfaces. The best solution to reduce working time and acquire more details of the 3D surface is to create an innovative method of surface measurement on on-line production. The non-contact approaches widely used in advanced manufacturing are computer vision techniques. They are widely utilised in the physical characteristics of 3D surface measurement especially in form and surface roughness measurements (Lee and Tarng, 2001; Solomon and Ikeuchi, 1996).

The optical techniques can also be used to obtain the 3D information about physical surfaces, but they are not suitable to be applied to the on-line measurement because of their setting systems. As a result, we propose applying the 3D freeform surface measurement on CMM using the PS method that can obtain 3D surface information and install an on-line measurement. This chapter first discusses and reviews the optical technique used for surface measurement. This is followed by surface measurement especially object shape as measured by the PS method and then the multi-view and multi-source PS methods, which are used to eliminate the effects of shadows and specularities for a shiny object. Finally, the knowledge gap for three special issues where there is currently a lack of clarity on scientific understandings is identified along

with a discussion of why and how these issues are significant in surface roughness and form measurement need to be studied in this research.

2.2 Surface-recovering method

A simple imaging system is shown in Figure 2.1. The z-axis of the coordinate system is used as the viewing direction, which points toward the camera. A right-handed coordinate system is then supposed. The viewing direction is perpendicular to the x and y axes, which intersect between the origin of the diagram at the z-axis and the observed plane. The shape of a surface may be formed either by using the height of every point above a reference plane or the gradient vector of the surface at each position.

The general equation of a 3D plane is given by

$$Ax + By + Cz + D = 0 \Longrightarrow \frac{A}{C}x + \frac{B}{C}y + z + \frac{D}{C} = 0 \qquad (2.1)$$

The components (p_n, q_n) of the slope of the surface are calculated by the first partial derivative of z which relates with x and y.

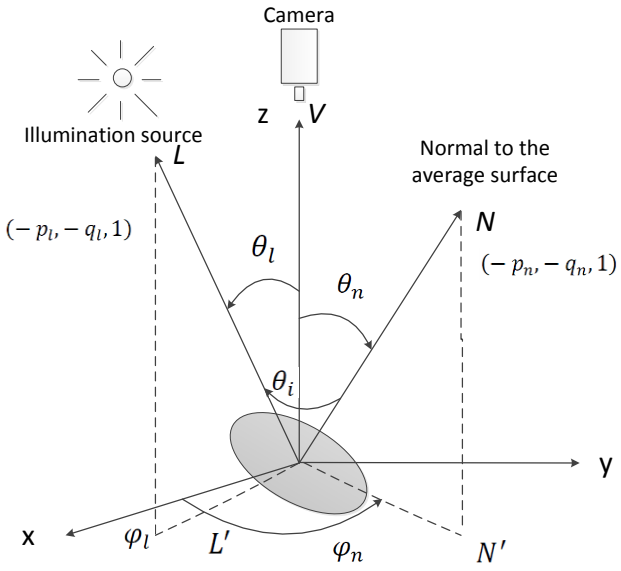

Figure 2.1 Imaging geometry

By describing surface shape as a distribution of surface normal vectors, the task becomes one of surface normal determinations. Consider a smooth 3D surface defined as

$$z = f(x, y) \tag{2.2}$$

The direction of a given surface normal vector may be explained as the partial derivatives.

$$\frac{\partial z}{\partial x} = -\frac{\mathrm{A}}{C} = -p_n \tag{2.3}$$

$$\frac{\partial z}{\partial y} = -\frac{\mathrm{B}}{C} = -q_n \tag{2.4}$$

or

$$\left[-\frac{\mathrm{A}}{C}, -\frac{\mathrm{B}}{C}, 1\right]^T = [-p_n, -q_n, 1]^T \tag{2.5}$$

where the terms p_n and q_n are the gradient of the surface at any location in the x and y directions, the surface normal is then illustrated as the vector $[-p_n, -q_n, 1]$. All locations (p_n, q_n) can be shown as forming gradient space, the origin of which corresponds to a normal vector pointing directly at the view plane.

The view vector can be expressed within the gradient space domain as $[-p_n, -q_n, 1]$ and the light vector can also be expressed within the gradient space domain as $[-p_l, -q_l, 1)$(Horn, 1989).

Another definition, which is also utilized in this chapter, is based on the representation of a plane by using equation $\vec{r} = \vec{a} + \alpha\vec{b} + \beta\vec{c}$, where $\vec{r}$ is the position vector of any position on the plane illustrated in Figure 2.3, $\vec{a}$ is the position vector of a specific known point on the plane. The normal to the plane is then given by the cross product $\vec{b} \times \vec{c}$; for instance, the nonparallel vectors placed on the plane are written as

$$\vec{b} = [1,0, p_n]^T \tag{2.6}$$

$$\vec{c} = [0,1, q_n]^T \tag{2.7}$$

The normal vector, which is orthogonal to the surface, is defined as

$$\vec{b} \times \vec{c} = [-p_n, -q_n, 1]^T \tag{2.8}$$

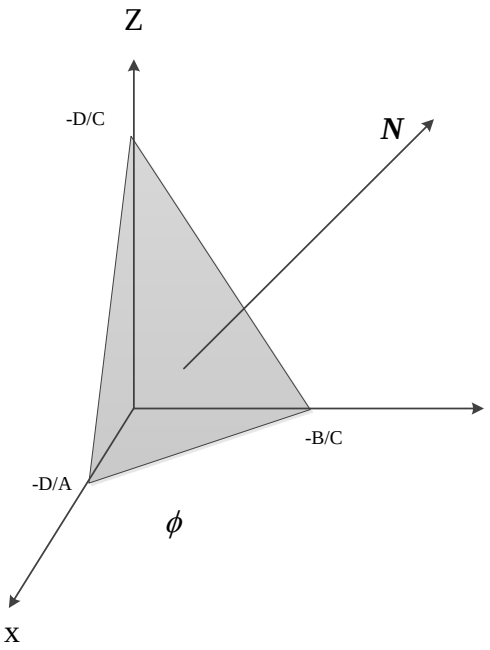

Figure 2.2 A plane and its normal vector

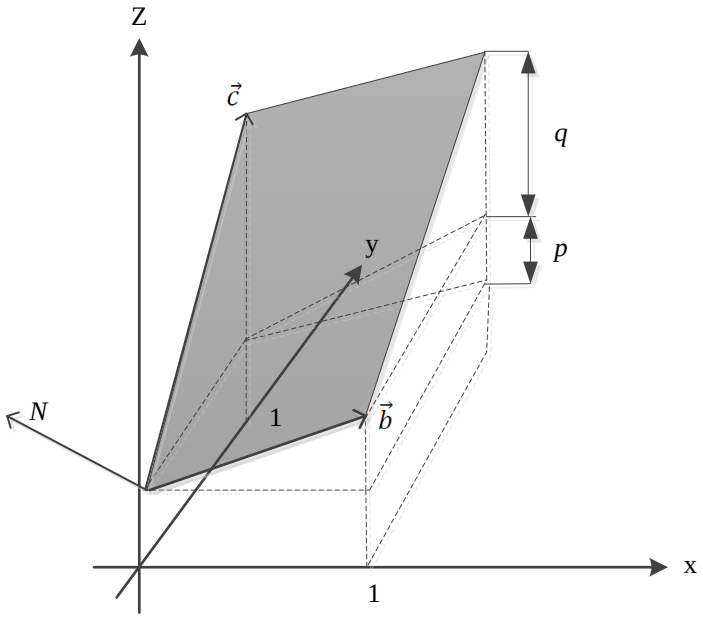

Figure 2.3 The slope of a surface patch can be illustrated as p and q

The surface normal defined to be a unit of length can now be written as

$$\vec{N} = \frac{(-p_n, -q_n, 1)^T}{\sqrt{p_n^2 + q_n^2 + 1}} \tag{2.9}$$

There are two things which can be stated from the above information. When the normal vector $\vec{N}$ or vector $(-p_n(x,y), -q_n(x,y), 1)^T$ of every component (x,y) building up the

surface, which is shown in equation (2.8) and (2.9), is known, the shape of surface could be found. On the other hand, we can say that the shape of surface can be found by knowing the distance of every point (x,y) of the surface from the reference plane. However, a single image intensity or radiance value, acquired from a unique facet orientation or point distance, cannot create the shape of surface because a maximum number of surface orientation is to be displayed to the even value of image intensity and the equation $(-p_n(x,y), -q_n(x,y), 1)^T$ have two degrees of freedom. As a result, additional information to determine local surface orientation has to be considered.

As Woodham (1980) explains, there are many techniques to obtain 3D information about surfaces. These techniques are mainly separated by direct methods and indirect methods. Direct methods are the method to attempt direct measurement such as a pulsed laser based system; for instance, where depth information is the only information available. Indirect methods attempt to measure distance by measuring parameter calculated from images of the illuminated object. Several indirect methods have been widely used such as binocular stereo, shape from shading, and photometric stereo.

2.2.1 Binocular stereo/ stereo system

Binocular stereo has been one of the most widely explored topics of 3D vision (Barnard and Fishler, 1982). A traditional stereo system typically comprises two cameras placed side by side for capturing stereo image pairs. The depth information of the captured scene is calculated and applied from the geometry of triangulation to calculate the distance from the disparity map of two images, as illustrated in Figure 2.4. The surface depth z is obtained as

$$Z = fd/x_1 - x_2 \tag{2.10}$$

where f is the camera focal length, d is distance between the two cameras, x_1 and x_2 are the coordinate positions of images of the same physical point on the two focal planes of the cameras, with respect to coordinate systems that are fully aligned, but each is centered on the axis of the corresponding camera lens.

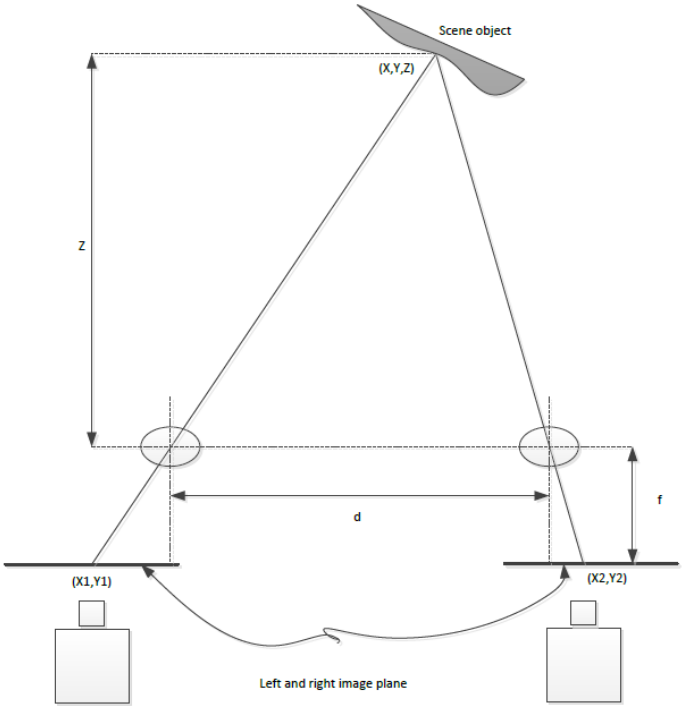

Figure 2.4 Geometry of Binocular stereo method

Binocular stereo involves a relationship between points of interest in one scene on one camera and the same points in another frame on the second camera, taking us to the well-known correspondence problem (Zhengzhen and Tianding, 2009). Binocular stereo has been used successfully in many works to reconstruct the 3D model of a surface, but there are disadvantages making it inapplicable in this study. Firstly, the depth information is to be recovered (as shown in Figure 2.4) rather than the surface orientation as required for this study. Secondly, a specimen is manufactured from high reflective materials. The PS method works well with a rough surface and varying surface reflectance, while binocular stereo does well with a smooth surface and uniform surface properties (Nayar, et al., 1989; Ikeuchi, 1987; Horn, et al., 1978).

2.2.2 Shape from shading from single image

Shape and shading were one of the first subjects of study in computer vision which was started and carried out by Horn (1975). Shape from shading is the method used to explore the relationship between brightness and object shape. Almost all of the work on shape from shading, working on the lambertain surface, has been focused on smoothly curved objects, where surface normal varies continuously with a position on the surface.

Many researchers working on machine vision do not clearly reveal the data contained in the brightness values recorded in a scene. The different values of average intensities in neighbouring regions are applied to segment the image. The best approach to managing the information is comprised of the image brightness values. It has been shown that the relationship between image brightness and surface orientation can be utilized very well with a surface shape. The benefit of this method is that the shape information can be gathered one image input, which is the least amount of input. Nevertheless, there is a disadvantage of less image information being available. The method is not accurate enough because the intensity of each pixel provides only one variable, but the description of surface shape calculated by surface gradient or surface normal requires at least two variables (Horn, 1989; Horn, 1986; Horn, et al., 1978).

2.2.3 Photometric Stereo

The PS method was firstly proposed by Woodham in the eighties and has been extended an experimental treatment by many types of research. It is a method that calculates local surface reflection and orientation through the variation of the incident light source, using multiple images with different illuminations or image sequences with moving a light source (Woodham, 1980). Multiple light sources are placed at various angles but equal distance apart from the object as shown in Figure 2.5.

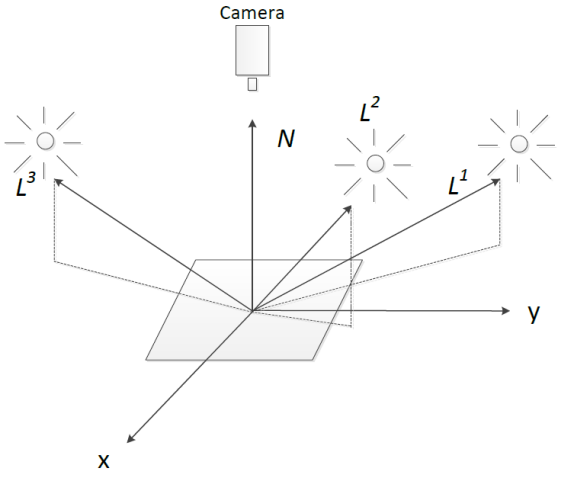

Figure 2.5 Illustration of photometric stereo geometry

The pixel of the each image acquired at the same location is assumed to correspond to the same object point. The method was originally based on the use of the so called

reflectance maps. A calibrated sphere was utilized to create the reflectance maps for determination of surface orientation, which in turn was used to measure image brightness. Two images are therefore able to create the surface gradient after the reflectance factor or surface albedo at each surface point is known. On the other hand, surface albedo is not able to know. Additional images are applied to find both gradient and reflectance factor. This method is extremely suitable for Lambertain surfaces due to their not being sensitive to noise. The main assumption of PS is that the object's surface is Lambertain and that the surface reflectance follows Lambert's Law. The reflectance can be varied to be a proportion of the surface.

2.3 Coordinate measuring machine, CMM

Coordinate measuring machine (CMM) is defined as "*measuring system with the means to move a probing system and capability to determine spatial coordinate on a workpiece surface*" (ISO 13360-1, 2001). In general, a CMM is made up of three linear moving axes that allow a contacting spherical stylus tip to move in three mutually orthogonal directions and touch an object to be measured. The position of each of the three axes is recorded during the measurement. Corrections are applied to the computer for stylus tip diameter and probing direction and sometimes for the geometric errors of the machine itself, and associated dimension is calculated. CMMs range in size from small workshop machines that can measure within a 300 mm cube or large size with 3 m or 5 m. CMMs are widely used to measure the three-dimensional sizes, forms, and positions of manufacturing parts. However, CMM measurement inaccuracy occurs when there is an error in the relative position between the measured points and the probing points. CMM errors directly influence the quality of product inspections. Therefore, CMM must be calibrated on installation and verified periodically during their operation.

2.3.1 CMM error sources

The accuracy of a CMM is affected by many sources. These error sources may cause a change in the geometry of the machine's components present in their mechanical structure such as the guideways, the scales, and the probing system (kinematic errors), the environments in which the CMM is operated these are the ambient temperature, temperature gradients, humidity and vibration (thermo-mechanical errors). In addition, the CMM software used to estimate the geometry of the workpiece is a source of CMM error (motion control and control software error). However, kinematic errors are a major

source of errors. They are errors in the machine components due to imperfect manufacturing or alignment during assembly (Barakat, et al., 2000).

For kinematic errors, a moving component always produces six errors of deviation from the nominal path as shown in Figure 2.6. One positional deviation in the direction of motion (linear error), two linear deviations orthogonal to the direction of motion (straightness errors), and three angular deviations or called rigid body rotations (roll, pitch, and yaw). Moreover, there are the three squareness errors between pairs of axes. Therefore, a CMM has 21 sources of kinematic errors. Analysing the geometrical errors of a CMM depend on the machine geometry and the purpose of the parameter evaluations. It can be decided between "direct" and "indirect" method. Direct measurement method allows the measurement of mechanical errors for a single machine axis without the involvement of other axes. For examples, positioning error measurement of an axis by a laser interferometer, measurement of straightness errors comparing with mechanical straightness standard, angular error measurement by an autocollimator, and measurement of squareness errors by the mechanical square standard. On the other hand, indirect measurement method requires multi-axes motion of the machine for movement to measure positions at different *X*, *Y*, *Z* positions such as measurement of 1D artifacts (e.g. a step gauge, and a series of gauge blocks), 2D artifacts (e.g. a ball plate, and a hold plate) and 3D ball plate, or indirect measurement based on displacement measurements such as using laser trackers (Mears, et al., 2009; Barakat, et al., 2000).

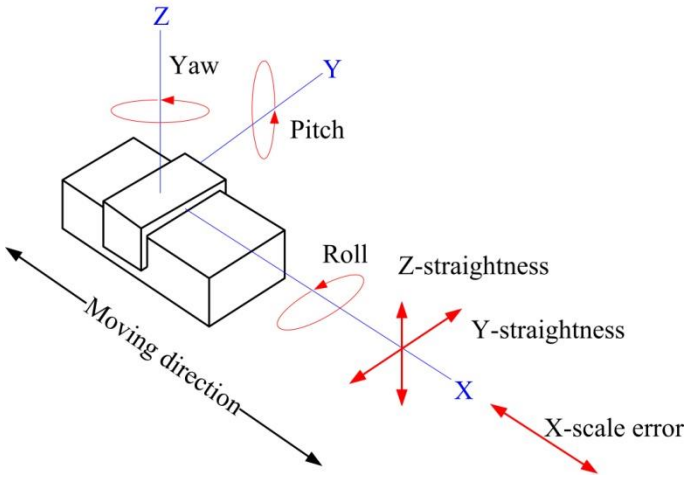

Figure 2.6 The individual error parameters for one axis

2.3.2 Maximum permissible error

The term of maximum permissible error of indication of a CMM for size measurement is defined by ISO 10360-1 as the extreme value of the error of indication of a CMM for size measurement $E_{L,\,MPE}$, permitted by specifications, regulation, etc. for a CMM (ISO 13360-1, 2001). Error of indication of a CMM for size measurement means that the error of indication from which the size of a material standard of size can be determined with a CMM, the measurement being taken through two opposite probing points on two nominally parallel planes and normal to one of planes, when the probing points are approached from opposite direction (Sun, et al., 2009). The maximum permissible error of indication of a CMM for size measurement error, $E_{L,\,MPE}$ is stated in one of three forms:

a) $E_{L,\,MPE}$ = ± minimum of ($A + L/K$) and B (see Figure 2.7 (a)),
b) $E_{L,\,MPE}$ = ± ($A + L/K$) (see Figure 2.7 (b)),
c) $E_{L,\,MPE}$ = ± B (see Figure 2.7 (c)).

Where;

A is a positive constant, expressed in micrometers and supplied by the manufacturer;

K is a dimensionless positive constant supplied by the manufacturer;

L is the measured size, in millimeters;

B is the maximum permissible error $E_{L,\,MPE}$ in micrometers, as stated by the manufacturer.

The expressions apply for any location and orientation of the material standard of size within the measuring volume of the CMM.

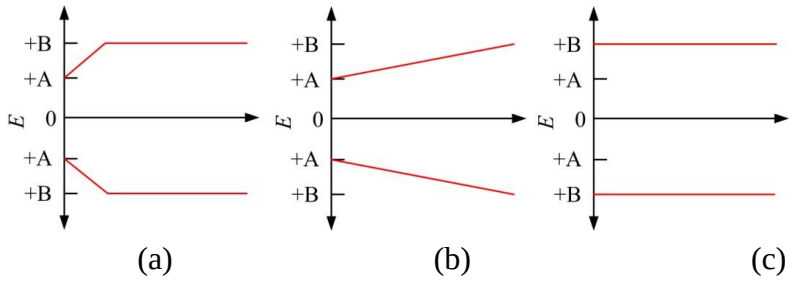

Figure 2.7 CMM maximum permissible error of indication for size measurement error

It should be noted that the maximum permissible error of length measurement, E_L is newly defined as the extreme value of length measurement error permitted by specification as shown in part 2 of the ISO 10360:2009, L = 0 mm and L = 150 mm (default values of ram axis stylus tip offset which means the distance (orthogonal to the ram axis) between the stylus tip and a reference point), are specified (ISO 10360-2, 2009; EAL-G17, 1995).

2.4 Surface metrology

2.4.1 Contact instrument (Stylus instrument)

Surface measurement usually yields information of two types, the roughness and the waviness. These parameters can be used to explain and predict the performance and problems of machine tools. Filtering techniques are applied to separate the surface topography into roughness and waviness (Whitehouse, 2002). The definition of each element of a standard stylus instrument has been detailed in the International Standards (ISO 3274, 1998). As can be seen from the Figure 2.8, the schematic diagram is comprised many parts such as a stylus, a pick-up unit, an amplifier, a filter and a recorder.

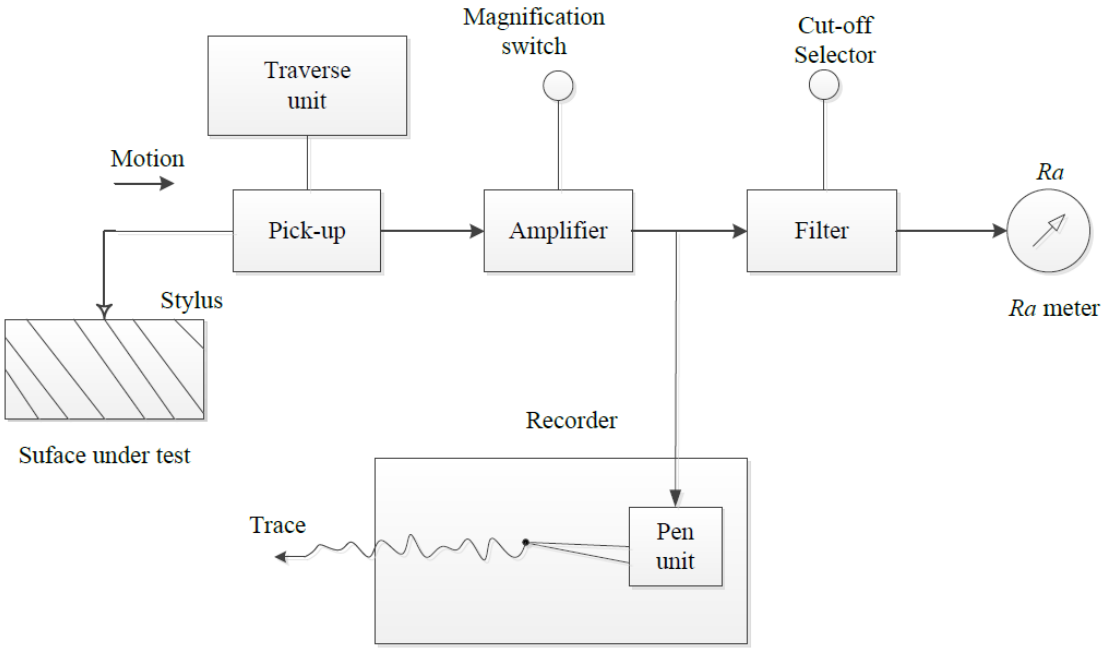

Figure 2.8 Schematic diagram of a standard stylus instrument (Smith, 2002)

The stylus technique in Figure 2.8 can be explained. The stylus traverses through the surface peaks and valleys on the surface of the object being examined. The transducer produces an electrical signal, which is proportionally converted from stylus's vertical motion. It is likely to be analysed using either a digital technique or analogue technique. The resulting charge is then amplified and electronically integrated by the amplifier, which generates signals proportional to the surface profile. A filter selection, using for analysis a range of structure in the entire surface profile, is utilized to eliminate a waviness profile. The surface roughness profile is stored in a recorder and the measurement results are shown by pen unit (Vorburger, et al., 2007).

1) Stylus

The stylus is design either a conic with a spherical tip or a four-sided pyramid with a truncated flat tip. Two standard cone angles, 60^{o} and 90^{o}, are used with conical type. The size of tip radius has a range of scale from less than 0.1 μm to 12 μm. In the case of a pyramid stylus, a stylus width 2 μm will provide wider transversely to the direction than a stylus width 0.1 μm. The size and shape of a stylus must be selected appropriately with measured surface. For example, if the slope angle of the valley on a surface texture is as steep as the half angle of the side of a conical stylus, the stylus would not be able to contact all of the surface features (Smith, 2002).

2) Pick-up operation

The purpose of a pick-up or transducer is the conversion of the minute vertical movements in which the stylus trace along the surface into an electrical signal. The basic requirement of sensitivity for its transformation with stylus movements should be around 0.1 nm. Pick-ups can be commonly classified into two groups by operating principles: analogue and digital transducers.

The analogue transducer has been widely used in the past with large stylus instruments. In the present, it is widely applied to sophisticated hand-held measuring instruments. The pick-up gives a signal proportional to displacement.

The digital transducer has been typically used with optical instruments. These optical configurations vary with each device company, but all of their instruments use a laser as a light source because it has a standing wavelength which is suitable for high precision roughness measurement (Smith, 2002; Leach, 2001).

2.4.2 Optical technique for surface texture assessment

Several optical technical designs have been developed for surface texture and form measurement. To date, the most common techniques used to perform surface texture and form have been laser interferometers (Sherrington and Smith, 1988).

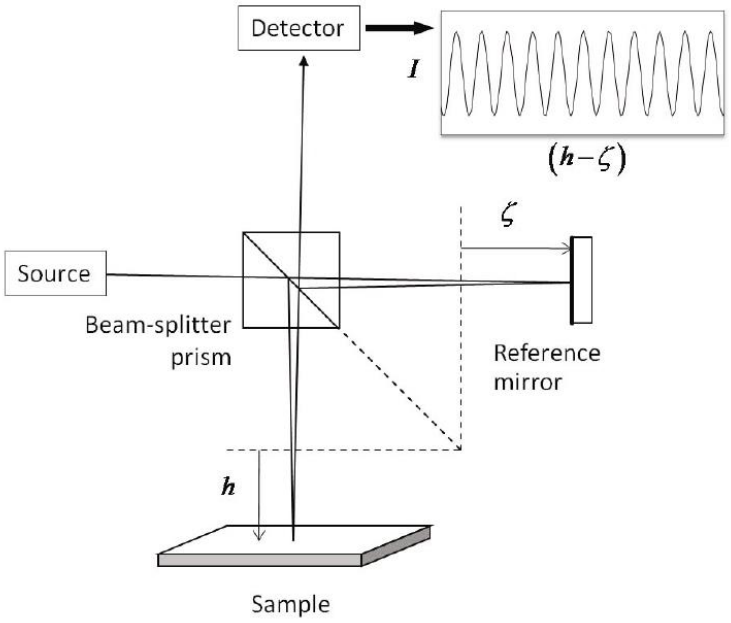

Figure 2.9 Michelson interferometer (Leach, et al., 2008)

These have included conventional Michelson and Twyman-Green interferometers, Schmalz light sectioning microscopes, Linnik microinterferometer, Tolansky multiple beam interferometers, and fringes of equal chromatic order (FECO) interferometers (Leach, 2011). The fringe images produced by interferometers demonstrated very high accuracy, which traced precisely the peaks and valleys of the surface texture with the high resolution of the vertical axis. Nevertheless, these methods were developed to rapidly compute the analysis of fringe automation that could digitize topography profiles in an automated way. Its usefulness compared with the stylus instrument was very competitive.

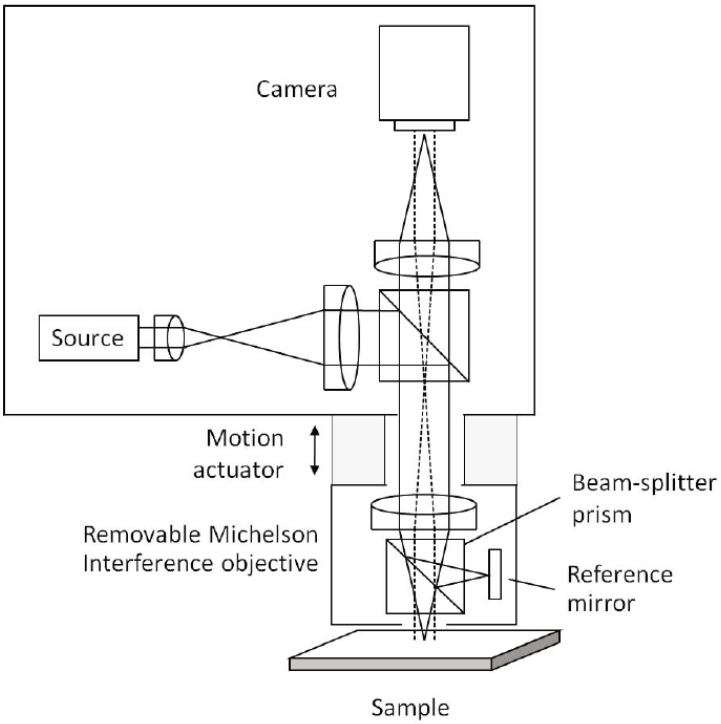

Figure 2.10 Interferometer for areal surface measurement employing a Michelson-type interference objective (Webb, 1996)

Figure 2.10 shows the optical configuration of a microscope that provides interchangeable interference objectives by using an ordinary interferometer design, based on the Michelson geometric transformation of Figure 2.9. There are various techniques used to achieve a high degree of accuracy on interference fringes such as phase shifting interferometry, coherence scanning interferometry, digital holographic microscopy, and imaging confocal microscopy (Leach, 2011). In this review, the optical techniques discussed in this chapter are the most common techniques for areal surface characterization in industrial manufacturing and laboratories.

1) Phase Shifting Interferometry

The phase shifting interferometric (PSI) microscope was built in the early 1980s to be the most useful method for measuring smooth optical surfaces (Leach, 2011).

PSI is a well-established technique that can provide 3D surface profiles with very high resolution. Moreover, the repeatability in the measurement system is less than 1 nm, and it is independent of field size. This technique has relied on the digitisation of the interference pattern obtained in order to control any phase shift. This sequencing is usually introduced by a controlled mechanical oscillation of an interference objective. Surface and form measurements can be acquired from a range of particular interference objectives. Such objectives are installed on the microscopes for interferometry (Hariharan, 2003; Whitehouse, 1997). However, for measuring surface roughness details, broadband (multi-wavelength) techniques, such as VSI are a more practical solution although other limiting issues (for example, that of 'skewing') in any optical method must be considered carefully in any surface roughness study (Rhee, et al., 2006).

Phase shifting interferometry's extreme sensitivity, including vibration and air turbulence, affects the measurement results. In many situations, the measurement accuracy is limited by the environmental condition, and sometimes the environment is sufficiently bad that the measurement cannot be performed. As a result, it can only work well in controlled areas and laboratories.

2) Coherence Scanning Interferometry

Davidson (1987), who developed coherence scanning interferometry (CSI), applied the CSI technique to perform with smooth surface and semiconductor applications. The technique was utilized to upgrade the lateral resolution of fine features (Davidson, et al., 1987). The CSI system was powerful enough to provide surface measurement with sufficient roughness that was able to generate random speckle. The capabilities for measuring both rough surface and smooth surface testing did not include the spatially unwrapped fringes. Moreover, the CSI system can also perform autofocus at every point in the field of view and eliminate untrue interference from scattered light (Leach, 2011; Lee and Strand, 1990). A schematic diagram of typical configurations of CSI is illustrated in Figure 2.11

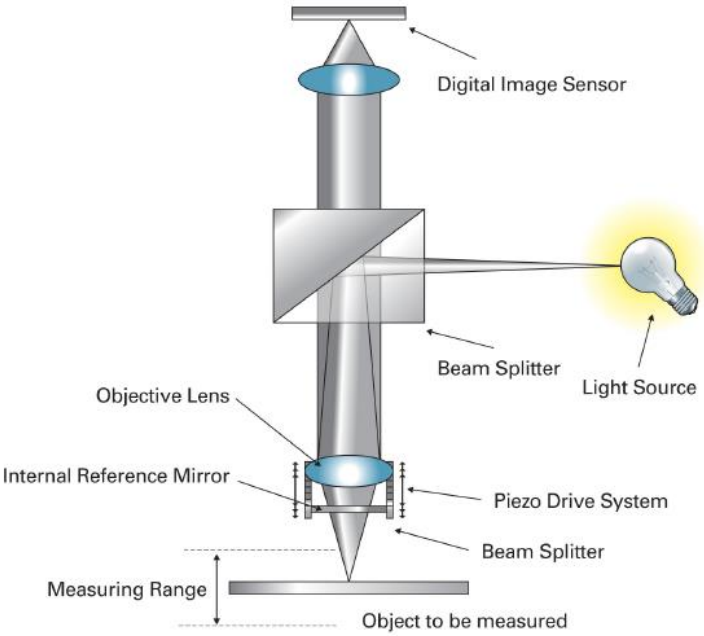

Figure 2.11 Schematic diagram of typical configurations of CSI (Leach, et al., 2008)

Light source (white light) used for CSI has a shorter coherent length than monochromatic light to prevent ambiguity in the fringe order evaluation. The illumination beam splitter is used to conduct light directly from the light source to objective lens. The light source is separated into two beams by the objective lens; one beam of light run directly to the object to be measured, and the other beam of light run directly to an internal reference mirror. The two beams are recombined and transmitted toward the digital image sensor. This sensor performs an intensity measurement of the light and then the interference objective is to scan the movement in the z direction to obtain the interference maximum. During scanning, intensity data for each image point or pixel in successive camera frames is recorded by a computer controller. The light intensity can be used to calculate the position of surface characteristics. The design of CSI instruments is normally similar to that of a conventional microscope, which can replace other interference objectives, such as the Michelson, Mirau, or Linnik type (Leach, 2011; Leach, et al., 2008).

3) Confocal Microscopy

The technique of confocal microscopy was first created by Marvin Minsky in the period from 1950-1959. This technique is an efficient system for the 3D measurement of

surface topography. A confocal microscope has a slightly different technology from the conventional microscope. A point of illumination from the light source is used to focus on a minute viewpoint on the object's surface rather than imaging on the whole of the illuminated surface. The confocal microscope is used for the acquisition of a sequence of confocal images through the depth of focus of the microscope's objective. There are two essential pinholes with different installed positions. The essential pinhole installed near a sensitive photodetector restricts and reduces the illuminated regions on the specimen by means of a structured illumination pattern. Therefore, reflected light from the other levels from the specimen does not have an effect on the measurement result. As a result, confocal microscopes are suitable instruments that can be used to increase the accuracy of the measurement of the contour surfaces (Leach, 2011). A schematic diagram of a typical confocal microscope is illustrated in Figure 2.12.

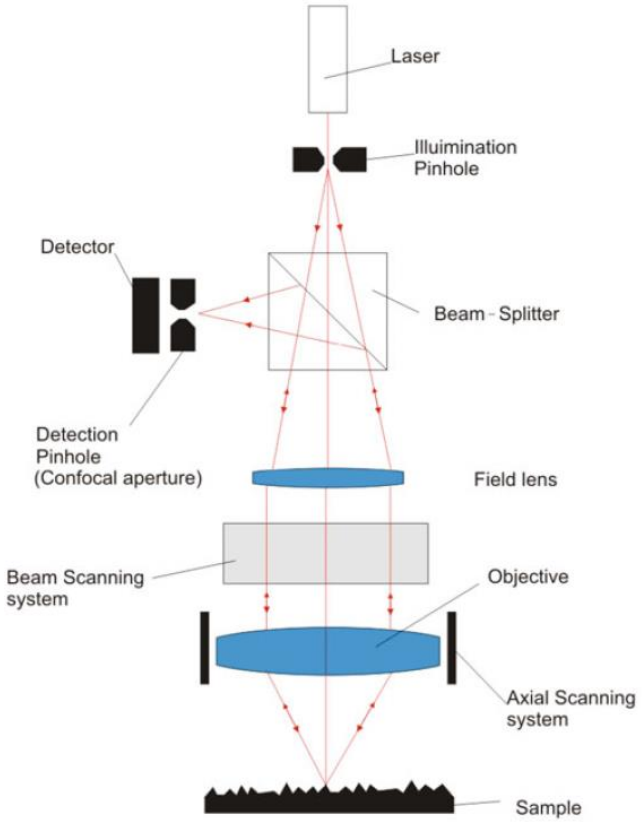

Figure 2.12 Schematic diagram of a typical confocal microscope (Leach, 2011)

The focused spot on the specimen and located pinhole before a detector are shown in Figure 2.12. In such a configuration, the method to acquire surface topography is by

moving the illuminating spot in the x and y directions to scan the whole surface perpendicular to the optical axis in the z axis. The mechanical scanning used to move the microscope's objective is generally performed by a piezoelectric actuator. The developed techniques using the scanning of a laser beam by the rotation of mirrors and the use of a pinhole disk, called a Nipkow disk, have been developed (Webb, 1996; Xiao, et al., 1988). Fiber optics is utilized in a confocal microscope system. The single mode optical fiber was used to launch and detect the confocal signal as well as providing the reference beam (Rea, et al., 1996). Nowadays, many commercial instruments, based on the basic confocal microscopy technique, can be categorized as belonging to one of three types of confocal microscopes: laser scanning confocal microscope, disc scanning confocal microscope, programmable array scanning confocal microscope (Leach, 2011).

The limitation of confocal microscopes is that the instruments are not able to provide high accuracy measurements regarding the slope of surface exceeding 15^{o} and the limited speed for surface measurement is rather low, with a profile record at 1 mm long using a minimum period of 10 min (Sherrington and Smith, 1988).

2.5 Surface texture measured by the PS method

The PS method is a successful approach for measuring object shape and facial appearance. It was first introduced in computer vision and graphics by Woodham (1980), who exploited the PS method to recover local surface orientation of Lambertian surfaces by using three point light sources. Ikeuchi (1981) then developed the traditional PS method for measuring objects with a specularly reflecting surface, which was useful in industrial applications. Onn and Bruchstein (1990) investigated two images of a Lambertain surface which were obtained using different illumination conditions, determining the local surface normals up to two possible orientations. They presented a novel method to recover a height profile from a smooth surface and concluded that it was possible to use only two shaded images provided by the PS method for recovering the smooth surface. Nayar, et al. (1990) proposed the structured highlight inspection method using 127 point sources, illuminating the object to be inspected. They developed the shape extraction system for shiny objects for on-line inspection. The theory of photometric stereo for a large class of non-Lambertain surfcaes was proposed by Tagare and Defigueiredo (1991); they showed that the traditional PS method was

sufficient to estimate the surface normal and the illuminant strength. Many researchers have improved the approach for recovering the shape of specular spike objects, and this approach has subsequently received extensive attention.

Healey and Binford (1988) proposed the Torrance-Sparrow specular model considering the underlying physics of specular reflection from rough surfaces. In their model, the properties of a specular feature in a scene and the local properties of the proportional surface had a powerful correlation. The model was able to separate the image intensities from specularity in image pixels. Smith, et al. (1999) developed the PS technique to apply for the detection of characteristic surface faults such as scratches, indentations, or small protrusions. Sun, et al. (2007) developed the PS system for reconstructing scenes of several properties of non-Lambertain rough surfaces. At least six lights are used to recovery the surface finish of different profiles on convex objects. This research can be properly applied to deep reliefs of topographic features. Hernandez (2008) proposed the Multiview PS technique to reconstruct texture-less shiny objects. Recently, the four-source PS method was used for measuring the warpage of injection modeled parts in polymer processing, which is a central task in the quality control of production processes. The research was developed for form measurement by using gradient fields in polar coordinates to direct surface reconstruction from gradients for the use of the PS technique in advance manufacturing (Radler, et al., 2016).

2.6 Research gaps and literature review summary

In this chapter, a non-contact method based surface and form measurements were presented along with the review of different techniques. Most of the researchers found that traditional non-contact instruments are suitable for measuring objects in a laboratory because they are very sensitive to the environment. This problem is directly involved with measurement results. In the review, use of the PS method for measuring the surface characteristics is discussed. Many researchers are using the PS method for recovering surface defects and surface characteristics. However, all the above-mentioned methods suffer from some serious limitations. They are only performed and improved the method for recovering 3D topographical information. Therefore, this study makes a major contribution to research on surface and form measurements using the PS method, which can identify the measurement accuracy and measurement uncertainties of measurement results. Moreover, measurement traceability of the PS

system for measuring surface roughness specimens is proposed, making links to national measurement standards through the surface roughness standards calibrated by using a stylus instrument, as will be explained in the next chapter.

The gaps identified to be investigated this research are as follows:

1) Previous research methods of surface and form measurements have been suitable to determine measurements in the laboratory. In this thesis work, the PS method will be applied and combined with the CMM to study tilt and slant angles by using the precision movement of CMM's probing system for measuring surface and form measurements. Hence, the system can be applied in the on-line measurement within the engineering industry.
2) Previous studied of operation parameter in the PS method for measuring surface topography are very limited, the PS system cannot be performed to determine surface and form measurements at the same time. In this research, I will investigate the method to increase the performance of the PS technique using a Gaussian filter. This will provide a novel way to separate surface roughness and form profiles on one-time measurement.
3) Previous research of the PS method for measuring surface has been done on the how to improve the performance of surface normals from the 3D profile. In this thesis work, the measurement uncertainty of the PS system will be investigated to optimise the accuracy of the measurement system, and the EN ratio will be used as the equation that evaluates the performance of the PS system for measuring surface texture.

It is believed that the progress in this study of surface and form measurements using the PS method is going to fill some unfilled gaps in knowledge of this new filed, and enable the further development of surface and form measurements on in-line manufacturing.

Chapter 3 The establishment of reference values for surface roughness measurement

3.1 Introduction

The basic method for surface inspection has been comparison of sensations from our finger running across precision reference specimens being and across objects manufactured from an industrial machine. But examining surface by this approach is insufficiently accurate when working with smooth surfaces. To determine a reasonable result, contact and non-contact for measuring surfaces have been built. They have been appropriately called stylus and optical instruments. The former method consists of a stylus that physically contacts the surface being measured and a traducer converting its vertical movement into an electrical signal. The latter method is named as following their optical techniques such as Laser triangulation, interference, reflection, and scattering. In this chapter, the stylus instrument has been utilized for measuring surface roughness standards. These results are used as reference values performing the linear regression with the results acquired from the photometric stereo method. In this chapter, the details of surface characteristics and description of the material used in the research have been provided, and then the method for calibration of surface roughness standards has been discussed.

3.2 Surface characteristics

A largescale combination in the natural world mimics surfaces discovered in engineering being desert, which is comprised sand grains - roughness. The ripples in a surface are waviness, and the undulating nature of the land is a profile. From an engineering point of view, the surface is separated from two distant media, the components, and its working environment (Smith, 2002). When mechanical parts are designed, they would be produced following drawing, including the production methods and its specific geometric tolerance. According to the method of manufacture, surface attributes have to be combined by roughness and waviness. The levels of these two attributes depend on a number of factors such as:

- the influence of the material's microstructure;
- the surface production including the tool's cutting action, tool geometry,

cutting speed;

- the machine's efficiency during the manufacturing process;
- the method for holding an object between the manufacturing process;

Based on consideration of these factors from the surface production, a smooth or rough surface would be created by a designer who realises a functional surface condition.

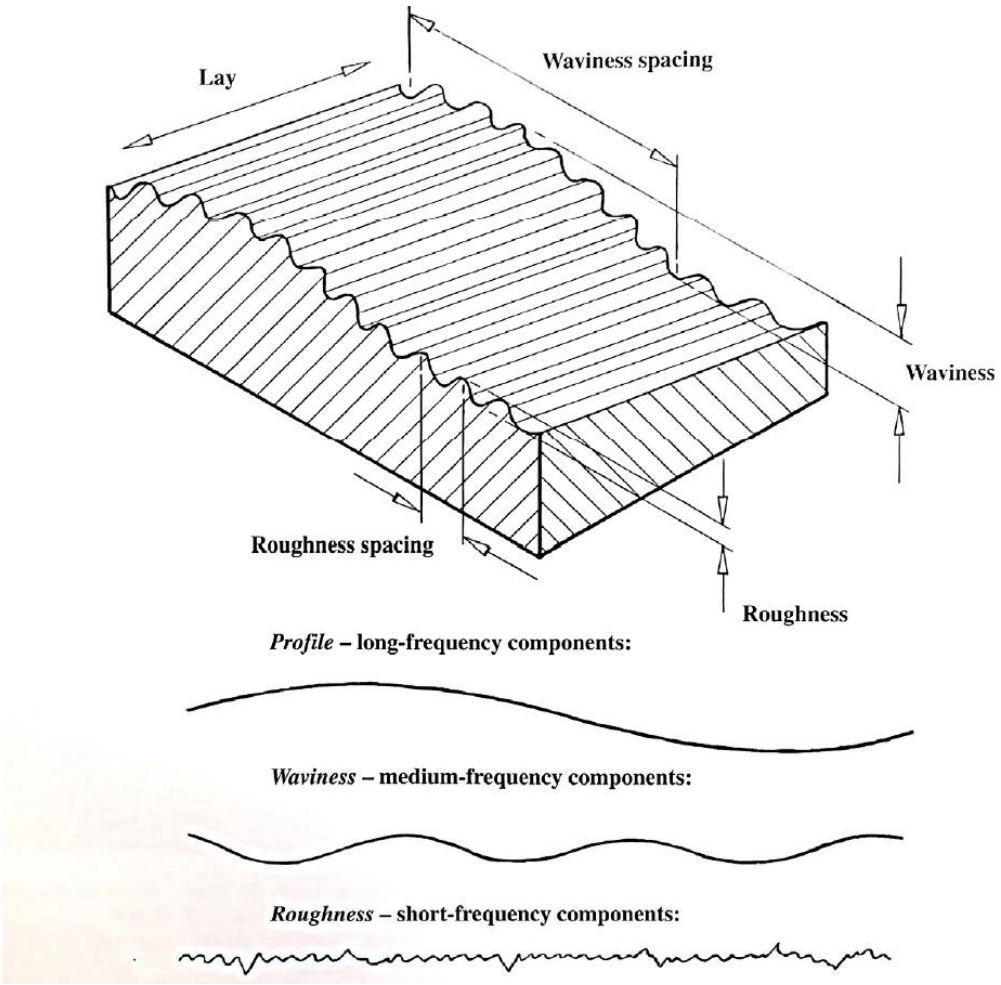

Figure 3.1 The major components that constitute a typical surface texture

The roughness (high-frequency components) is inevitable because it is the mark of the production. On the other hand, the waviness or medium-frequency components could be eliminated and avoided by understanding the influence for surface production, for example, vibration caused by an imbalance of machinery can be prevented by repaired and overhauled rotating parts following the operating time of their devices. The profile (low-frequency components) is the overall shape of the surface, separated from

roughness and waviness variations. The error case will happen from the deviation of shape required and specified by the designer (Smith, 2002; Whitehouse, 2002).

The coordinate system of roughness measurement generally uses rectangular system x, y and z-axes. The x-axis is a coordinate that a stylus instrument traverses on the surface. The y-axis is a coordinate that parallels with the lay of surface and the z-axis are the coordinate that perpendicular to the x-axis. The lay of any surface is essential when we attempt to describe its potential functional performance (ISO 4287, 1998). If the trace direction of the stylus is created incorrectly, the measurement profile and measurement result will have entirely misrepresentative values as illustrated in Figure 3.2.

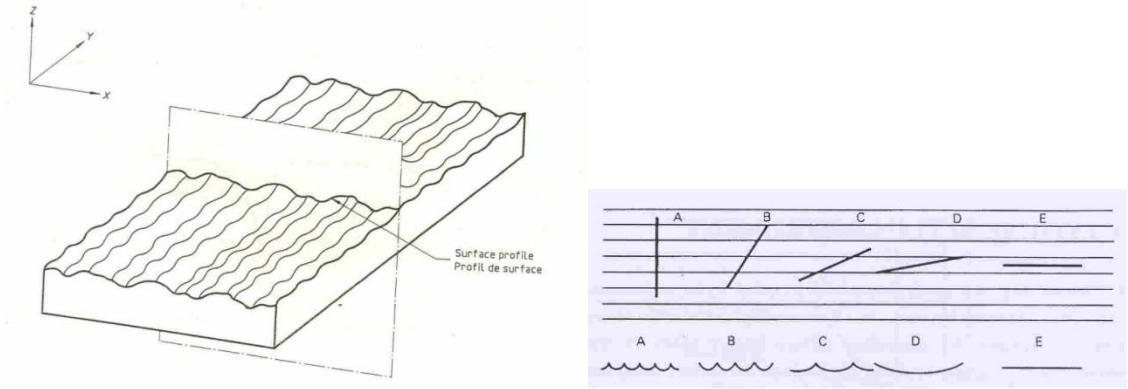

Figure 3.2 Effect of the measurement direction (ISO4287, 1997)

The surface profile usually chooses a plan with a normal that nominally lies parallel to the real surface and in a suitable direction. If the surface is assessed from a wrong direction, the measurement result will be false. Choosing a correct orientation is the main assessment criteria for surface roughness measurement.

Surface roughnesses manufactured by different processes are shown in Figure 3.3. Such features are a natural consequence of any particular form of the manufacturing process. There are a lot of problems with the instrument maker as many different forms of surfaces have specific roughness values. There are many types of contact and non-contact instruments used for measuring surface roughness such as stylus, optical, X-rays and ultrasonic. The user should choose the instrument whose range is suitable for the magnitude of the feature being measured. The roughness parameter R_a is defined in the following section (Whitehouse, 2002).

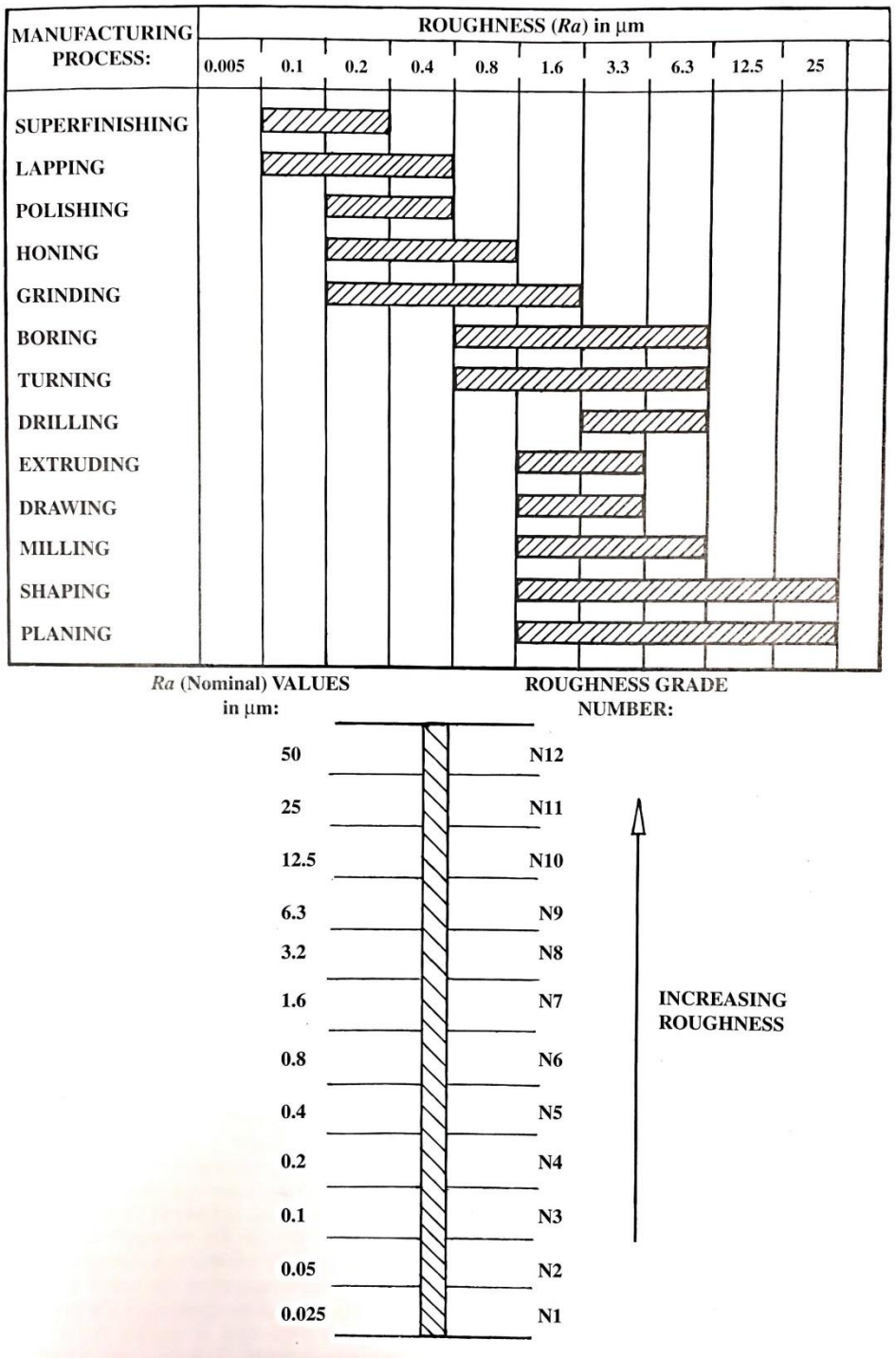

Figure 3.3 Typical roughness value obtained by different finishing processes (ISO1302, 2001)

3.3 Filters

The fundamental role of filtering for surface profile assessment is to select and analyse a range of structures in the surface profile judged to be of significance to a particular situation. Surface geometry is generally included roughness, waviness, and profile. Numerical algorithms can separate these profiles through the selection of suitable

characteristic functions of each profile. The technique for separation each profile is called as profile filter and defined (ISO 4287:1997) to be a filter dividing profiles into long-wave and short-wave components as shown in Figure 3.4.

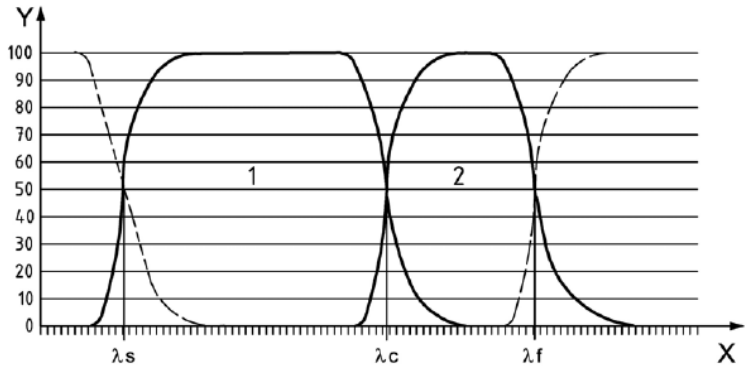

Figure 3.4 Transmission characteristic of roughness and waviness profiles

There have been three types of filtering which are used for surface texture analysis. Firstly, λ_s is the profile filter which defines the intersection between the roughness and the prior short-wavelength components in a surface. λ_s is used to eliminate irrelevant information, such as instrument noise and imperfections. Secondly, λ_c is the profile filter which defines the intersection between the roughness and waviness components in a surface. λ_c is used to eliminate waviness component. Finally, λ_f is the profile filter which defines the intersection between waviness and longer wavelength components presenting in a surface. λ_f is used to remove any other profiles on the surface.

3.4 Surface roughness standards

The surface profile parameters are defined by ISO 4287:1998, which encompasses five groups of texture parameters, including amplitude parameters (peak and valley), amplitude parameter (average of ordinates), spacing parameters, hybrid parameters, and curves and related parameters.

3.4.1 Amplitude parameters

A number of different diagnostic two-dimensional amplitude parameters are defined by height variation measurements on material surfaces made on a given reference level. These parameters are summarized in Figure 3.5.

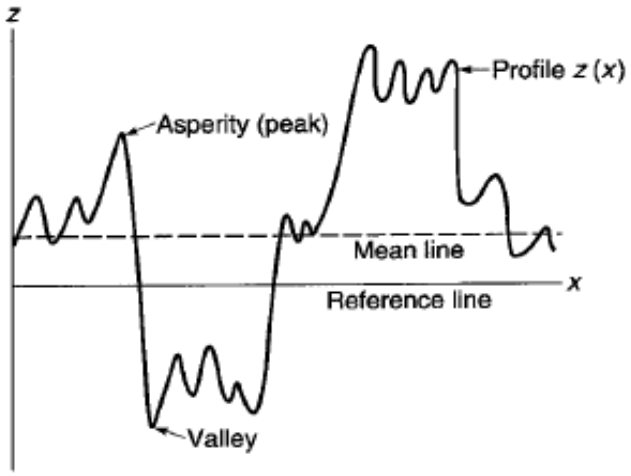

Figure 3.5 Schematic of a surface roughness profile indicating the key features from that amplitude parameters is defined and determined. Reproduced from (Bhushan, 2001)

These comprise the arithmetic (or center line) average height (R_a), and the maximum peak to valley height (R_z). These are the roughness parameters stated in the experimental section. Other height parameters encompass root mean square height (R_q), maximum valley height (R_v) and maximum peak height (R_p) (Bhushan, 2001). They are useful in surface analysis, but since they were not measured in this research, These parameters will not be considered further.

R_a is the average of a number (n) of absolute height values (z_k) evaluated on the mean line through the full profile obtained over a provided sampling length (x):

$$R_a = \frac{1}{n}\sum_{k=1}^{n}\left|z_k\right| \tag{3.1}$$

Ranges of individual R_a values give for a number of standardized roughness grading systems. One that is commonly referred to is the grading number (N). Table 3.1 presents the maximum value of R_a that corresponds to *N1 – N12* that cover the majority of surface textures encountered in material science and engineering applications.

Table 3.1 The relations of roughness grading number and their R_a values. Adapted from (Bhushan, 2001)

Maximum R_a value / μm	Roughness grading number (N)
0.025	N1
0.05	N2
0.1	N3
0.2	N4
0.4	N5
0.8	N6
1.6	N7
3.2	N8
6.3	N9
12.5	N10
25.0	N11
50.0	N12

R_z is the highest peak-mean line height plus lowest valley-mean line height) over the measured sampling length:

$$R_z = R_p + R_v \qquad R_p = \max\{z_k\} \qquad R_v = \min\{z_k\} \tag{3.2}$$

Skewness (R_{sk}) of the assessed profile is proportional to the mean cube of the height values recorded. It is an indicator of the asymmetry of the distribution around its midpoint:

$$R_{sk} = \frac{1}{Rq^3}\left[\frac{1}{N}\sum_{k=1}^{N} Z_k^3\right] \tag{3.3}$$

The value of the skewness determines whether the bulk of the material is located above the middle line (negative values) or below the middle line (positive values). When two surfaces have a similar R_a, the skewness parameter provides a way of distinguishing them. Richard Leach provides an excellent example of the usefulness of the skewness parameter in his Good Practice review: "*A characteristic of a good bearing surface is that it should have a negative skew, indicating the presence of comparatively few spikes that could wear away quickly and relative deep valleys to retain oil traces. A surface with a positive skew is likely to have poor oil retention because of the lack of deep valleys in which to retain oil traces. Surfaces with a positive skewness, such as turned surfaces, have high spikes that protrude above the mean line.* R_{sk} *correlates well with load carrying ability and porosity.*" (Leach, 2001)

Kurtosis (R_{ku}) of the assessed profile is proportional to the mean fourth power of the height values recorded. It is an indicator of the spikiness/bumpiness of the surface:

$$R_{ku} = \frac{1}{Rq^4}\left[\frac{1}{N}\sum_{k=1}^{N} Z_k^4\right] \tag{3.4}$$

A spiky surface would have a high value of kurtosis and a bumpy surface a low value. This parameter is useful for predicting surface wear and lubrication properties (Leach, 2001).

3.4.2 Spacing parameters

Apart from the perpendicular amplitude deviations used to characterize surfaces, other descriptive parameters have been established to characterize surface details in the parallel direction (Bhushan, 2001; ISO 4287, 1998). These include peak density (N_p) - the number of peaks (of any amplitude value) present in a profile per unit length across a surface, and the zero crossings density (N_0) that indicates the number of times a profile crosses the mean line per unit length. The reciprocal of the peak density ($1/N_p$) gives a measure of the average spacing between consecutive peaks and is therefore called the mean peak spacing (A_R).

3.4.3 Hybrid parameters

As the name implies, these alternative parameters incorporate a combination of height and spacing data in a profile feature. Two of the most important parameters of this type are the average slope and average curvature of a peak or a valley (Bhushan, 2001; ISO

4287, 1998). The latter is of particular importance as its magnitude indicates whether, upon contact from a stylus, a peak on the sample surface would return to its former shape (elastic deformation) or remain distorted (plastic deformation). These parameters were not investigated in the experimental part of the project and so are not discussed in any further detail.

The surface roughness standards used in the experiment were a standard made from tungsten metal with roughness parameter Ra values of 3.2, 6.3, 12.5, 25 and 50 μm, respectively (ISO 5436, 2000). They were calibrated by the standard contact method, using a stylus instrument (Surfcorder ET4000A) to determine the average roughness values and measurement uncertainties. Specifications and measurement protocols for the instrument are now detailed.

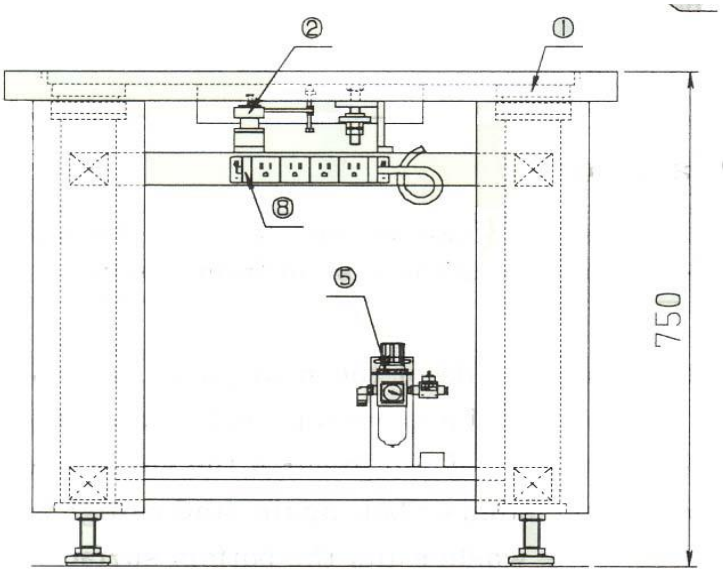

Figure 3.6 Schematic diagram of the pneumatic vibration isolation table system

All measurements reported in this experiment were performed on vibration isolation systems as shown in Figure 3.6. It is absolutely essential that environmental vibrations are dampened because their frequencies overlap significantly with the mechanical frequencies of the measurement systems. The surface roughness standards used in our research are shown in Figure 3.7.

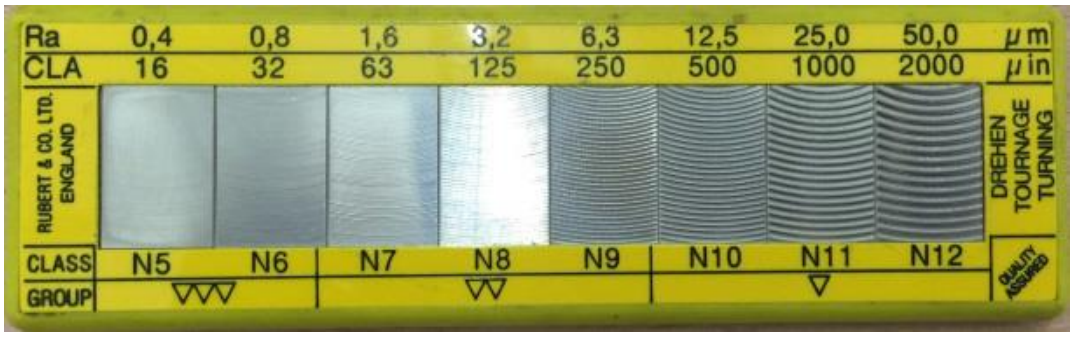

Figure 3.7 Surface roughness standard utilized in the research

The surface roughness standard as shown in Figure 3.7 must be cleaned before initiation of measurement by the standard cleaning procedure. The following cleaning procedure is applied:

1) Clean the surface roughness standard by using ethyl alcohol and wipe off with soft lint-free cloth or appropriate wiper.

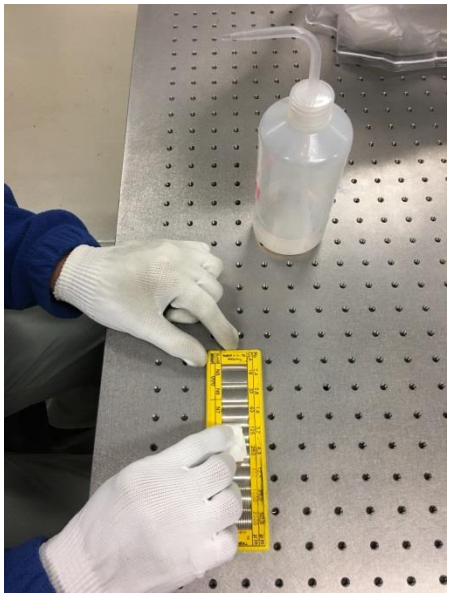

Figure 3.8 Cleaning process

2) Stabilize the surface roughness standard for at least 1 hour before measurement. The stabilization process is necessary because of the geometric parameters of the standard, as well as of the measurement instrument, depends on temperature and, to a lesser extent, atmospheric pressure. For this reason, calibration samples should be stored near the instrument in an environment that has been stabilized on temperature and humidity.

3.5 Setting up stylus instrument

3.5.1 Initial setup of stylus instrument

Below is a step-by-step protocol that is followed for the preparation and operation of the stylus-based instrument, including screen shots from the related software packages. Brief comments are also included on the purpose of each of the procedures performed. Stylus instrument specifications are as follows:

- Model: *Kosaka Laboratory ET4000AK*
- X-axis – measuring range of 100 mm, resolution of 0.01 μm
- Z-axis – setting range of 52 mm, LVDT transducer, measuring range of 32 μm, resolution of 1 nm, tip force range of 0.5-500 μN, tip radius of 2 μm
- The ambient temperature measured by a digital thermometer at 20 ± 1 ºC / relative humidity at 50 ± 10%.

The start-up sequence is as follows:

1) Turn on the pneumatic vibration isolation system. This ensures that the system is adequately insulted from the mechanical noise present in its environment.
2) Check the air pressure from the pressure gauge under the pneumatic vibration table. Ensure that, the pressure gauge is between 0.45 MPa and 0.55 MPa (Figure 3.7). This ensures that the table floats at its optimum height.

Figure 3.9 Pressure gauge

3) Turn the power on to remote control unit, amplifying operation unit, CCD unit, main unit and personal computer in roughness measuring instrument (see the schematic

diagram above) and leave it to be stabilized for least 30 minutes. The stabilization period is necessary because the electrical characteristics of the electronics are temperature-dependent and the temperature distribution takes the time to reach the equilibrium state after the system is powered on.

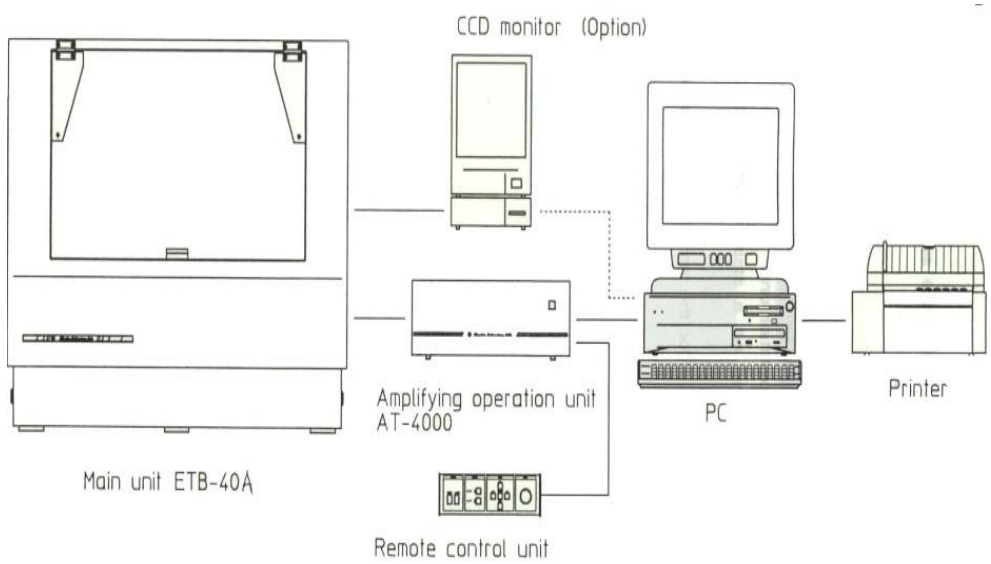

Figure 3.10 Schematic diagram of the stylus instrument

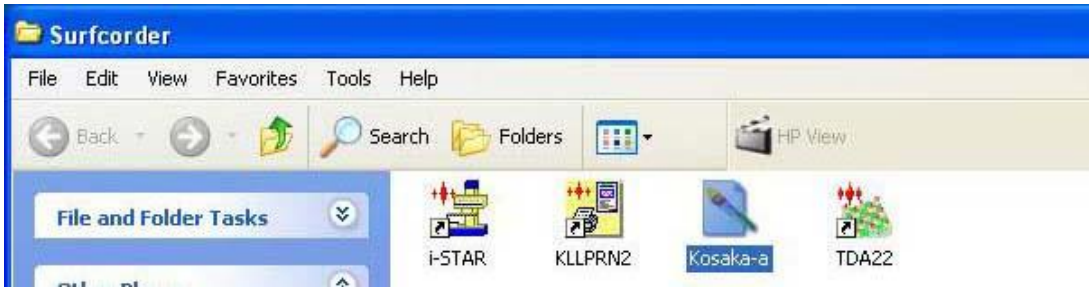

Figure 3.11 Screenshot of the Windows Program Manager folder containing the stylus software start-up icons

4) Double click i-STAR icon in the Surfcorder folder (see the screenshot above). After that, the screen displays “Start the initialization” box. Select OK in “Start the initialization” box. After that, the instrument will initialize along X and Y axes.
5) After that, screen displays “Initialize the pick-up”. Select "Pick-up init" in the initialization box. The instrument will initialize along the Z axis. After that, the screen display “Initialization finished”. Press the "close" button. The screen will launch into I-Star program.

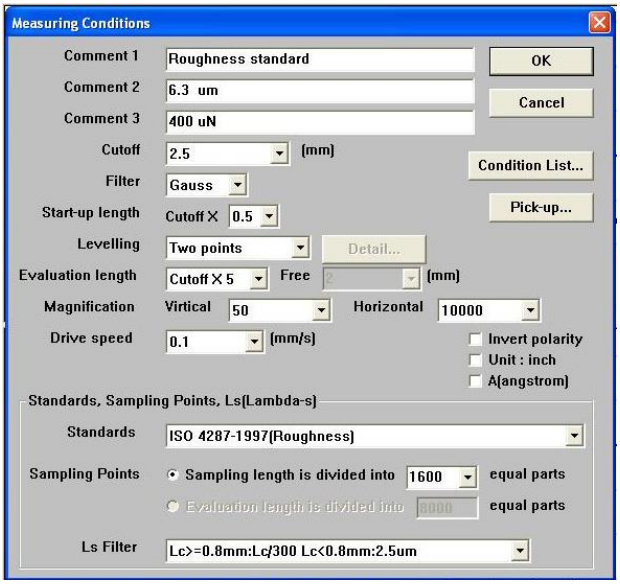

Figure 3.12 Parameter selection window of the stylus profilometer control software

The parameter selection window of the measurement process is largely self-explanatory – the parameters in question have been described in the introduction chapters above.

3.5.2 R_a measurement

The R_a measurement sequence on the stylus instrument is as follows:

1) Put the surface roughness standard in the middle position of instrument table as shown in Figure 3.13.

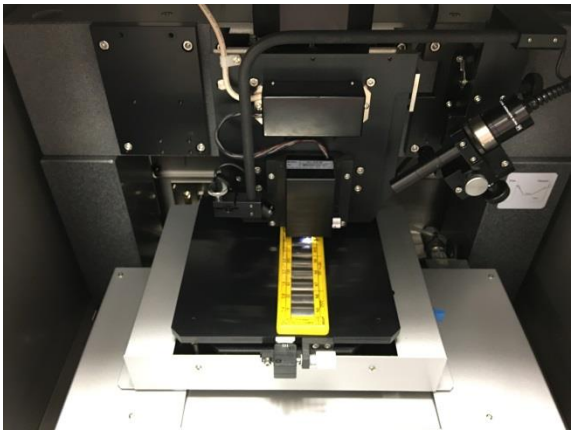

Figure 3.13 The surface roughness standard is placed in the middle of instrument

2) Move Z axis by observation the pick-up unit of instrument close to the surface of the surface roughness standard using remote control unit.
3) Press “AUTO” button on the remote control unit. The pick-up unit is to be moved automatically to the surface of the surface roughness standard until the stylus moves to middle measurement range.
4) Design the measuring area. A number of traces must not be less than twelve and shall be distributed over the measuring area (ISO 5436, 2000).
5) Align the measurement area in X and Y axis by the remote control unit and adjusting the surface roughness standard by hand and the traversing direction should be perpendicular to the direction of the lay unless otherwise indicated.
6) Tilt the measurement plane of the step height standard using ‘Tilt’ adjusts command in Control menu of I-Star program.
7) Select X auto adjust button on “Tilt adjust window”. The X-tilt Auto Adjust will display. Insert the tilting length into the windows. Note: Tilting length must be cover the measurement length of the surface roughness standard
8) Select ‘Done’ button on X-tilt Auto Adjust window. The instrument will tilt the measurement plane of the surface roughness standard. Then select ‘Close’ button on X-tilt Auto Adjust window.
9) Select ‘Measuring Conditions’ menu and set using following criteria;
    - Standards: ISO 4287-1997.
    - Cutoff: 5 sampling lengths.
    - Filter: Gaussian.
    - Evaluation length: depends on the average roughness value which can follow as ISO 4287-1997.
    - Magnification Vertical: 50 / Horizontal: 10000.
    - Drive speed: 0.1 mm/s.
    - Sampling points: 8000 points.
10) Select “Measure toolbar”. The instrument is to be automatically started measurement. The number of repeat measurements n = 5.
11) After finishing, select “Save toolbar” for saving measurement data.
12) Move the pick-up unit to next line on surface roughness standard and repeat measuring step until all measurements are complete.
13) Save the results of measurement to ASCII text file format for subsequent analysis in a spreadsheet program.

14) After finishing measurement, move the stylus tip from the surface roughness standard and remove the surface roughness standard from the table.

3.5.3 Measurement results

The values of surface roughness standard used in our experiment were included 3.2, 6.3 12.5, 25, 50 μm. In this experiment, they were measured to find true values from the stylus instrument. In the case of evaluation the test data from measurement system, to determine whether adequate process control has been built, statistical analysis is adopted. If systematic or random errors does not influence the metrological process, then the process is called to be a normal system and any process data is valid. Two statistically derived mathematical expressions are needed to define whether a process is behaving correctly: there is the arithmetic mean and its accompanying standard deviation (Taylor, 1997). Actually, the arithmetic mean is conveniently shortened to mean, this being denoted by the symbol $\bar{x}$. Its value is the mean of all value of *x* can be derived from the following expression:

$$\bar{x} = \frac{1}{n}\sum_{i=1}^{n} x_i \tag{3.5}$$

where $\bar{x}$ arithmetic mean, $\sum x$ = sum of x and n = number of readings.

The overall process of calculation the estimated standard deviation for a series of n measurements can be mathematically expressed in the following manner:

$$s = \sqrt{\frac{1}{n-1}\sum_{i=1}^{n}(x_i - \bar{x})^2} \tag{3.6}$$

where x_i is the result of the *i*th measurement and $\bar{x}$ is arithmetic mean of *n* results considered.

The stylus profiling measurements were made at several different positions on the surface to assess the stability of the roughness values (Vorburger et al., 1996). To enough sufficient statistics for the roughness measurement using the stylus method, 60 independent measurements were performed from 12 lines on surface roughness standard, and each line was measured five times to find the standard deviation of measurement (ISO 12179, 2000). The results of measurement measured by the stylus instrument 12 lines are illustrated in the table below. Table 3.2 is shown the raw experimental data of Ra at nominal value 3.2 μm.

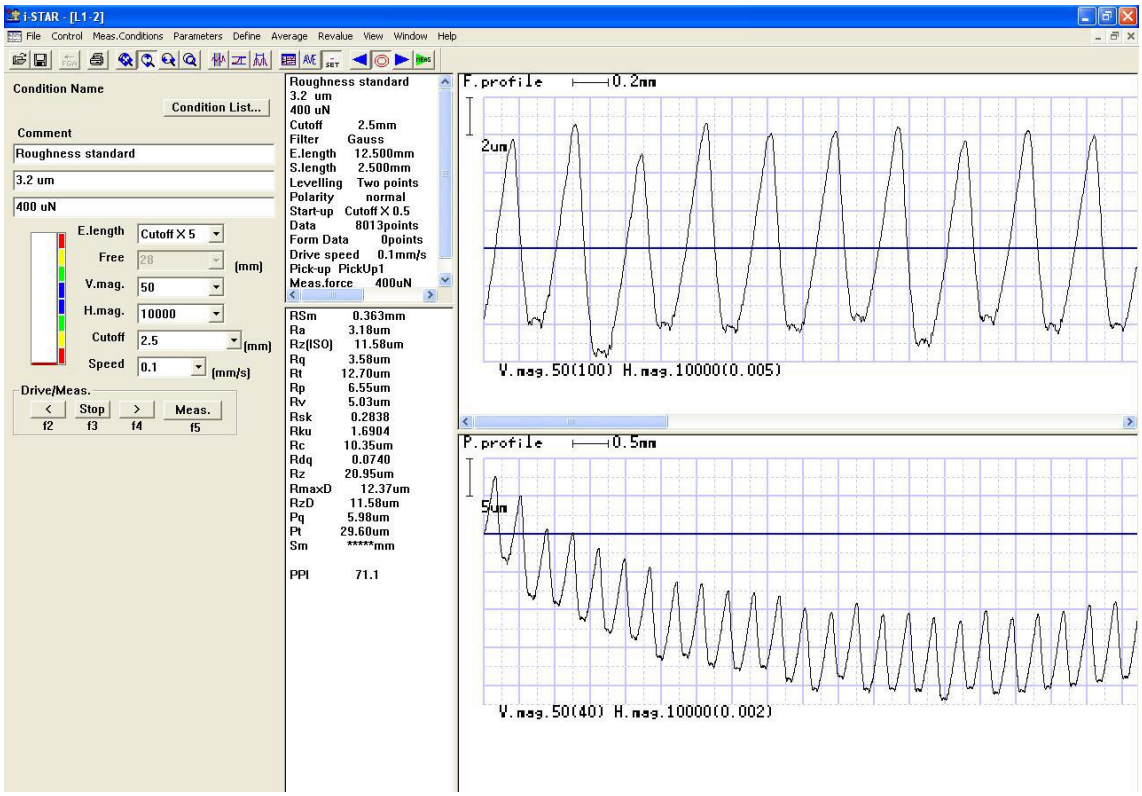

Figure 3.14 The Ra profile at 3.2 μm measured by the stylus instrument

Table 3.2 Ra value measured by the stylus instrument at 3.2 μm

Line Number	Ra value measured by the stylus instrument, (μm)					$\bar{x}$	S
	1	2	3	4	5	μm	μm
R_a Line 1	3.15	3.16	3.16	3.15	3.15	3.15	0.005
R_a Line 2	3.17	3.18	3.17	3.18	3.15	3.17	0.012
R_a Line 3	3.15	3.15	3.15	3.14	3.14	3.15	0.005
R_a Line 4	3.20	3.20	3.20	3.19	3.20	3.20	0.004
R_a Line 5	3.20	3.19	3.19	3.18	3.20	3.19	0.008
R_a Line 6	3.14	3.14	3.19	3.19	3.18	3.17	0.026
R_a Line 7	3.15	3.15	3.16	3.16	3.16	3.16	0.005
R_a Line 8	3.16	3.16	3.15	3.15	3.15	3.15	0.005
R_a Line 9	3.18	3.18	3.17	3.14	3.16	3.17	0.017
R_a Line 10	3.15	3.15	3.15	3.15	3.16	3.15	0.004
R_a Line 11	3.17	3.17	3.17	3.16	3.16	3.17	0.005
R_a Line 12	3.17	3.16	3.16	3.16	3.15	3.16	0.007

The nominal value of surface roughness standard is 3.2 μm. The mean of the measured value is evaluated by the sum of averaged values from lines 1 to 12 whose values are divided by the number of the line measured on the surface. The Ra's true value of surface roughness standard at 3.2 μm is 3.17 μm. Table 3.3 is shown the raw experimental data of Ra at nominal value 6.3 μm.

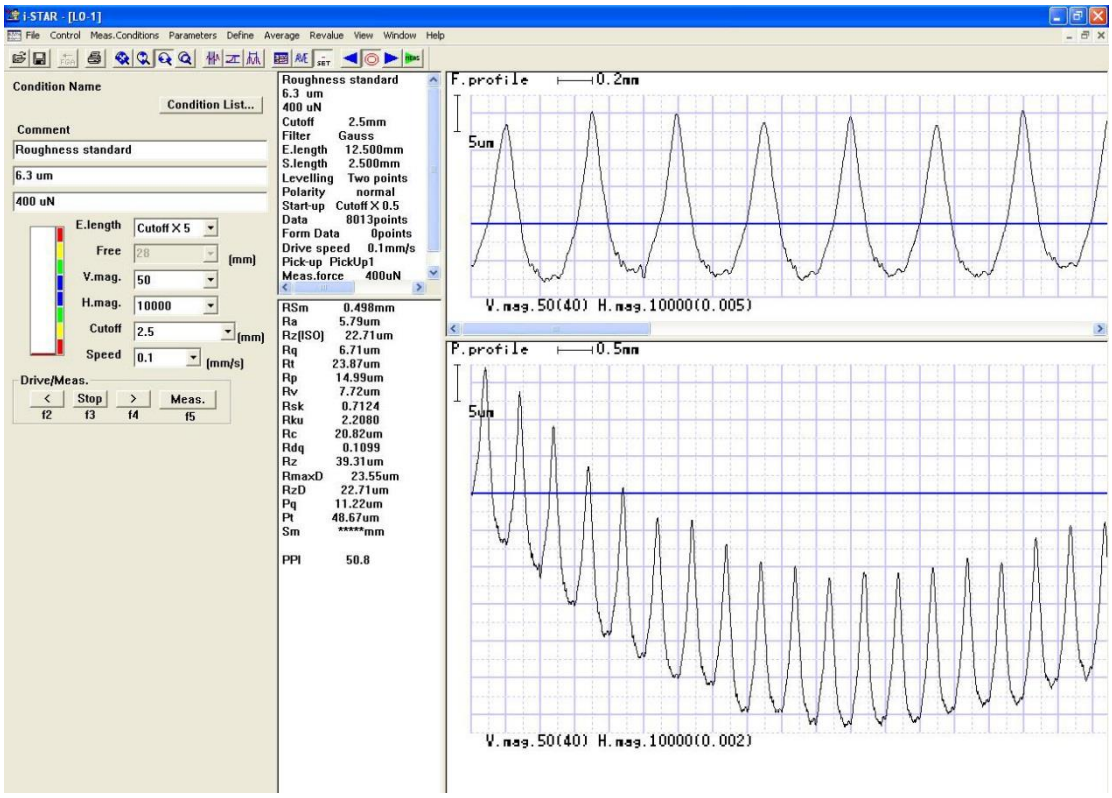

Figure 3.15 The Ra profile at 6.3 μm measured by the stylus instrument

Table 3.3 Ra value measured from the stylus instrument at 6.3 μm

Line Number	Ra value measured by the stylus instrument, (μm)					$\bar{x}$	S
	1	2	3	4	5	μm	μm
R_a Line 1	5.79	5.78	5.79	5.77	5.79	5.78	0.003
R_a Line 2	5.75	5.76	5.75	5.75	5.78	5.76	0.013
R_a Line 3	5.75	5.74	5.74	5.74	5.73	5.74	0.007
R_a Line 4	5.82	5.81	5.83	5.82	5.82	5.82	0.007
R_a Line 5	5.92	5.92	5.95	5.92	5.92	5.93	0.013
R_a Line 6	6.02	6.01	6.03	6.00	6.01	6.01	0.011
R_a Line 7	5.87	5.86	5.88	5.86	5.86	5.87	0.009
R_a Line 8	5.78	5.79	5.78	5.79	5.78	5.78	0.006
R_a Line 9	5.92	5.93	5.92	5.92	5.98	5.93	0.026
R_a Line 10	5.93	5.92	5.94	5.92	5.92	5.93	0.009
R_a Line 11	5.75	5.75	5.74	5.74	5.74	5.74	0.006
R_a Line 12	5.74	5.74	5.73	5.76	5.74	5.74	0.011

The nominal value of surface roughness standard is 6.3 μm. The mean of the measured value is evaluated by the sum of averaged values from lines 1 to 12 whose values are divided by the number of the line measured on the surface. The Ra's true value of surface roughness standard at 6.3 μm is 5.84 μm. Table 3.4 is shown the raw experimental data of Ra at nominal value 12.5 μm.

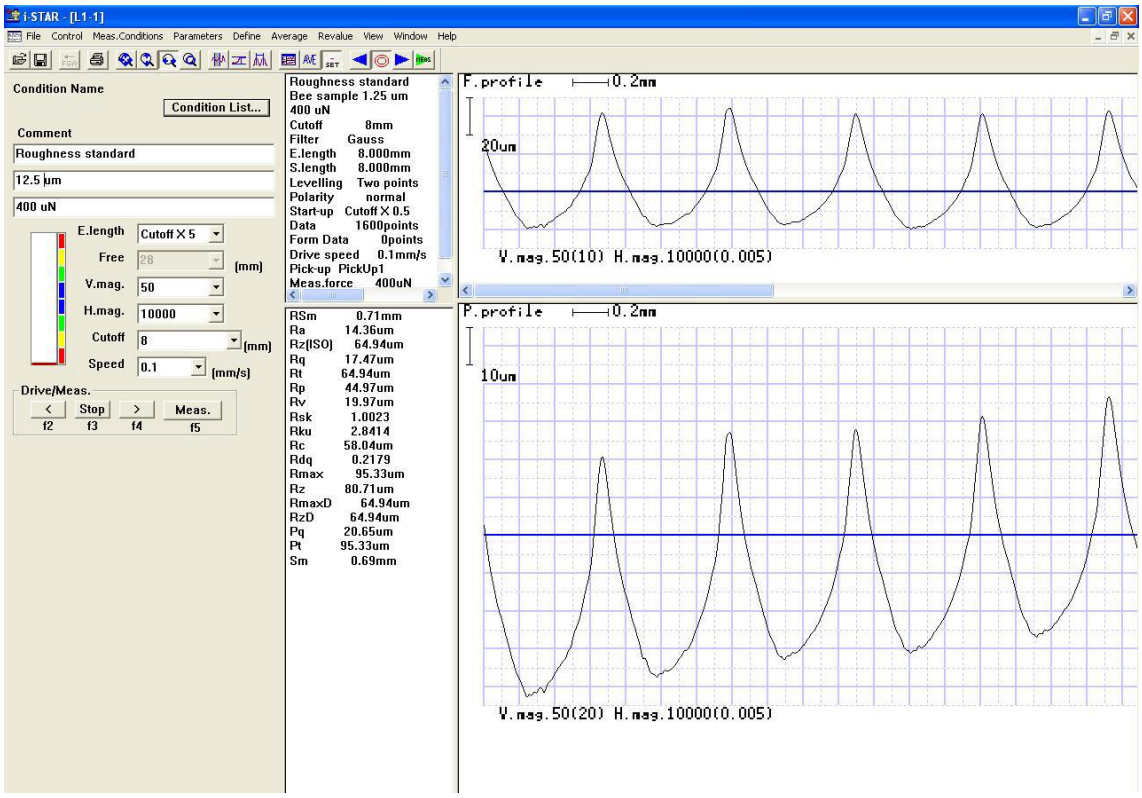

Figure 3.16 The Ra profile at 12.5 µm measured by the stylus instrument

Table 3.4 Ra value measured by the stylus instrument at 12.5 µm

Line Number	Ra value measured by the stylus instrument, (µm)					$\bar{x}$	S
	1	2	3	4	5	µm	µm
R_a Line 1	14.36	14.36	14.37	14.37	14.37	14.37	0.005
R_a Line 2	14.37	14.37	14.37	14.38	14.36	14.37	0.007
R_a Line 3	14.38	14.38	14.37	14.33	14.33	14.36	0.026
R_a Line 4	14.36	14.36	14.36	14.36	14.37	14.36	0.004
R_a Line 5	14.36	14.35	14.36	14.35	14.35	14.35	0.005
R_a Line 6	14.36	14.36	14.36	14.36	14.37	14.36	0.004
R_a Line 7	14.37	14.38	14.36	14.36	14.36	14.37	0.009
R_a Line 8	14.36	14.36	14.36	14.36	14.38	14.36	0.009
R_a Line 9	14.35	14.35	14.36	14.36	14.36	14.36	0.005
R_a Line 10	14.35	14.37	14.37	14.38	14.37	14.37	0.011
R_a Line 11	14.35	14.36	14.36	14.36	14.37	14.36	0.007
R_a Line 12	14.36	14.37	14.36	14.36	14.38	14.37	0.009

The nominal value of surface roughness standard is 12.5 μm. The mean of the measured value is evaluated by the sum of averaged values from lines 1 to 12 whose values are divided by the number of the line measured on the surface. The Ra's true value of surface roughness standard at 12.5 μm is 14.36 μm. Table 3.5 is shown the raw experimental data of Ra nominal value at 25 μm

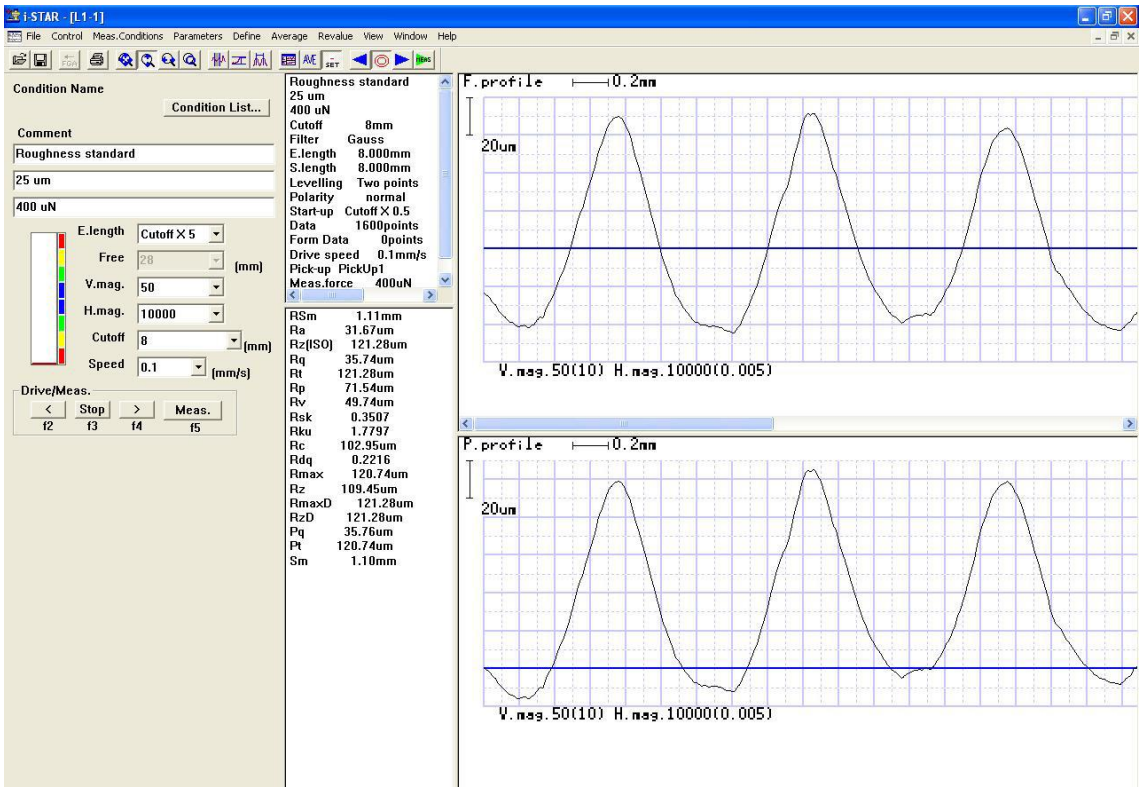

Figure 3.17 The Ra profile at 25 μm measured by the stylus instrument

Table 3.5 Ra value measured by the stylus instrument at 25 μm

Line Number	Ra value measured from the stylus instrument, (μm)					$\bar{x}$	S
	1	2	3	4	5	μm	μm
R_a Line 1	31.74	31.74	31.76	31.78	31.74	31.75	0.018
R_a Line 2	31.67	31.67	31.65	31.66	31.67	31.66	0.009
R_a Line 3	31.67	31.67	31.67	31.67	31.66	31.67	0.004
R_a Line 4	31.77	31.75	31.77	31.76	31.74	31.76	0.013
R_a Line 5	31.46	31.58	31.58	31.49	31.48	31.52	0.058
R_a Line 6	31.66	31.68	31.60	31.60	31.60	31.63	0.039
R_a Line 7	31.65	31.68	31.64	31.64	31.63	31.65	0.019
R_a Line 8	31.67	31.60	31.66	31.69	31.68	31.66	0.035
R_a Line 9	31.74	31.75	31.78	31.71	31.69	31.73	0.035
R_a Line 10	31.67	31.67	31.67	31.68	31.69	31.68	0.009
R_a Line 11	31.67	31.67	31.67	31.68	31.69	31.68	0.009
R_a Line 12	31.65	31.66	31.65	31.71	31.69	31.67	0.027

The nominal value of surface roughness standard is 25 μm. The mean of the measured value is evaluated by the sum of averaged values from lines 1 to 12 whose values are divided by the number of the line measured on the surface. The Ra's true value of surface roughness standard at 25 μm is 31.67 μm. Table 3.6 is shown the raw experimental data of Ra nominal value at 50 μm

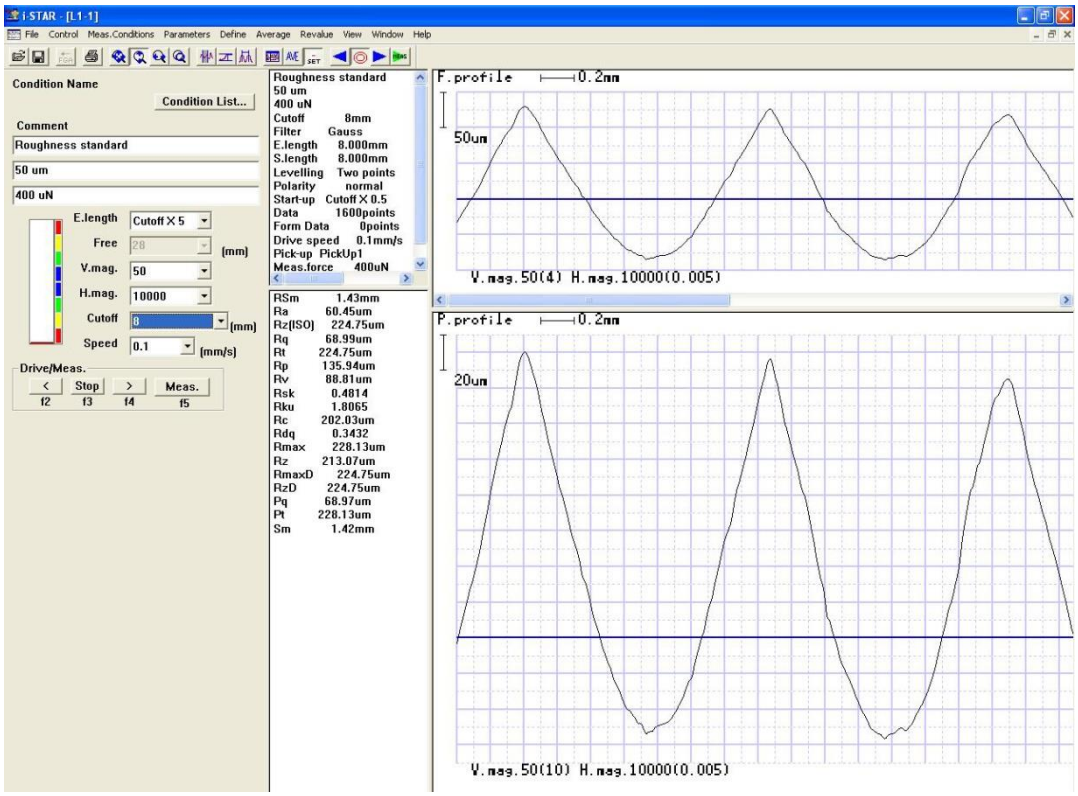

Figure 3.18 The Ra profile at 50 μm was measured by the stylus instrument

Table 3.6 Ra value measured by the stylus instrument at 50 μm

Line Number	Ra value measured by the stylus instrument, (μm)					$\bar{x}$	S
	1	2	3	4	5	μm	μm
R_a Line 1	60.45	60.45	60.40	60.41	60.42	60.43	0.023
R_a Line 2	60.45	60.45	60.45	60.43	60.42	60.44	0.014
R_a Line 3	60.45	60.45	60.41	60.42	60.41	60.43	0.020
R_a Line 4	60.36	60.39	60.33	60.33	60.36	60.35	0.025
R_a Line 5	60.30	60.28	60.42	60.58	60.57	60.43	0.143
R_a Line 6	60.61	60.61	60.57	60.57	60.58	60.59	0.020
R_a Line 7	60.61	60.61	60.58	60.57	60.56	60.59	0.023
R_a Line 8	60.61	60.60	60.57	60.58	60.57	60.59	0.018
R_a Line 9	60.27	60.27	60.33	60.45	60.44	60.35	0.088
R_a Line 10	60.45	60.27	60.28	60.44	60.28	60.34	0.092
R_a Line 11	60.45	60.45	60.47	60.48	60.45	60.46	0.014
R_a Line 12	60.27	60.29	60.28	60.45	60.45	60.35	0.093

The nominal value of surface roughness standard is 50 μm. The mean of the measured value is evaluated by the sum of averaged values from lines 1 to 12 whose value are divided by the number of the line measured on the surface. The Ra's true value of surface roughness standard at 50 μm is 60.45 μm.

3.6 Conclusion

In this experimental study, the aim was to calibrate the surface roughness standards and establish the references for surface roughness measurement. The calibration process was performed using automatic measuring process on stylus instrument. The five different surface roughness standards, which included R_a at 3.2, 6.3, 12.5, 25 and 50 μm, were measured in order to calculate the average of measurement values. Regarded to calibration process, each area of surface roughness standard such as at 3.2 μm was divided into 12 lines (for example R_a Line 1….. Line 12) and measured five times per line ,and then the average value was calculated and applied as the references for surface roughness measurement, as shown in Figure 3.19.

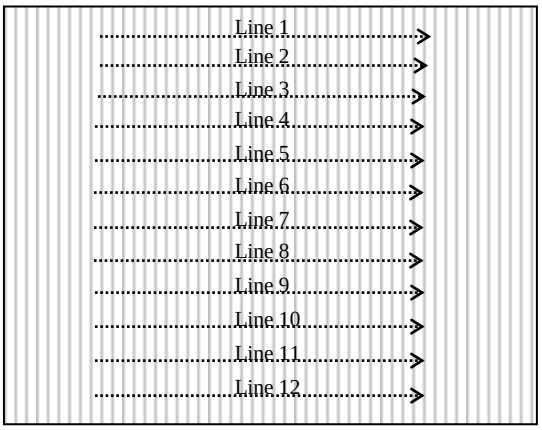

Figure 3.19 Measurement position of surface roughness standard

The measurement results were summarised in Table 3.7.

Table 3.7 The measurement results from surface roughness standards measured by the stylus instrument

Nominal value (μm)	Average (μm)	Standard deviation
3.2	3.17	0.016
6.3	5.84	0.094
12.5	14.36	0.065
25	31.67	0.062
50	60.44	0.096

As shown in Table 3.7, the nominal value is the expressed value that is stated on the specimen, originated from the manufacturer. The average values of these measurements showed slightly different from the values given by the manufacturer. The results of standard deviation were less than 0.1 and would be implied that the specimen presented a highly homogeneous material and the stylus instrument was the high-efficiency instrumentation. All R_a values on the surface roughness standards measured by the stylus instrument will be exploited to be reference values in the next chapter.

Chapter 4 Surface roughness measurement using photometric stereo method with coordinate measuring machine

4.1 Introduction

Computer vision has been extremely popular in measurement systems. The quality of the components produced is a major concern in industrial manufacturing, and it is closely related to dimensional accuracy, form and surface finish. Surface topography, especially surface roughness, plays an essential role in determining the functional performance of machine parts. The measurement of engineering surface roughness is becoming increasingly important. Several methods are utilized to determine surface information by measuring parameters calculated from images of the illuminated objects. This chapter focuses on the photometric stereo approach as applied for average roughness measurement. The method of recovery of the normal vector and the reflectance properties for every point of the surface, which is described in depth, is discussed in detail with regard to the 3-source photometric stereo technique. The five values of surface roughness standards measured by the stylus instrument in Chapter 3 were utilized as reference values for the PS system. The scenes captured by the camera were reconstructed by least square method to obtain the surface normal from the surface topography. The tangent plane method was utilized for recovering surface depths. Their surface profiles after recovery include form, waviness and roughness profiles. A Gaussian filter was used to separate them in order to acquire actual roughness profiles.

4.2 Operating principle

4.2.1 The reflectance model

Intensity values are known from image sets that record a reflected radiance from the illuminated objects. There are many contributing factors relating to the reflected radiance when the incident light has constant direction and intensity, e.g. the physical properties and shape of the measured object. If the surfaces are rough enough so that all incident light beams are diffusively reflected in all directions, these surfaces are called Lambertian surfaces (Woodham, 1989). According to the Lambertian reflectance surface (Woodham, 1989), this intensity is given by

$$i = \rho k \cos(\theta_i) \tag{4.1}$$

where i is the emittance (reflected power per unit area) from the surface, ρ is the albedo representing the amount of light reflected back from the surface, the intensity of light source is represented by *k* (incident power per unit area) and the angle between the light vector and the surface normal is represented by θ_i.

4.2.2 Photometric stereo (PS)

The PS method was firstly proposed by Woodham in 1980. This method calculates local the surface reflection and orientation through the location of an incident light source, with several images taken from a constant viewing direction (Smith, 1999; Woodham, 1989). The basic idea of the PS method is to solve equation 4.2 for the unknown surface normal.

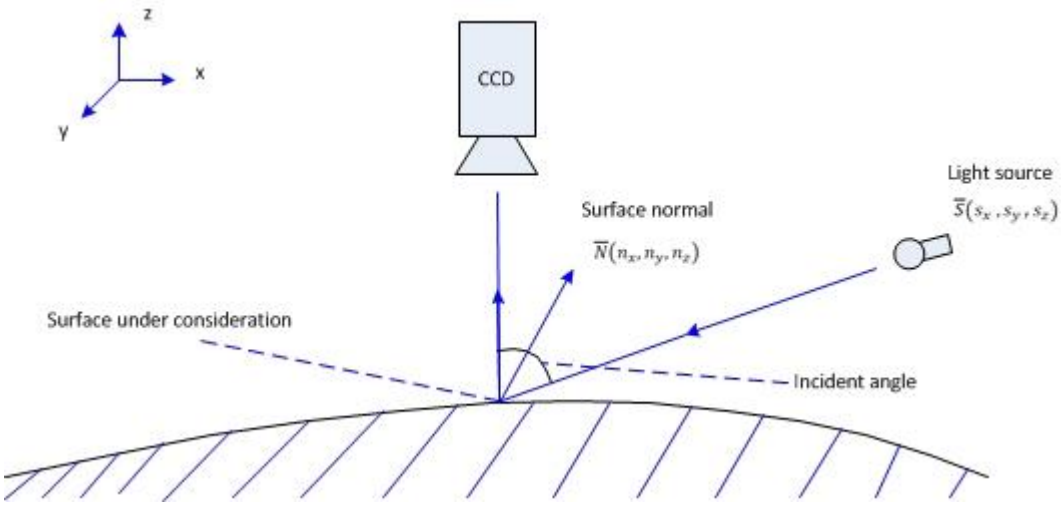

Figure 4.1 Photometric stereo system

When three images with the same view are taken under different lighting directions, three reflectance maps are provided to solve a linear system of three unknown surface normals (n_x, n_y, n_Z). The cosine of the incident angle can also be denoted as a dot product, as shown in Eq. (4.2), where $\overrightarrow{S}$ represents the unit vector of light source direction and the unit vector $\vec{N}$ represents the surface normal

$$\vec{I} = \rho(\vec{S} \cdot \vec{N}) \tag{4.2}$$

In the case of three images being utilized by the measurement system,

$$\begin{bmatrix} I_1 \\ I_2 \\ I_3 \end{bmatrix} = \rho \begin{bmatrix} s_{1x} & s_{1y} & s_{1z} \\ s_{2x} & s_{2y} & s_{2z} \\ s_{3x} & s_{3y} & s_{3z} \end{bmatrix} \begin{bmatrix} n_x \\ n_y \\ n_z \end{bmatrix} \quad (4.3)$$

In equation 4.3, (I_1, I_2, I_3) represent the image intensity values at image location (*x*, *y*). The unknown surface albedo is denoted by ρ. The unknown components of the surface normal are represented by (n_x, n_y, n_Z), and (s_x, s_y, s_Z) are the known components of the light source vector, where numbers 1, 2 and 3 indicate light direction. To solve the unknown surface reflectance factor and surface normal, the following relation has been used

$$\vec{I}(x,y) = \rho(x,y)[S]\vec{N}(x,y) \quad (4.4)$$

To determine the surface normal (*N*) in equation 4.4, the following relation can be utilized from equation 4.5, where the lighting directions, *S*, must not be coplanar to a plane.

$$\vec{N}(x,y) = \frac{1}{\rho(x,y)}[S]^{-1}\vec{I}(x,y) \quad (4.5)$$

The least squares technique can be utilized to calculate pseudo-inverse and local surface gradients $p(x,y)$ and $q(x,y)$. The local surface normal $\vec{N}(x,y)$ can also be calculated from the pseudo-inverse using equation 4.6 to 4.8 where $\vec{M}(x,y) = [m_1(x,y), m_2(x,y), m_3(x,y)]^T$

$$\vec{M}(x,y) = \rho(x,y)\vec{N}(x,y) = ([S]^T[S])^{-1}[S]^T\vec{I}(x,y) \quad (4.6)$$

$$p(x,y) = \frac{-m_1(x,y)}{m_3(x,y)}, q(x,y) = \frac{-m_2(x,y)}{m_3(x,y)} \quad (4.7)$$

$$\vec{N}(x,y) = \frac{[-p(x,y), -q(x,y), 1]^T}{\sqrt{p(x,y)^2 + q(x,y)^2 + 1}} \quad (4.8)$$

$$\rho(x,y) = \sqrt{m_1^2(x,y) + m_2^2(x,y) + m_3^2(x,y)} \quad (4.9)$$

Note that because all three simultaneous in equation 4.3 are required, the lighting positions will determine the available range of recoverable surface orientation. In other words, the observed surface must be illuminated by all three light sources (Smith, 1999).

4.3 System designs

Figure 4.2 illustrates the PS system setting up on the CMM for surface roughness measurement. The roughness standard was mounted on the centre of the measuring table. The light source was assumed to be a point source with a constant incident illumination over the measured object. When images were captured from the system, the external lighting source was controlled. The measurements were performed in a dark room to avoid the effects of the ambient light.

Figure 4.2 The PS system on the CMM for measuring surface texture

4.3.1 Light source position estimation

The general assumption that the light vector is the same at every point (pixel) is mostly not true in practice. The first step for calculating a normal map is to calibrate the light source. A hemisphere is utilized to evaluate the light vector at several different locations in the image area whereby the brightest spot of each picture is used to identify the direction of the light source (Ahmad, et al., 2014).

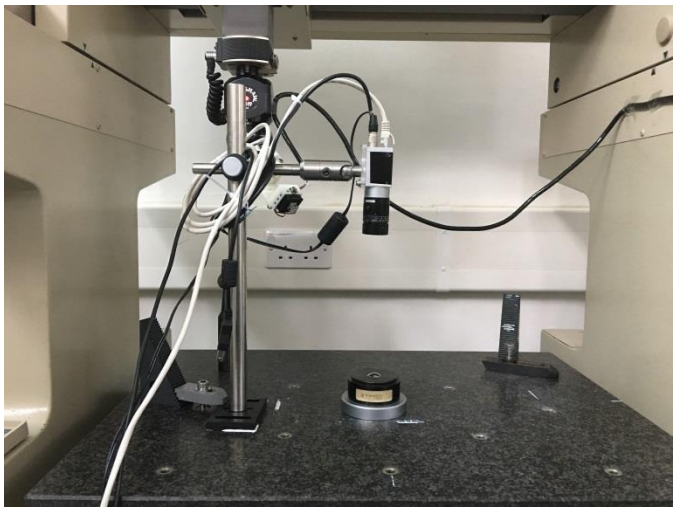

Figure 4.3 Calibration setup for light position calculation

The light source is moved around the hemisphere in order to calculate the light directions as shown in Figure 4.3.

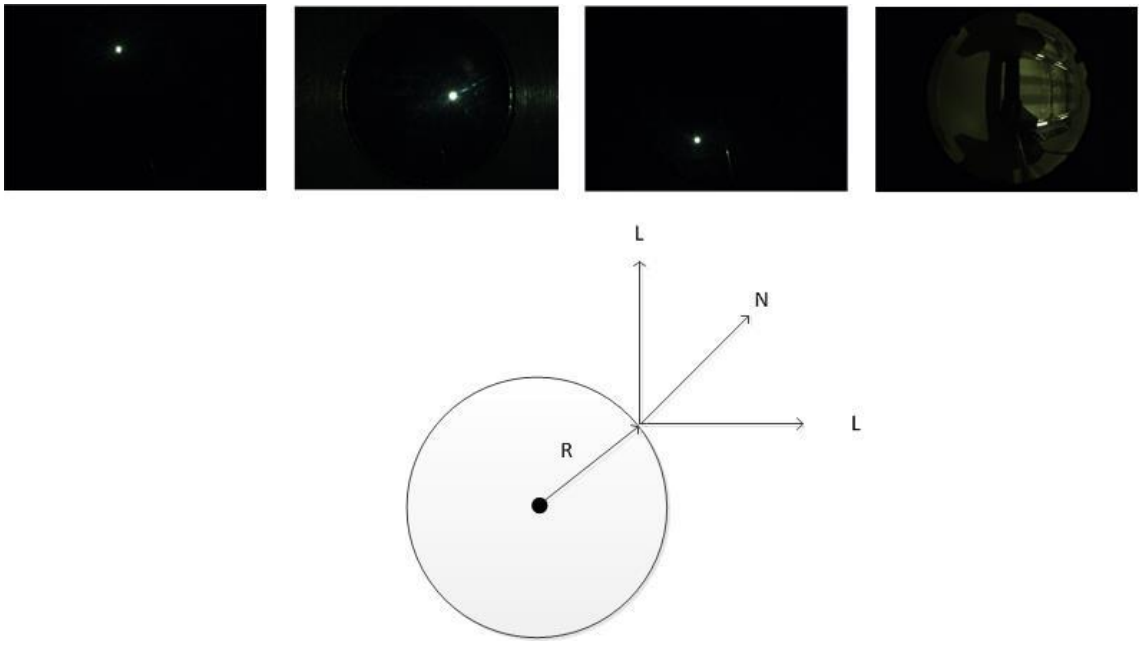

Figure 4.4 The method for finding light direction

The position of the light sources is known by the location of the brightest points of each picture on the hemisphere images. In order to calculate light vectors (L), equation (4.10) is used:

$$L = 2(N \cdot R)N - R \tag{4.10}$$

-where R is the reflection direction taken as [0,0,1], N is the unit surface normal, N = (N_x,N_y,N_z), N_x = P_x-C_x, Ny = P_y-C_y and N_z = $\sqrt{\left(R^2 - N_x^2 - N_y^2\right)}$. The location of the brightest point on the sphere image is at [P_x, P_y] and [C_x , C_y] is the pixel coordinates of the sphere centre. The radius of the hemisphere in the image plane is represented by R. When the light vectors are known, the next step of the experiment is to find the optimal placement of the illumination for three image photometric stereo acquisitions of surface textures (Spence and Chantler, 2003). In the research, the optimal slant and tilt angles are investigated by the precise movement of the CMM to obtain the suitable angles for recovery image topography. Spence and Chantler (2006) worked with three lights of equal slant, and using numerical optimisation, they concluded that the normals are best recovered when the light sources are 120^o apart at a slant of 55^o. This corresponds to orthogonal light directions and is in full agreement with the results derived from the theory presented here.

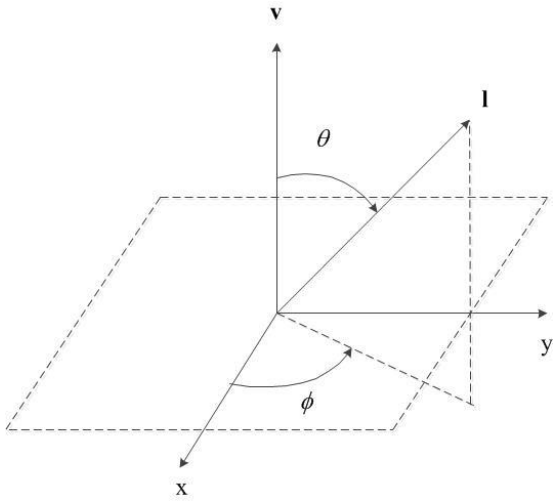

Figure 4.5 Slant and tilt angles of a light source

In Figure 4.5, the angle between the light source (**l**) and the viewing vector (**v**) is the slant angle (θ). The tilt (ϕ) is the angle between the projection of **l** onto the viewing xy plane and the x-axis. In this experiment, the slant angles (θ) were investigated at 30^o, 37.5^o, 45^o and 52.5^o to find the optimum angle for measuring the surface roughness

standard. The slant angle was held constant whilst the tilt angle was swept through a complete rotation in 120^{o} intervals. Three images were captured at 120^{o} intervals over a complete rotation at each of the three slant angles.

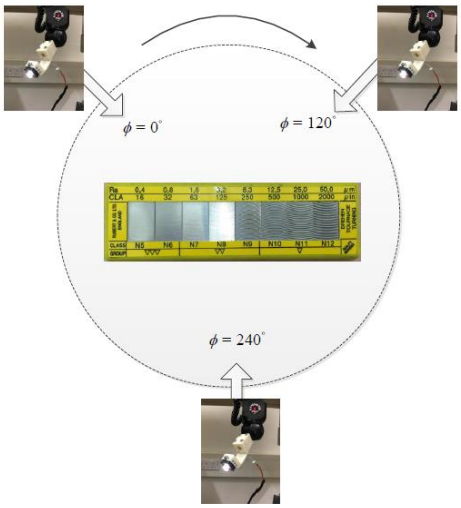

Figure 4.6 Illumination conditions for the tilt angle experiments

The hemisphere used to find the light vectors of the PS system was positioned in the centre of CMM. The angle of light was moveable via the movement of the CMM to find the suitable tilt and slant angles. In terms of tilt angles, the samples were illuminated at angles of 0^{o}, 120^{o}, and 240^{o}. The light source attached to the CMM's probe was sequentially shifted along the tilt angles every 120° around the hemisphere, which used slant angles of 30^{o}, 37.5^{o}, 45^{o} and 52.5^{o} respectively from each cycle of tilt angles, to find the best direction of the light source to recover surface roughness standard profiles.

4.3.2 Light source

A neutral white LED was used as the light source as shown in Figure 4.7. It is properly designed for industrial lighting and provides high illumination intensity of 230 lumens at a 700 mA driver. A narrow beam (17.7^{o}) optical lens was used for increasing the efficiency of the light source. A 3D printing machine was used to create lightweight parts for the installation of the light source with CMM's probe.

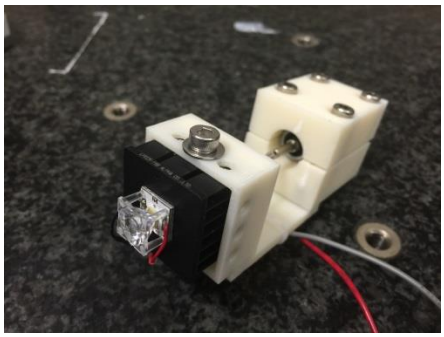

Figure 4.7 Light source

4.3.3 The PS setup and image acquisition

A digital gigabit ethernet camera with a 25× optical zoom lens was utilized to capture pictures from the PS system. The resolution of the acquired images is 659×494 pixels, with the pixel size of 7.4 μm×7.4 μm. All of the images were directly captured by using a gigabit ethernet interface, being the high speed port of the camera. The system was concisely designed for running our system by using a laptop. The light source and captured images were controlled by the Arduino board and LabVIEW software as shown in Figure 4.8.

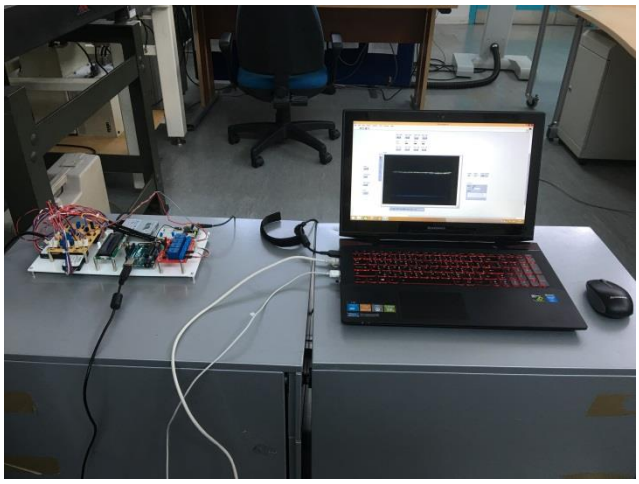

Figure 4.8 Arduino board and LabVIEW software

For our experiment, when the three images are sequentially taken to create a 3D profile from the PS system for the evaluation of surface roughness, a pixel size needs to be

changed for the length measurement. A working standard glass was used to modify the pixel size to be millimetre. The PS method for measuring surface texture can be presented as a block diagram, as shown in Figure 4.9.

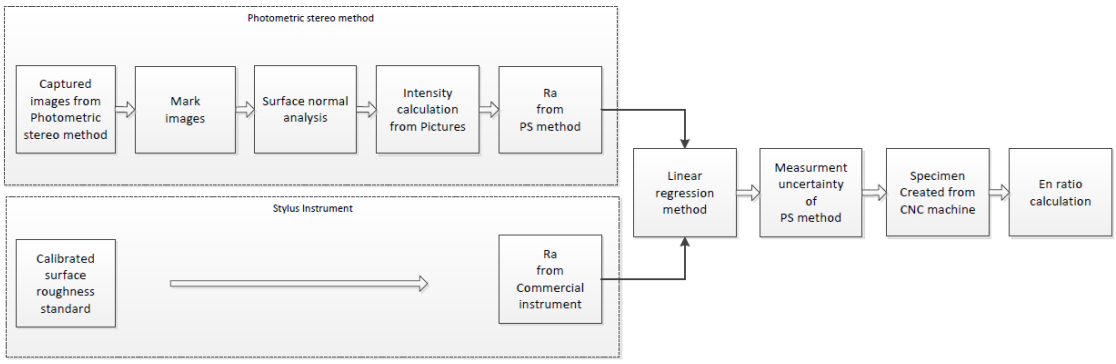

Figure 4.9 Measurement Strategy

The block diagram shows the steps of the measurement method. The light source is used to create a stable and well-controlled illumination condition. The images with a size of 512 × 320 pixels are captured from the camera with a 25× optical zoom lens. Each tilt angle is precisely positioned by the CMM's movement. In marking images, the area of interest is selected by Matlab programming. The gradient space plots are generated and analysed for all standard surface roughness. The surface normals are calculated by the least squares technique. Accurate surface reconstruction can then be achieved. Twelve profiles from the measured surfaces are then chosen for surface normal calculation and compared with the roughness standards. The surface roughness standards are calibrated by the stylus instrument to confirm the true values and to acquire the value of the measurement uncertainties. The linear regression method is utilized to find the best slant angle of the standard surface roughness determined by the PS method. The sources of measurement uncertainties of the PS method have been methodically evaluated in accordance with GUM (1993). The roughness specimen manufactured from the CNC machine is exploited to confirm the efficiency of our proposed method.

4.3.4 Surface roughness standard recovery system

The raw images of surface roughness standards at 3.2, 6.3, 12.5, 25, and 50 μm under three light directions taken from the PS system at each slant angles are shown in Figure 4.10, 4.11, 4.12, 4.13 and 4.14.

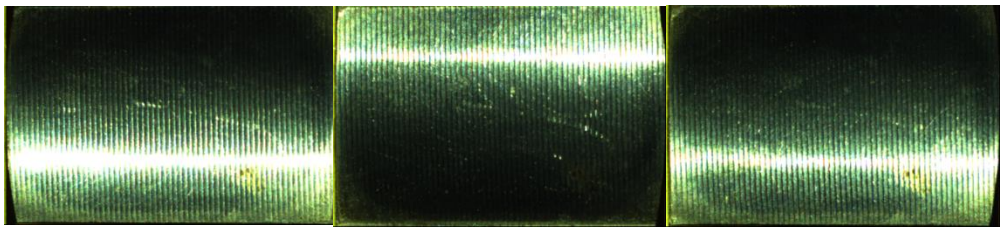

a – 0^o **b – 120^o** **c – 240^o**

Figure 4.10 Three images of roughness standard 3.2 μm illuminated from each tilt angle

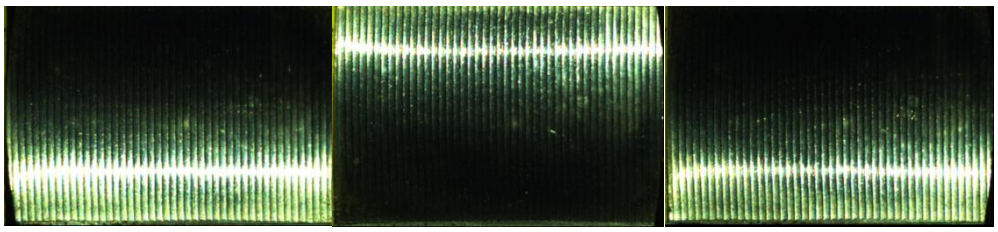

a – 0^o **b – 120^o** **c – 240^o**

Figure 4.11 Three images of roughness standard 6.3 μm illuminated from each tilt angle

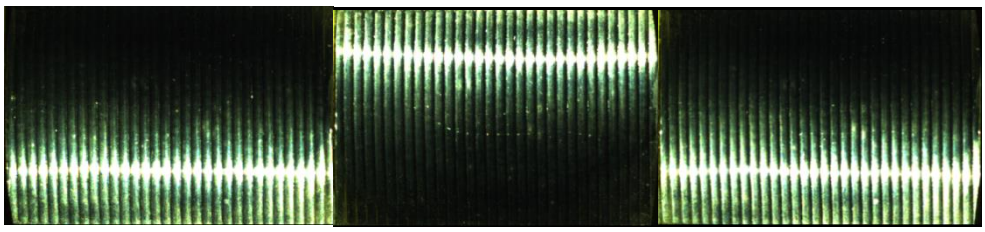

a – 0^o **b – 120^o** **c – 240^o**

Figure 4.12 Three images of roughness standard 12.5 μm illuminated from each tilt angle

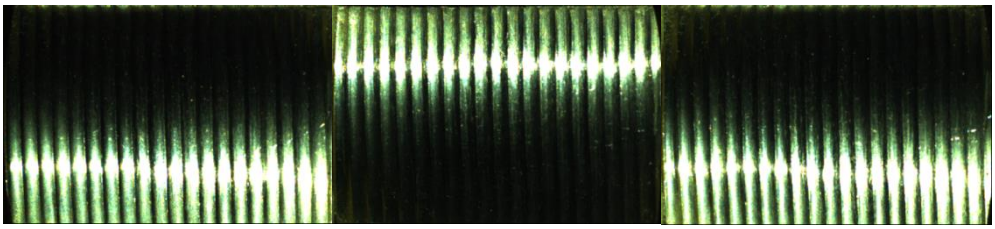

a – 0^o **b – 120^o** **c – 240^o**

Figure 4.13 Three images of roughness standard 25 μm illuminated from each tilt angle

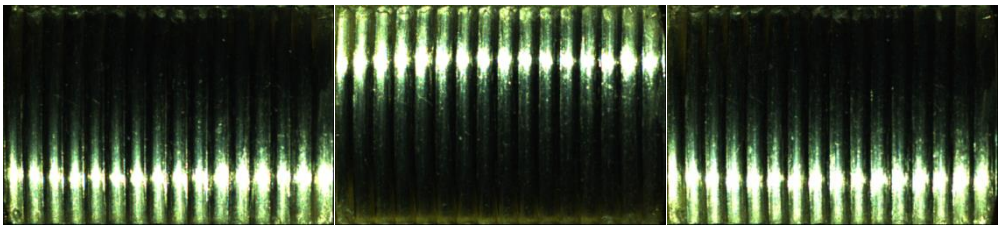

a – 0^o **b – 120^o** **c – 240^o**

Figure 4.14 Three images of roughness standard 50 μm illuminated from each tilt angle

The measuring area is manually selected by MATLAB software, as illustrated in Figure 4.15. The sample profiles were captured with its centre aligned with the camera's optical axis. Each image acquired from the camera covers an area of specimen of 300 × 30 pixels.

Figure 4.15 Marked image's area at 300 × 30 pixels

The scenes captured by the PS system are analysed by the least square method to extract the surface normals of points in the surface roughness standard. A tangent plane method is utilized to calculate its surface heights. According to the tangent plane

theorem, the surface normal is perpendicular to the lines on the plane. Therefore, the vector product of normal and this line is zero (Lv, et al., 2012).

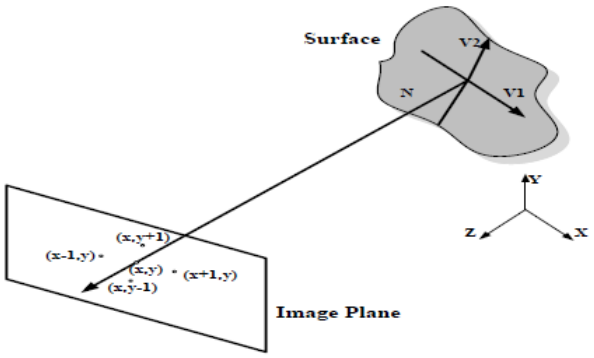

Figure 4.16 Tangent plane method

As shown in Figure 4.16, the vector V_1 composed of point (x,y) and (x+1,y) can be defined as follows:

$$V_1 = \left(1,0, z_{x+1} - z_{x,y}\right) \tag{4.11}$$

According to the tangent plane theorem, the correlation between *N* and V_1 is:

$$N \cdot V_1 = 0 \tag{4.12}$$

Then

$$\left(n_x, n_y, n_z\right) \cdot \left(1,0, z_{x+1,y} - z_{x,y}\right)^T = 0 \tag{4.13}$$

Therefore

$$-n_z z_{x,y} + n_z z_{x+1,y} = -n_x \tag{4.14}$$

The correlation between *N* and V_2, which starts from (x,y) to (x,y+1), can be found in a similar way as shown:

$$-n_z z_{x,y} + n_z z_{,y+1} = -n_y \tag{4.15}$$

Two constraint equations, which include equation 4.14 and 4.15, are therefore created for each point. However, taking account of the boundary condition of images, point (x-1,y) or (x,y-1) is used to produce the constraint equation defined as follows:

$$n_z z_{x-1,y} + -n_z z_{x,y} = n_x \quad (4.16)$$

$$n_z z_{x,y-1} + -n_z z_{x,y} = n_y \quad (4.17)$$

As mentioned before, determining how to establish two constraint equations for each point is discussed. The formation of constraint equations of all the pixels in the scene is shown.

Table 4.1 A picture with 6×6 pixels

(1,1)	(1,2)	(1,3)	(1,4)	(1,5)	(1,6)
(2,1)	(2,2)	(2,3)	(2,4)	(2,5)	(2,6)
(3,1)	(3,2)	(3,3)	(3,4)	(3,5)	(3,6)
(4,1)	(4,2)	(4,3)	(4,4)	(4,5)	(4,6)
(5,1)	(5,2)	(5,3)	(5,4)	(5,5)	(5,6)
(6,1)	(6,2)	(6,3)	(6,4)	(6,5)	(6,6)

Table 4.1 is assumed to be a picture including 6×6 pixels. The picture is to be divided into four parts for discussion.

(1) For dealing with the pixels from (1,1) to (5,5), since pixels exist on the right and below, constraint equations are created based on equations (4.14) and (4.15).

$$-n_z z_{x,y} + n_z z_{x+1,y} = -n_x \quad (4.18)$$

$$-n_z z_{x,y} + n_z z_{x,y+1} = -n_y \quad (4.19)$$

(2) For dealing with the pixels from (6,1) to (6,5), since pixels exist on the right but not on the below, constraint equations are created based on equations (4.14) and (4.17).

$$-n_z z_{x,y} + n_z z_{x+1,y} = -n_x \quad (4.20)$$

$$n_z z_{x,y-1} + -n_z z_{x,y} = n_y \quad (4.21)$$

(3) For dealing with the pixels from (1,6) to (5,6), since pixels only exist on the below but not on the below, constraint equations are created based on equations (4.15) and (4.16).

$$n_z z_{x-1,y} + -n_z z_{x,y} = n_x \quad (4.22)$$

$$-n_z z_{x,y} + n_z z_{,y+1} = -n_y \quad (4.23)$$

(4) For dealing with the pixels from (6, 6), since pixels do not exist on the right and below, constraint equations are created based on equations (4.16) and (4.17).

$$n_z z_{x-1,y} + -n_z z_{x,y} = n_x \quad (4.24)$$

$$n_z z_{x,y-1} + -n_z z_{x,y} = n_y \quad (4.25)$$

Therefore, based on equations (4.14), (4.15), (4.16) and (4.17), the constraint equation for all the pixels in the picture is applied to recover the surface heights.

The 3D topography of overall surface roughness standard is shown in Figure 4.17, 4.18, 4.19, 4.20 and 4.21. These profiles are reconstructed by 3-source photometric stereo technique for using Matlab2012b.

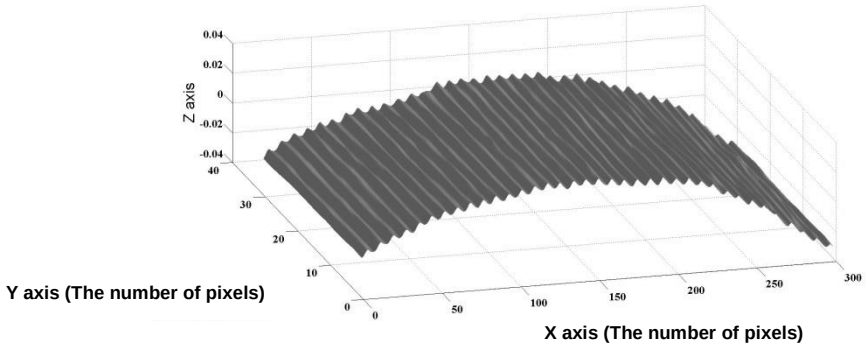

Figure 4.17 The 3D roughness standard surface at 3.2 μm determined by the PS method

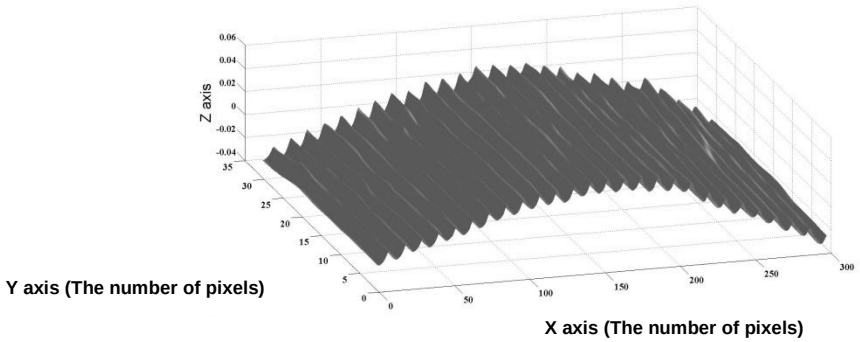

Figure 4.18 The 3D roughness standard surface at 6.3 μm determined by the PS method

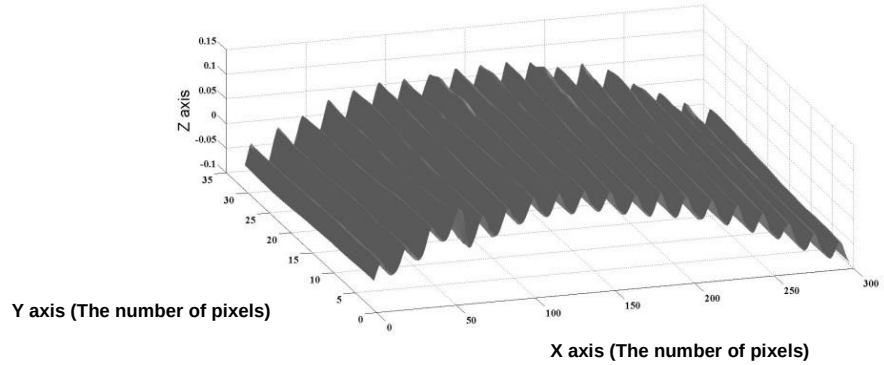

Figure 4.19 The 3D roughness standard surface at 12.5 μm determined by the PS method

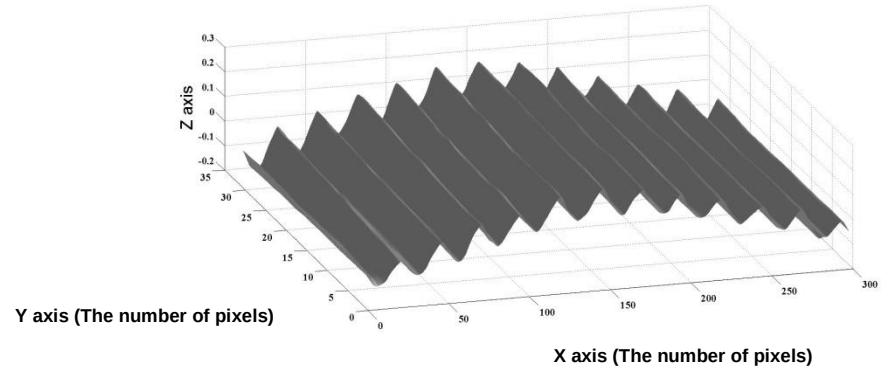

Figure 4.20 The 3D roughness standard surface at 25 μm determined by the PS method

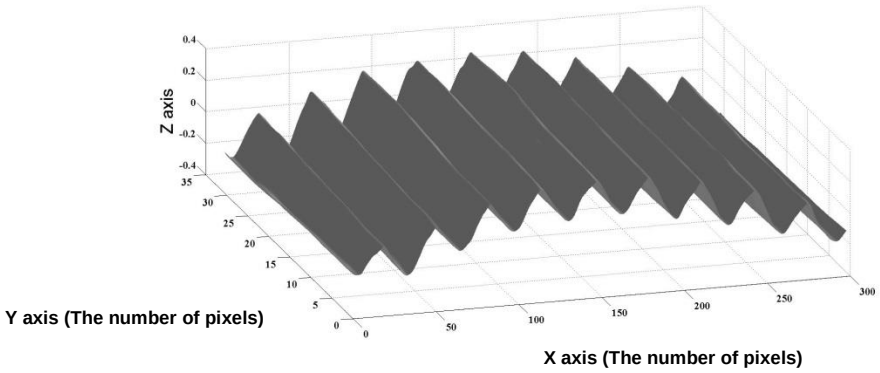

Figure 4.21 The 3D roughness standard surface at 50 μm determined by the PS method

The x and y axes from all figures are indicated as the number of pixels. The method used to convert those pixels into length measurement (mm) is to compare them with a working standard scale. The working standard scale is a special ruler produced from low expansion glass as shown in Figure 4.22.

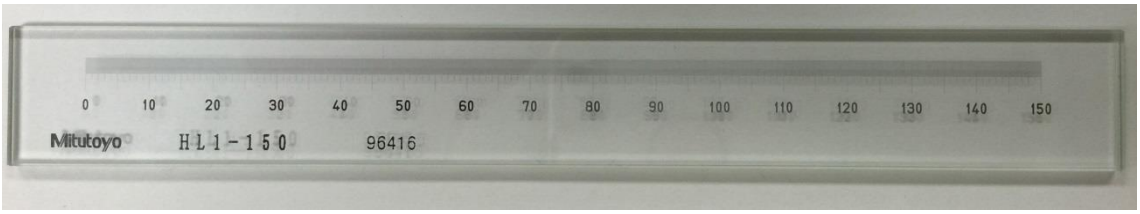

Figure 4.22 Working standard scale

It has generally been used for checking the magnification accuracy of profile projectors and microscopes, and the table feeding accuracy of measuring equipment. In this research, it was utilized to verify the conversion of the pixels to a length measurement.

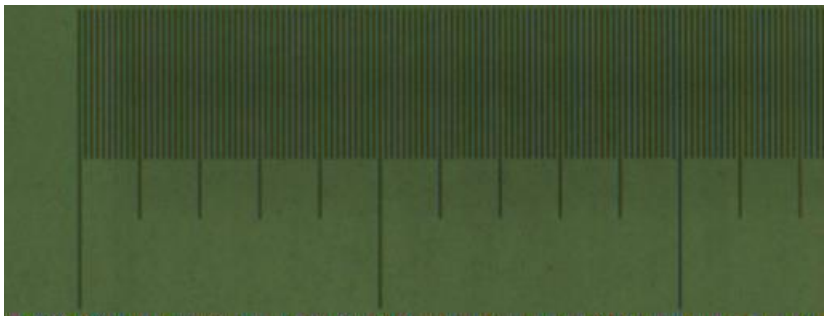

Figure 4.23 The scale on the working standard scale

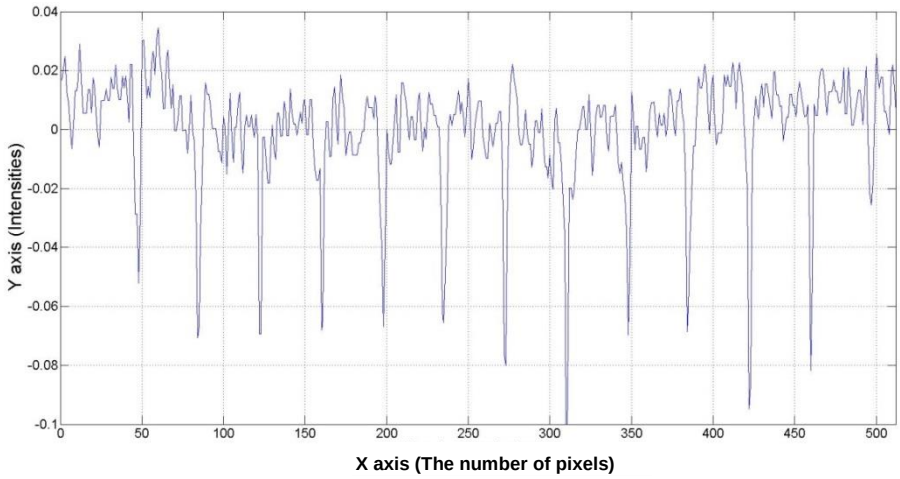

Figure 4.24 The pixel size was calibrated by a working standard scale

Figure 4.23 is the scene captured from the camera to have a scene size of 520×320 pixels. It is performed to change the length measurement at 10 mm to the number of pixels as shown in Figure 4.24. By using MATLAB software, measuring the length at 10 mm is precisely exchanged to be the number of pixels, as shown in Table 4.2.

Table 4.2 The results of pixels calibration

Measuring length (mm)	The number of pixels					Average of the number of pixels
	1	2	3	4	5	
10	376	376	376	376	376	376

By using equation (4.25), the result obtained for 1 pixel is equal to 0. 026 mm.

$$1 \text{ pixel} = (10\ mm)/(376\ pixels) \quad (4.25)$$

= 0.026 mm

As mentioned in Figure 4.17, 4.18, 4.19, 4.20, and 4.21, the area used to recover the surface roughness profiles is 300×30. To find the true length measurement, the x and y axes are multiplied by 0.026 mm, as shown in equation (4.26).

$$\text{Scene's x axis} = 300 \times 0.026 \text{ mm} \quad (4.26)$$

$$= 7.8 \text{ mm}$$

$$\text{Scene's y axis} = 30 \times 0.026 \text{ mm} \quad (4.27)$$

$$= 0.78 \text{ mm}$$

In terms of the z axis, the conversion to the length measurement (mm) is made by comparing it with the true results, which were measured using the stylus instrument from Chapter 3. It is described after filtering the surface roughness profiles.

4.4 Filtering

After the 3D surface roughness standards were reconstructed from the PS method, the profiles comprised form, roughness, and waviness. Form and waviness should be removed from profiles for surface roughness assessment.

The simple way to realize the engineering surface is a range of spatial frequencies that combine the sinusoidal functions of different amplitudes and wavelengths. High-frequency and small-wavelength sinusoidal functions are explained as a roughness profile, all medium-wavelength sinusoidal functions are interpreted as a waviness profile, and a form profile comprises all large-wavelength components (Raja, et al., 2002).

The fundamental of engineering surface is that the assessment of a datum line is in profiles measuring from an instrument. The precision of a datum line directly influences the evaluation of a surface parameter. The mean line is the reference line applied for surface assessment. The traditional methods for determining mean lines include the least squares method and the 2RC filter. However, there are disadvantages to the two approaches. The former method produces mean lines that influence the location of the sampling lengths on the surface profiles. They cannot assess continuous profiles from each cut-off length within the entire evaluation length. The latter method leads to

distortion of the true profile due to its nonlinear phase characteristic (Yuan, et al., 2000). The most widely used filter for surface profile analysis is a Gaussian filter, which is recognized as an optimal filter. It solved the problem of the non-linear phase of the 2RC, and it could be implemented digitally quite easily. In the assessment of surface roughness, the Gaussian low pass filter has been utilized as a datum line, as explained in both the American Standard (ASME B46.1, 2002) and the International Standards (ISO 16610-21, 2012; ISO 11562, 1996).

The conversion between each profile is decided by user-defined wavelength cut-offs as those profiles are certainly represented by wavelength bandwidths. The requirement of two cut-offs is used to separate each band properly; the first cut-off is for the lower band, and another cut-off is for the upper band.

In the actual measurements, the capability of measuring instrument to apply a filter on its roughness assessment can only be specified for one cut-off to define roughness and waviness. For instance, the small-scale stylus size is used to create the short-wavelength cut-off through mechanical filtering appropriately. A long-wavelength cut-off in accordance with the measured profile may be adequate to acquire roughness.

Roughness is mathematically described as a high frequency deviation from the ideal surface. To determine the roughness of a surface form and waviness must be separated from the raw measured data. In our research, the idea is to eliminate form and waviness profiles. The weighting function for the phase correct filter corresponding to the equation of the Gaussian density function would be utilized. The definition of the weighting function is explained in the International Standards (ISO 16610-61, 2015; ISO 16610-21, 2012). Its weight function is given by

$$h(x) = \frac{1}{\alpha\lambda_{co}} exp\left[-\pi\left(\frac{x}{\alpha\lambda_{co}}\right)^2\right] \tag{4.28}$$

where x is the distance from the centre (maximum) of the weighting function, λ_{co} is the cut-off wavelength and the constant α is given by

$$\alpha = \sqrt{\frac{In\,2}{\pi}} \tag{4.29}$$

The different weight function results would be varied with the cut-off wavelength. To obtain the transfer functions $H(\lambda)$ of the respective filter, a Fourier transformation of $h(x)$ is necessary. $H(\lambda)$ is given by:

$$H(\lambda) = \int_{-\infty}^{\infty} h(x)\, exp\left[-i\frac{2\pi}{\lambda}x\right] dx = exp\left[-\pi\left(\frac{\alpha\lambda_{co}}{\lambda}^2\right)\right] \quad (4.30)$$

By substituting α in equation (4.29) into equation (4.30), $H(\lambda)$ becomes:

$$H(\lambda) = \frac{1}{2}^{\left(\frac{\lambda_{co}}{\lambda}\right)^2} \quad (4.31)$$

According to the weight functions in Figure 4.26, the respective transfer functions are illustrated in Figure 4.27. They show the cut off wavelength at which damping starts. The Gaussian transfer function created from equation 4.28 is the typical characteristic of the long-wave component (mean line). In term of calculating the short-wave component, its transmission characteristic is obtained by 1 - $H(\lambda)$. The filtering is performed by convolving the surface roughness standard profile with equation 4.28, which is the most widely used algorithm for evaluating the Gaussian filtered mean line.

In the value of surface roughness standards at 3.2, 6.3, 12.5, 25, and 50 μm, the choice of the correct cut-off wavelength (λ_{co}) is crucial for a meaningful filtering. For surface profilers, a standard is described in the International Standards (ISO 4288, 1998).

The 'raw' data acquired from the PS technique for surface texture measurement is to contain a mixture of, in this case, the desired property of roughness, but also of waviness that results from the manufacturing process.

The method to determine the surface texture of surface roughness standards is comprised three characteristic lengths: sampling length, evaluation length and traverse length (ISO 4287:1997). The assessment or evaluation length – the scale over that a roughness measurement is made, and the traverse length that refers to the distance physically traversed in the course of an individual measurement (see Figure 4.25). The evaluation length can be an arbitrarily selected value, but conventionally it is set at a value corresponding to 5 sampling lengths. The traverse length is usually greater than both sampling and evaluation lengths. It is used to exclude filter edge effects from the measurement result (Smith, 2002). Table 4.3, the roughness sampling length (l_r) is the cut-off wavelength (λ_{co}) in equation (4.28).

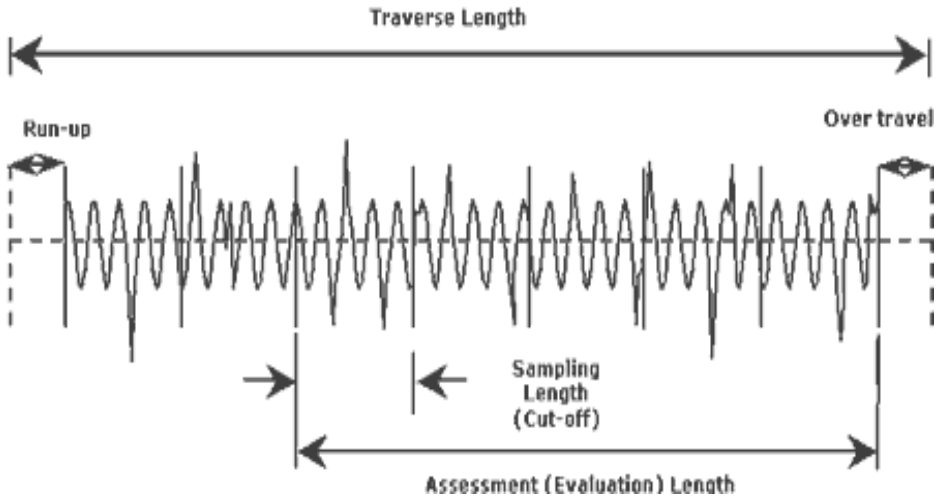

Figure 4.25 The method of assessment surface texture from characteristic lengths. Reproduced from Rapp Industrial Sales web site (http://www.rappindustrialsales.com/).

Table 4.3 Roughness sampling lengths for the measurement of *Ra*

R_a μm	Roughness Sampling length l_r mm	Roughness evaluation length l_n mm
$(0{,}006) < R_a \leq 0{,}02$	0,08	0,4
$(0{,}02) < R_a \leq 0{,}1$	0,25	1,25
$0{,}1 < R_a \leq 2$	0,8	4
$2 < R_a \leq 10$	2,5	12,5
$10 < R_a \leq 80$	8	40

In the experiment, sampling lengths at 2.5 and 8 mm are applied to separate the roughness profile, leaving form and waviness profiles. The convolution integral method is used as an algorithm for calculation of the Gaussian filtered mean line. It can be calculated by the number of pixels in each sampling length in the picture recovered

from the PS method divided by the sampling length from Table 4.3. The Gaussian filtered mean line in surface roughness standards at 3.2 and 6.3 μm is as follows:

$$= N/\lambda_{co} \quad (4.32)$$

$$= (300\ pixels)/(2.5\ mm)$$

$$= 120$$

and the Gaussian filtered mean line in surface roughness standards at 12.5, 25, 50 μm is as follows:

$$= N/\lambda_{co} \quad (4.33)$$

$$= (300\ pixels)/(8\ mm)$$

$$= 37.5$$

where λ_{co} is the cut-off wavelength, and N is the number of pixels in each sampling length in the picture recovered from the PS method; both numbers are used to establish the range of data from each surface roughness standard to be convolved with equation (4.28). The λ_{co} = 2.5 mm and λ_{co} = 8 mm are then created as Gaussian density functions, as illustrated in Figure 4.26.

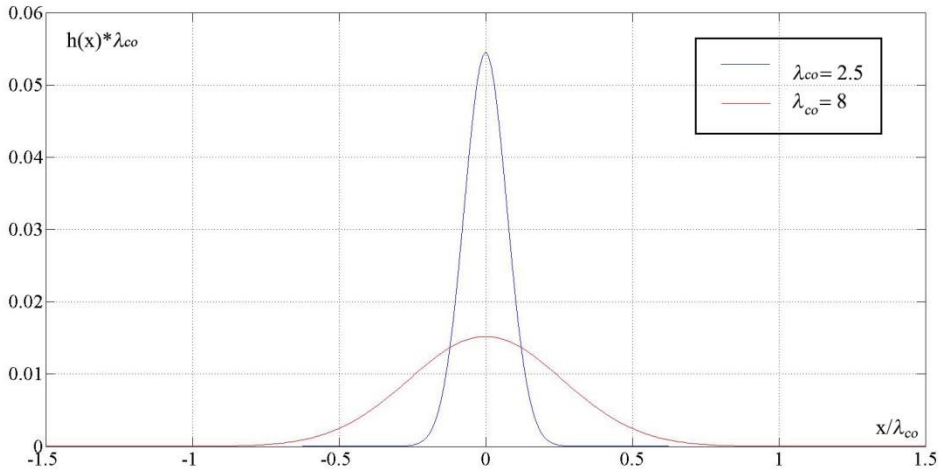

Figure 4.26 Gaussian density function for λ_{co} = 2.5 mm and λ_{co} = 8 mm

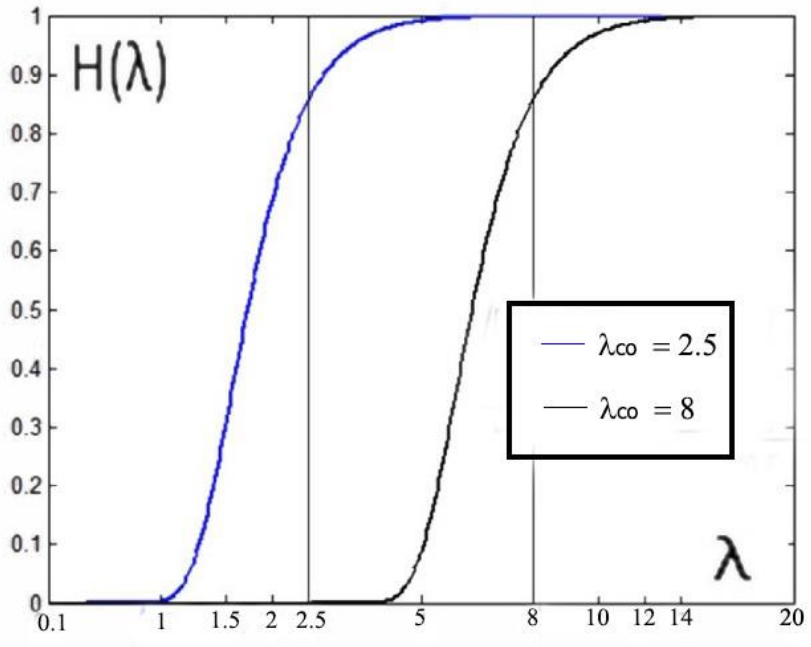

Figure 4.27 Gaussian transfer function for λ_{co} = 2.5 mm and λ_{co} = 8 mm

The Gaussian transfer functions are applied on surface roughness standard profiles at 3.2, 6.3, 12.5, 25 and 50 μm before filtering to separate the roughness profile from the form and waviness profiles, as shown Figures 4.28, 4.29, 4.30, 4.31, 4.32, 4.33, 4.34, 4.35, 4.36 and 4.37.

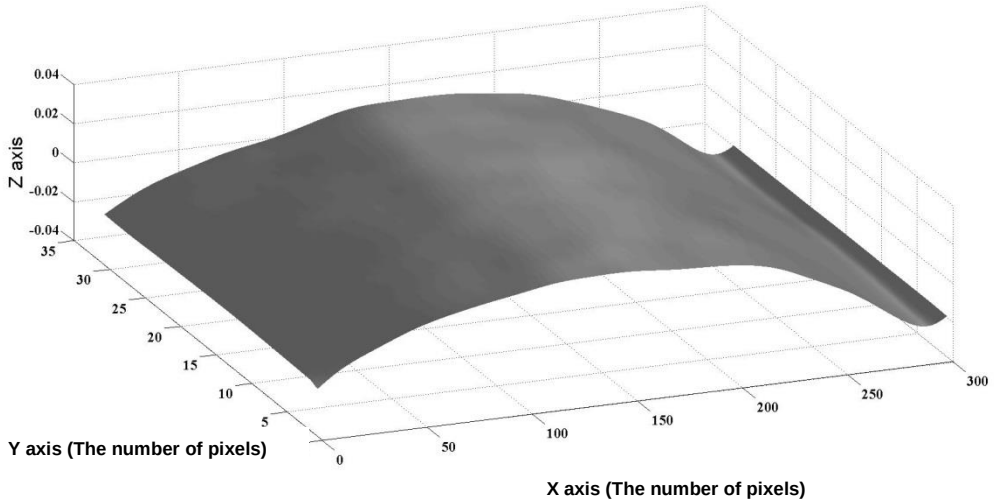

Figure 4.28 3D profile of waviness and form at roughness standard surface 3.2 um after applying the Gaussian transfer function

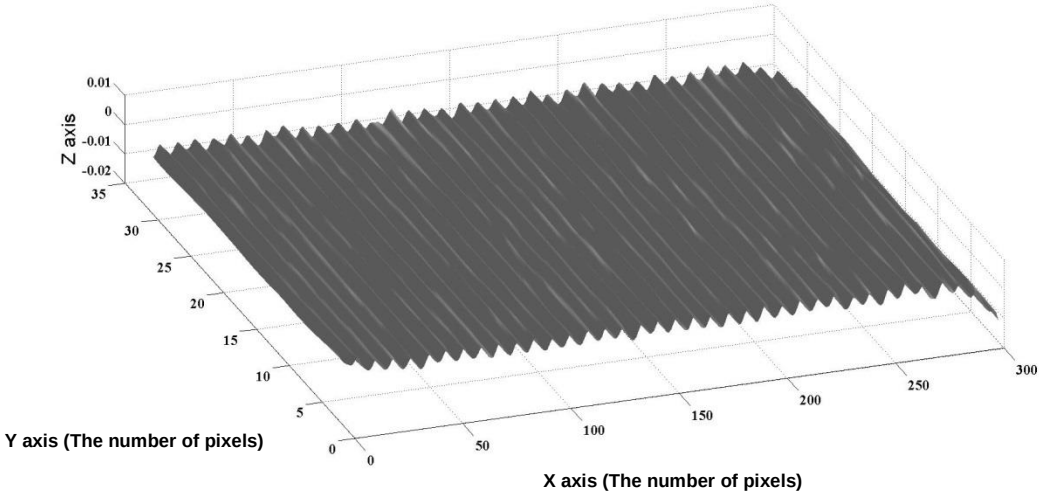

Figure 4.29 3D profile of surface roughness standard at 3.2 um

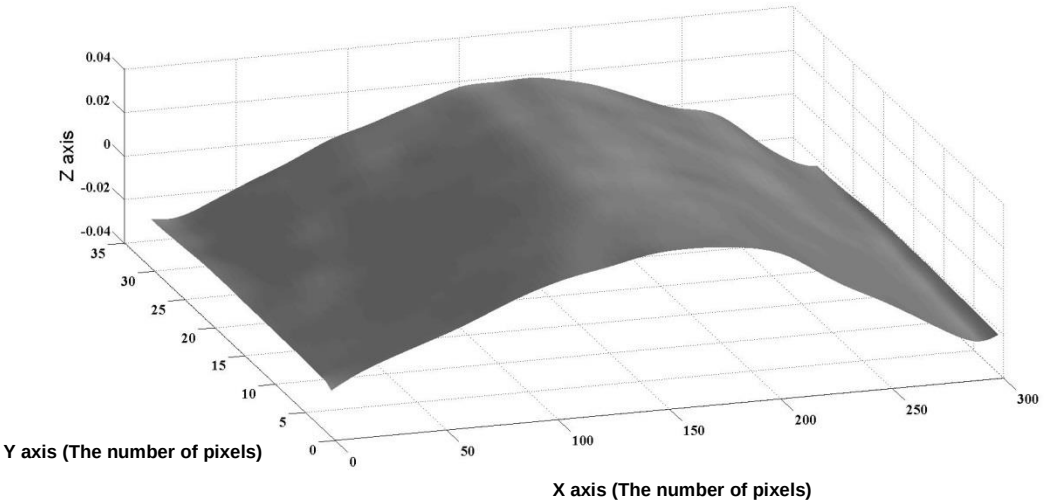

Figure 4.30 3D profile of waviness and form at roughness standard surface 6.3 um after applying the Gaussian transfer function

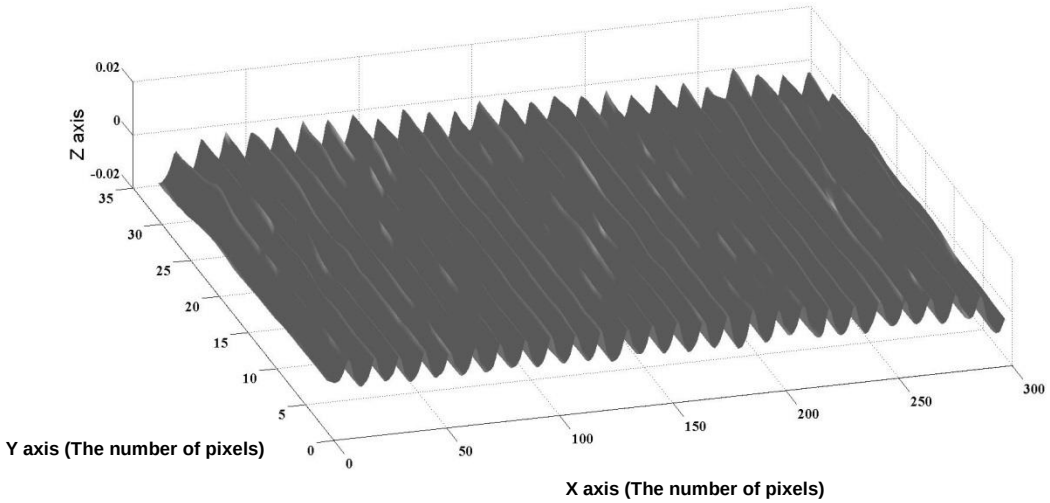

Figure 4.31 3D profile of surface roughness standard at 6.3 um

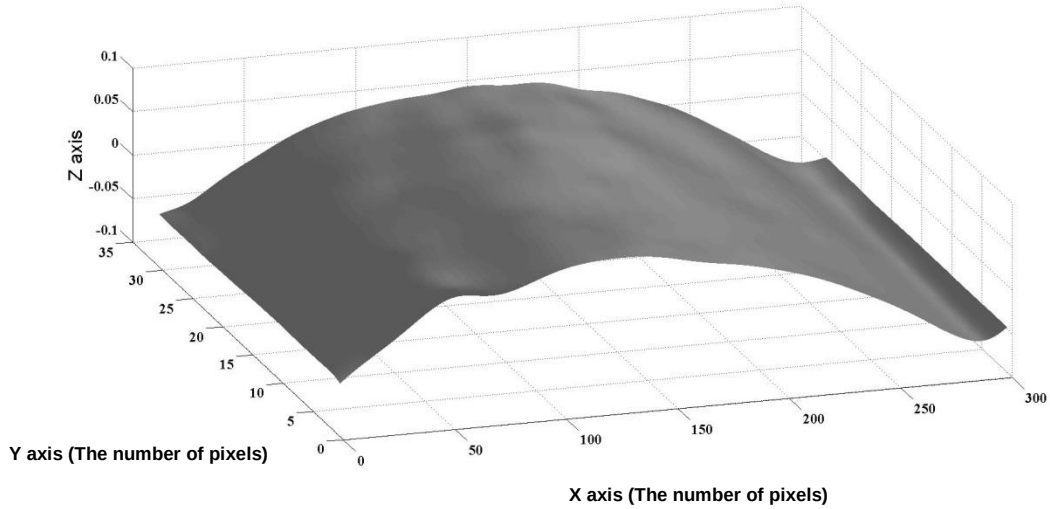

Figure 4.32 3D profile of waviness and form at roughness standard surface 12.5 um after applying the Gaussian transfer function

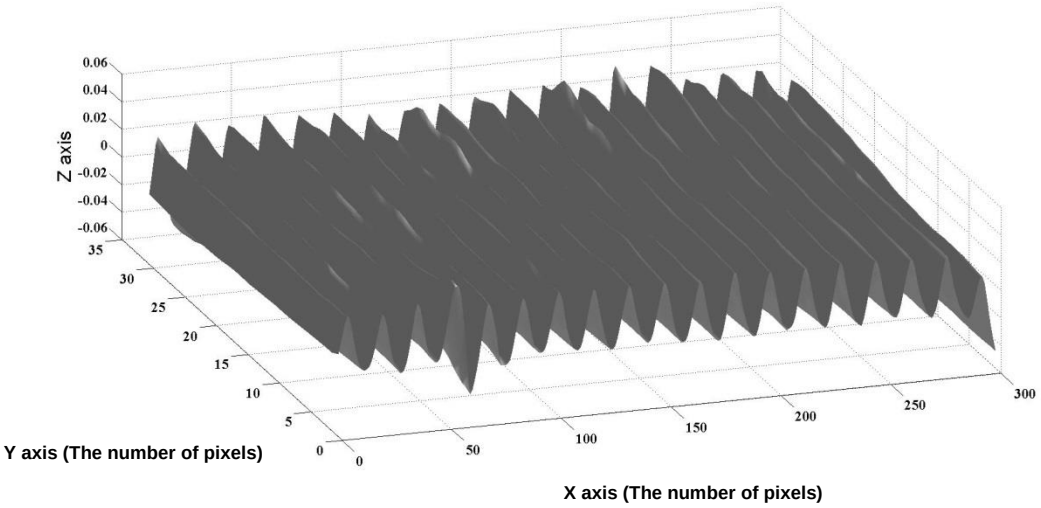

Figure 4.33 3D profile of surface roughness standard at 12.5 um

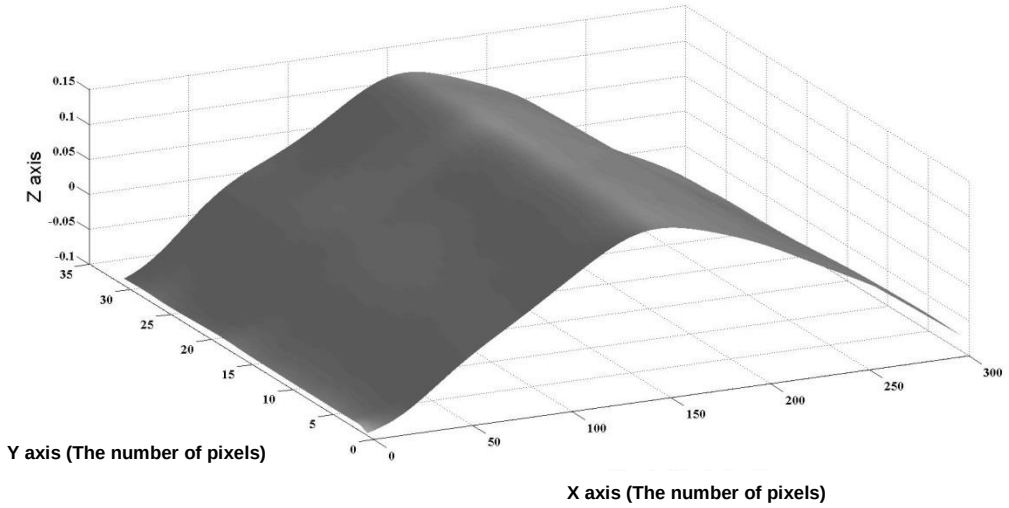

Figure 4.34 3D profile of waviness and form at roughness standard surface 25 um after applying the Gaussian transfer function

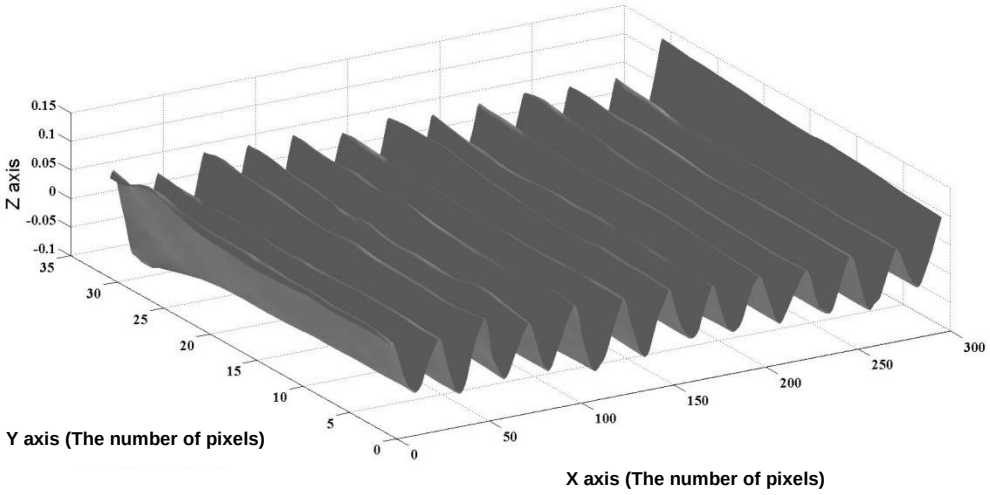

Figure 4.35 3D profile of surface roughness standard at 25 um

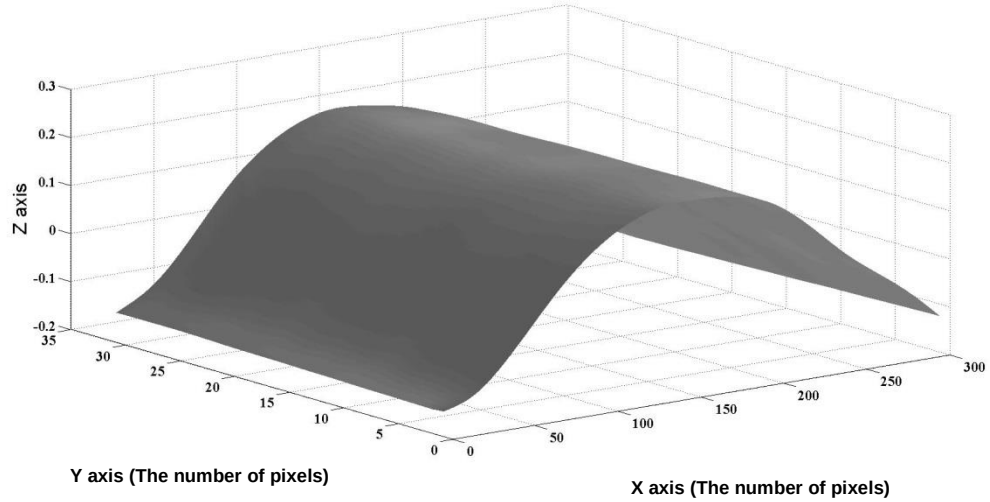

Figure 4.36 3D profile of waviness and form at roughness standard surface 50 um after applying the Gaussian transfer function

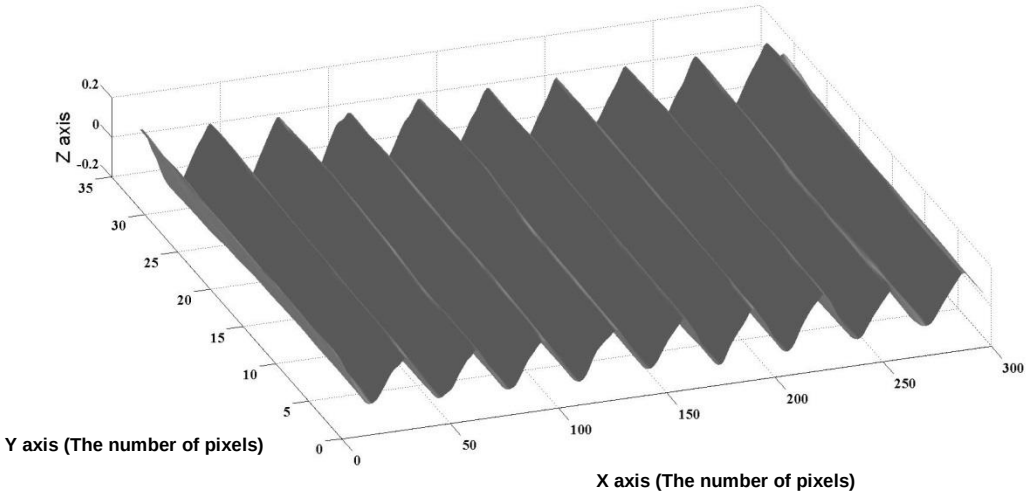

Figure 4.37 3D profile of surface roughness standard at 50 um

In the experiment, the centre lines from three-dimensional profiles are selected to compare the roughness profiles determined from the stylus instrument. The effect after the filtering process is that the data are shifted from their original location. Figure 4.38 shows that the data are shifted after the Gaussian transfer functions have been performed, and Figure 4.39 illustrates that the data are moved back to the correct position.

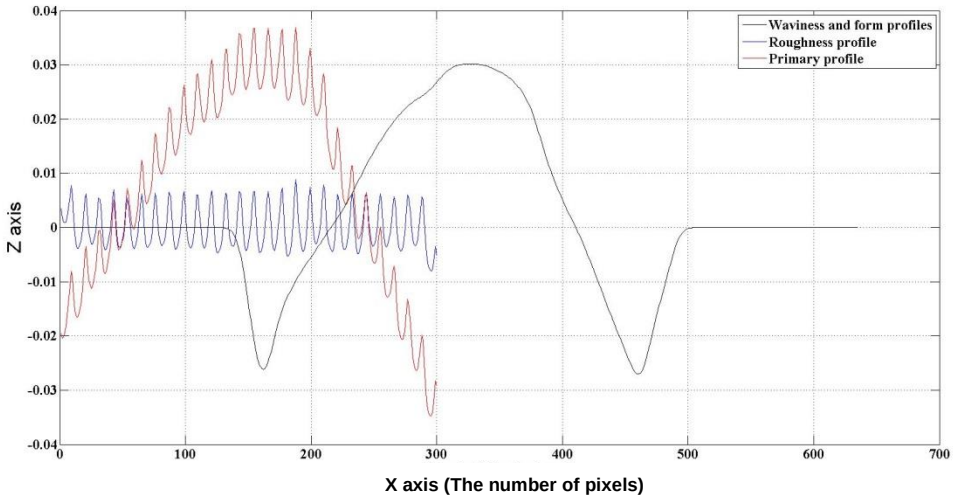

Figure 4.38 Roughness profile 6.3 um separated from primary profile by high pass filter before data are shifted

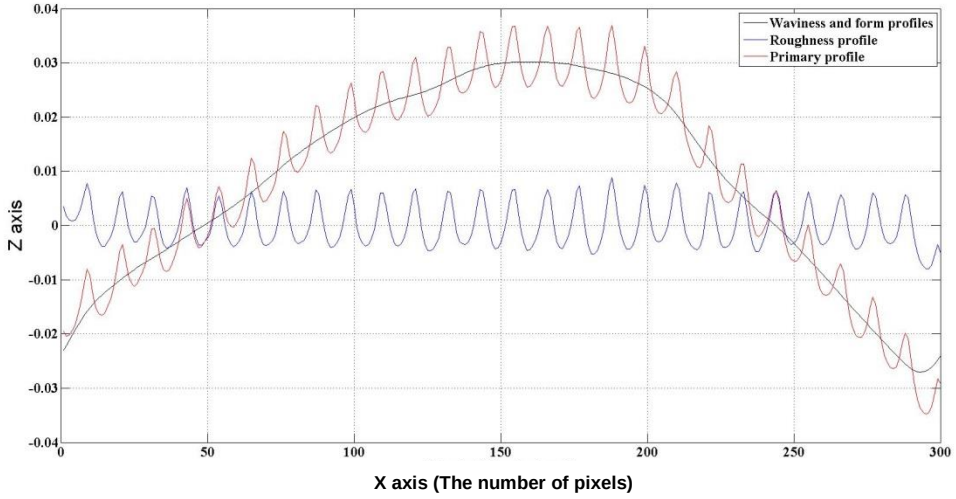

Figure 4.39 Roughness profile 6.3 um separated from primary profile by high pass filter after data are shifted

4.5 Measurement results

The surface roughness parameter determined throughout in this research is the R_a, as it is the surface finish parameter most widely used by researchers and industrial manufacturing (Smith, 2002). It is the arithmetic average of the absolute value of the heights of roughness irregularities from the measured mean value as shown in the following:

$$R_a = \frac{1}{n}(\sum_{i=1}^{n}|y_i|) \tag{4.34}$$

where y_i is the height of roughness irregularities from the mean value, and n is the number of sampling data. In this research, the z axis can be converted to the measuring length (um) by the feature of a surface image, called the arithmetic of the PS method ($Ra_{PS,}$), which is used to predict the actual surface roughness of the object. The Ra_{PS} can be evaluated as follows

$$Ra_{PS} = \frac{1}{n}(\sum_{i=1}^{n}|Ra_{PSi} - Ra_{PSm}|) \tag{4.35}$$

where Ra_{PSi} is the individual value in pixel of a surface image along one line, and Ra_{PSm} is the mean of all the pixel values of a surface image along one line. It can be determined as

$$Ra_{PSm} = \frac{1}{n}(\sum_{i=1}^{n} Ra_{PSmi}) \quad (4.36)$$

where Ra_{PSmi} is the individual value in each pixel of a surface image along one line. All of the surface images were evaluated and analysed after having been passed through the high pass filter (Kumar, et al., 2005). The average values of 12 lines from the sample profiles were then calculated according to the International Standard (ISO 4288, 1998). To reduce the statistical error of a measurement, it is necessary to perform several averages per position. The experiment was made at five times per 1 line of each sample profile. There were a few points that showed a high deviation from the surface model. It can then be expected that the standard deviation would be very small. The result of *Ra* profiles measured from the PS method after having been passed through the high pass filter is shown in Table 4.4.

Table 4.4 The measurement results of R_a determined from the PS method under different slant angles.

Slant	Standard Roughness Nominal value (um)	PS method Average value	Standard deviation
30 ^{o}	3.2	0.0016	0.00001
	6.3	0.0038	0.00002
	12.5	0.0156	0.00001
	25	0.0275	0.00002
	50	0.0373	0.00002
37.5^{o}	3.2	0.0016	0.00001
	6.3	0.0054	0.00002
	12.5	0.0098	0.00002
	25	0.0517	0.00001

	50	0.0547	0.00002
45^o	3.2	0.0015	0.00001
	6.3	0.0039	0.00002
	12.5	0.0121	0.00002
	25	0.0318	0.00001
	50	0.0762	0.00002
52.5^o	3.2	0.0043	0.00001
	6.3	0.0051	0.00001
	12.5	0.0121	0.00002
	25	0.0231	0.00002
	50	0.0321	0.00002

Each value of surface texture measured from the PS method and surface texture measured from the stylus instrument is solved by the system of linear equations (Karris, 2007; Palm, 2005). The solution for the scalar equation is given by

$$AX = B \tag{4.37}$$

A and B are matrices whose elements are known, and X is a matrix (a column vector) whose elements are unknown. A and X must be conformable for multiplication. To solve the matrix equation 4.37, multiplication of both sides by A^{-1} yields:

$$A^{-1}AX = A^{-1}B = IX = A^{-1}B \tag{4.38}$$

Where I is the identity matrix. The equation 4.38 can be solved as follows:

$$X = A^{-1}B \tag{4.39}$$

The equation 4.39 is used to solve any set of simultaneous equations having solutions. The equation can be drawn from the measurement system as follows:

$$X = \begin{bmatrix} m \\ b \end{bmatrix} \tag{4.40}$$

$$A = \begin{bmatrix} x_1 & 1 \\ x_2 & 1 \\ \cdots & \cdots \\ x_n & 1 \end{bmatrix} \tag{4.41}$$

$$B = \begin{bmatrix} y_1 \\ y_2 \\ \cdots \\ y_n \end{bmatrix} \tag{4.42}$$

where x_1, x_2,…, x_n are the data determined from the PS method, and y_1, y_2,…,y_n are the surface roughness standard values measured from the stylus instrument. The slope or gradient of the line is shown by constant m, and b is a point at which the line crosses the y-axis. The coefficient of determination, R^2, is used to determine the goodness of fit of the regression line. The best coefficient of determination was found at a 45^o slant angle. The linear regression model at a 45^o slant angle can be utilised for recovering three dimensional surface roughness standards. The measurement results are summarized in Table 4.5 as the coefficients of determination between the estimated R_a by the PS system against the surface roughness standard as determined from the stylus instrument.

Table 4.5 The linear regression model of Ra_{std} against Ra_{PS} at 30, 37.5, 45 and 52.5 slant angles

Slant angle (θ)	Linear regression model	Coefficient of determination
30°	$Ra_{std} = 1492.1Ra_{PS} - 2.51$	0.92
37.5°	$Ra_{std} = 825.8Ra_{PS} + 2.74$	0.84
45°	$Ra_{std} = 761.4\ Ra_{PS} + 3.98$	0.99
52.5°	$Ra_{std} = 1933.4Ra_{PS} - 6.57$	0.96

where Ra_{PS} is averaged from the 12 line profiles from the PS image measurement system and Ra_{std} is the roughness averaged from the 12 line profiles from the stylus instrument. Five values of the surface roughness standards were utilized for evaluating the PS system. The best coefficient is found at a 45^{o} slant angle. This equation can be used to calculate the average roughness measurement from the recovered surfaces.

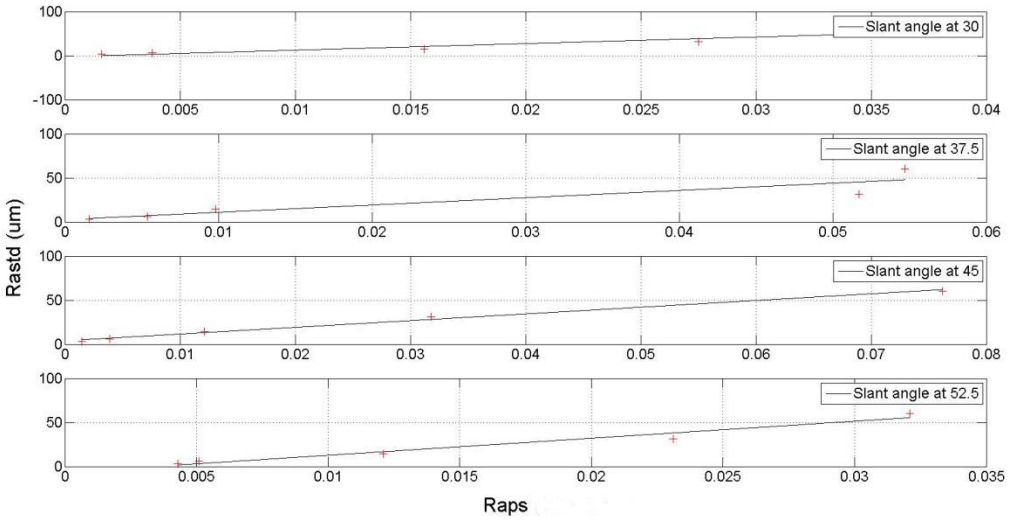

Figure 4.40 Linear regression of Ra_{std} against Ra_{PS} at 30, 37.5, 45 and 52.5 slant angles

Experiments performed on five values of surface roughness standards covering a range of textures were used for system evaluation. As shown in Figure 4.40, the coefficient of determination ranged from R^2 = 0.84 (at $\theta = 37.5^{\circ}$) to 0.99 (at $\theta = 45^{\circ}$). The highest coefficient of determination (R^2 = 0.99) was found at the slant angle of 45°.

The Linear regression model at 45° was utilized to estimate accurately the surface roughness from the recovered surface. The aim of recovering surface roughness profiles in a three-dimensional surface is to provide more information on the surface characteristics than the stylus instrument. Two-dimensional results acquired from the stylus instrument could be replaced by such multidimensional indicators as a power spectrum energy of wavelengths. The PS technique can be extended to analyse and evaluate large surfaces depending on the measurement setup. Each centre line from those profiles measured from the PS system is shown in Figure 4.41, 4.42, 4.43, 4.44 and 4.45. The x axes of measurement results in all Figures are also converted from pixel sizes to length measurement in mm unit based on the camera calibration and the linear

regression model at 45° is then used to transfer the surface normals from each pixel into the length measurement (μm).

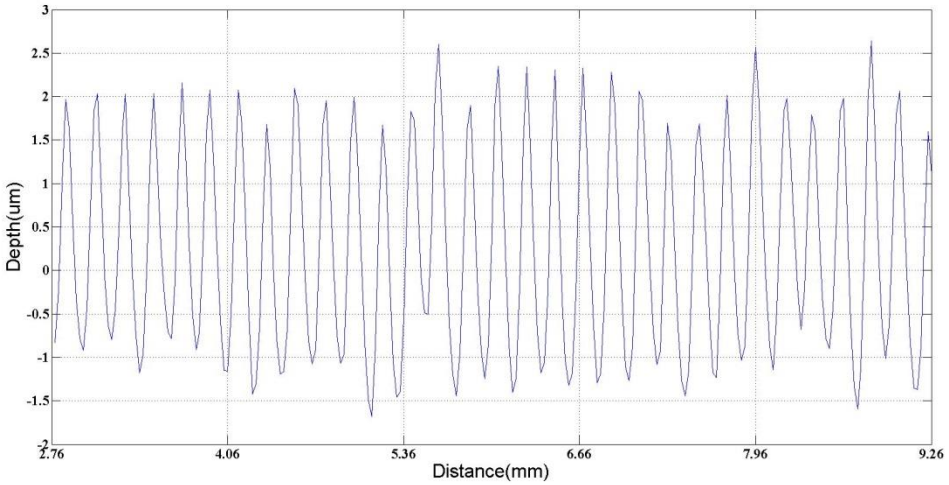

Figure 4.41 Standard surface roughness profile at 3.2 μm after having been passed though the linear regression model

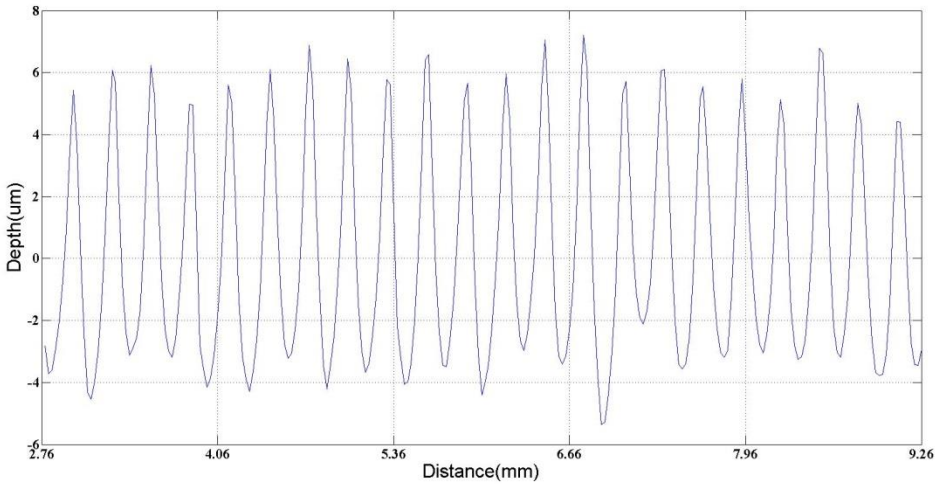

Figure 4.42 Standard surface roughness profile at 6.3 μm after having been passed though the linear regression model

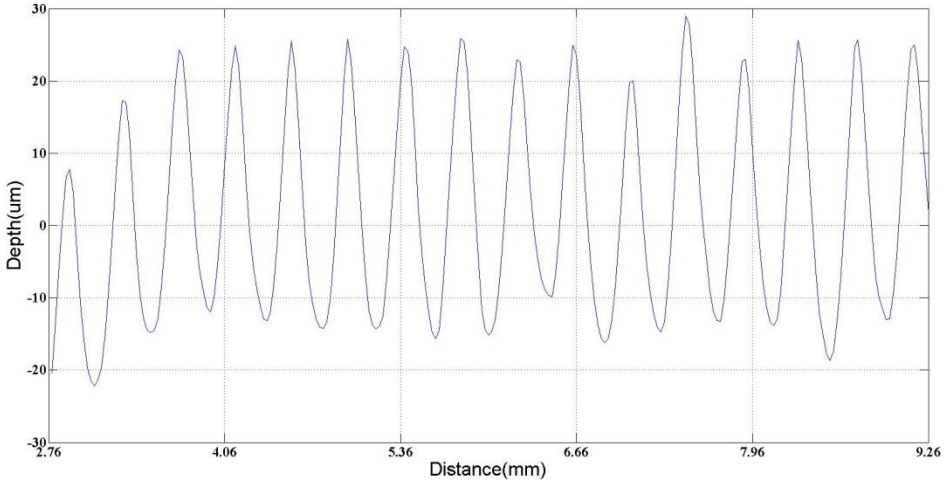

Figure 4.43 Standard surface roughness profile at 12.5 μm after having been passed though the linear regression model

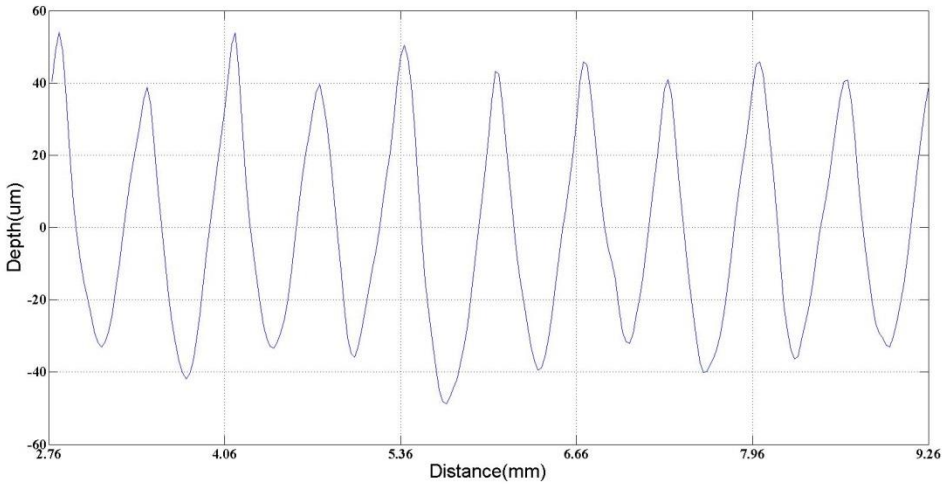

Figure 4.44 Standard surface roughness profile at 25 μm after having been passed though the linear regression model

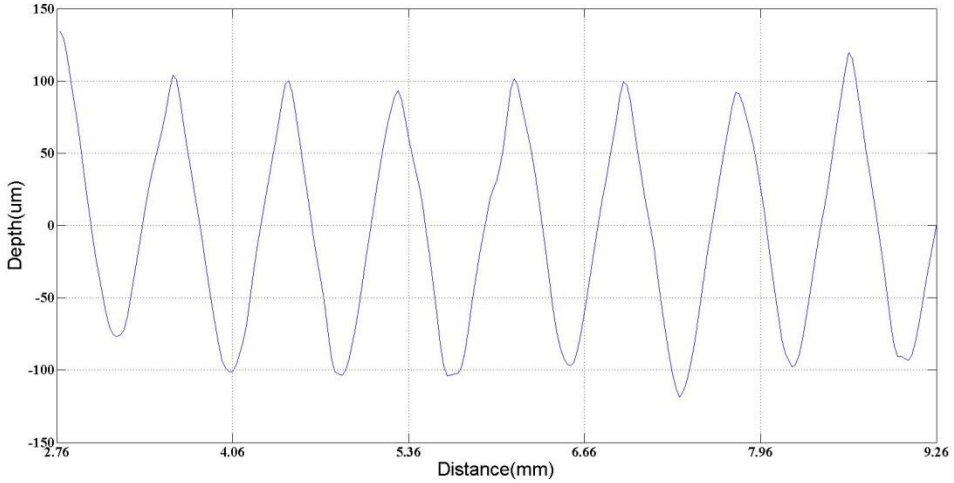

Figure 4.45 Standard surface roughness profile at 50 μm after having been passed though the linear regression model

4.6 Conclusion

The PS technique based surface roughness measurement is developed and the experiment results show that the new approach for textural examination using the PS method makes it possible to determine the Ra values of workpieces at higher level than 3.2 um. The 3D surface profiles can be obtained using the gradient, calculated from photometric stereo images. Although, 3D surface profiles can be recovered by the PS method, there are few assumptions and limitations. In the case of high reflection area, it is not possible to recover the 3D surface profiles as the saturated pixel values. As a result, the PS method is not suitable for objects having high reflection material. Moreover, the limitation of angle of CMM's probing has the direct effect with the experimental approach because the slant angles are limited to movement no more four different slant angles: 30^o, 37.5^o, 45^o and 52.5^o. The best slant angle from the experiment for measuring the surface roughness standard was 45^o as evaluated by the coefficient of determination. The three-dimensional surface was perfectly reconstructed from the surface normals and the corresponding light source intensity. The Gaussian transfer function used for mean line creation worked well to separate the roughness profile from the form and waviness profiles. A proper cut-off frequency has been specified in the standard ISO 16610-21:2012. Further verification and experimental validations will be conducted and reported in Chapter 5. The specimen will be created to confirm the measurement efficiency of surface roughness from the proposed

approach. In addition, the measurement uncertainty of the PS system is to be assessed to create the confidence of measured values.

Chapter 5 Uncertainty estimation and validation method of surface roughness measurement on a coordinate measuring machine using the photometric stereo method

5.1 Introduction

In the past few decades, the real importance of calibration measurement has been realized. Many more industrial manufacturers are using instruments for measuring their products. These tools need to be calibrated following the quality control properly. Moreover, measurement results can be linked to the international standard by an unbroken chain of accredited comparisons. In this chapter, the measurement uncertainty for the PS system will be evaluated to increase confidence in measurement results, and then measurement traceability will be made through surface roughness standards which are calibrated by the stylus instrument, at National Institute of Metrology (Thailand).

5.2 Measurement

Measurement units have been officially defined according to the international system of units (SI). The abbreviation SI comes from the French name ‘’Systeme International d’Unites’’, and it was established in 1960 by the General of Weights and Measures. Seven quantities based on the SI units have been defined as following a particular physical quantity. They include time (second), length (metre), mass (kilogram), electrical current (ampere), thermodynamic temperature (kelvin), amount of substance (mole), and luminous intensity (candela) (Leach, 2010). Measurement is a set of operations that have the object of determining a value of quantity. The property of an object can be determined by giving a number in a measuring system. Instruments such as rulers, stopwatches, weighing scales, and thermometers are all basic measuring instruments, which are necessary for everyday life, and whose numbers tell us about physical volume (Bell, 2001). Measurement results can be separated into two parts: measurement result, and measurement uncertainty. For example, the measurement result of the scale named on the certificate 1000.001$\pm$0.001 kg can inform the result of measurement of 1000.001kg and measurement uncertainty of the scale of 0.001 kg.

Measurement is a technical operation performed the instruction to compare between the quantities being measured with the volume of a standard, which represents the

measurement unit that means instrumentation. The measuring method and instrumentation are based on the level of accuracy of the measurement being acquired. These include the expertise in the measurement of the measurable components. Moreover, if the instrument used in the measurement process has not been calibrated correctly, it is not possible to have confidence in the measurement results.

When reporting the result of a measurement of a physical quantity, some quantitative indication of the quality of the result should be given, so that whoever uses it can assess its reliability. Without such an indication, measurement results cannot be compared, either among themselves or with reference to values given in a specification or standard. It is, therefore, necessary that there be a readily implemented, easily understood, and generally accepted procedure for characterizing the quality of a result of a measurement that is for evaluating and expressing its uncertainty (Bell, 2001). The concept of uncertainty is that when all of the known or suspected components of error have been evaluated, and the appropriate corrections have been applied, there remains an uncertainty about the correctness of the stated result, that is, a doubt about how well the result of the measurement represents the value of the quantity being measured.

5.3 Uncertainty of measurement

A common sentence to explain the uncertainty of measurement is that it is the residual error which may exist in an instrument or workpiece after calibration has been performed to obtain corrections (Dietrich, 1991). The sources of uncertainties can be categorised into various types. The following lists shown sequentially are not exhaustive but cover most of the principal sources of uncertainty.

- uncertainties occurring standards or in calibration equipment,
- uncertainties caused by human error,
- resolution or discriminations uncertainties,
- uncertainties in environmental measurements, including temperature effect, variation of power supplies; Lack of repeatability-instability uncertainties,
- functional uncertainties, caused by the malfunctioning of equipment,
- uncertainties due to lack of cleanliness,

- uncertainties resulting from inadequate quality surface texture and erroneous geometry,
- uncertainties due to manufacturer's specification,

There are two methods to estimate measurement uncertainties. The uncertainty of measurement associated with the input estimates is evaluated according to either a "type A" or a "type B" method of evaluation (Forbes, 2012; Bell, 2001).

The statistical analysis of an observation series was applied to produce the Type A evaluation of standard uncertainty. In this case, the standard uncertainty is the experimental standard deviation of the mean that follows from an averaging procedure or an appropriate regression analysis as follows

$$u_A = s(\bar{q}) \tag{5.1}$$

where $s(\bar{q})$ is the termed experimental standard deviation of the mean. The type A evaluation of standard uncertainty can be applied when several independent observations have been made for one of the input quantities under the same conditions of measurement.

The type B evaluation of standard uncertainty is the method of evaluating the uncertainty by means other than the statistical analysis of the series of observation series. In this case, the evaluation of standard uncertainty is based on scientific knowledge. Usually, the standard uncertainty $u(x_i)$ is evaluated by scientific judgments based on all available information on the possible variability of x_i. Values belonging to this category may be derived from previous measurement data, such as a manufacturer's specifications, data provided in calibration and other certificates, uncertainties assigned to reference data taken from handbooks, published in formation, and common sense (GUM, 1993).

For uncorrelated input quantities, the square of standard uncertainty associated with the output estimation *y* is given by equation (5.2), called combined standard uncertainty.

$$u_c^2(y) = \sum_{i=1}^{N} u_i^2(y) \tag{5.2}$$

The quantity $u_i(y)$, where (i = 1, 2,… N), is the contribution to the standard uncertainty associated with the output estimate y resulting from the standard uncertainty associated with the input estimate x_i as

$$u_i(y) = c_i u(x_i) \tag{5.3}$$

where c_i is the sensitivity coefficient associated with the input estimate x_i. It is determined from the partial derivative of the mathematical model function of the measurement. The sensitivity coefficient c_i describes the extent to which the output estimate y is influenced by variations of the input estimate x_i.

The measurement uncertainty is generally considered to be an expanded uncertainty of measurement (U), obtained by multiplying the standard uncertainty $u_c(y)$ of the output estimate y by a coverage factor k, ($U = ku_c(y)$). In cases where a normal distribution (Gaussian) can be attributed to the measurand and the standard uncertainty associated with the output estimate has sufficient reliability, the standard coverage factor k = 2 shall be used. The assigned expanded uncertainty corresponds to a coverage probability of approximately 95%. These conditions are fulfilled in the majority of cases encountered in calibration work. The result of a measurement is then conveniently expressed as $Y = y \pm U$, which is interpreted to mean that the best estimate of the value attributable to the measurand Y is y, and that $y - U$ to $y + U$ is an interval that may be expected to encompass a large fraction of the distribution of values that could reasonably be attributed to Y. Such an interval is also expressed as $y - U \leq Y \leq y + U$ (Schwenke, et al., 2000; EA-4/02, 1999).

5.4 The uncertainties of measuring surface texture

Measuring surface texture involves a very complicated system depending on a number of factors because there are many parameters involved in determining the surface texture of workpieces. For this reason, calculating measurement uncertainties is not simple way to perform these calculations (Leach, 2001). The surface roughness parameter used throughout in this study is the arithmetical mean of the surface profile (*Ra*). This parameter is also the surface finish parameter most widely used by researchers and industries.

5.4.1 Roughness standard calibration (*Ra* parameter ISO 4287:1997)

According to ISO 4287:1997, the definition of *Ra* is

$$R_a = \frac{1}{l}\int_0^l |R(x)|dx \tag{5.4}$$

where l is the sampling length, and $R(x)$ is the roughness profile.

Equation 5.4 can be modified as shown in equation 5.5

$$R_a = \frac{1}{N}\sum_{i=1}^{N} R_i \tag{5.5}$$

The uncertainty of *Ra* can be shown as the following equation

$$u^2(R_a) = C_{R_i}^2 \cdot u^2(R_i) \tag{5.6}$$

$$u^2(R_a) = \left(\frac{\partial R_a}{\partial R_i}\right)^2 \cdot u^2(R_i) \tag{5.7}$$

$$u^2(R_a) = \frac{1}{N}\sum_{i=1}^{N}\frac{\partial R_i}{\partial R_i} \cdot u^2(R_i) \tag{5.8}$$

$$u^2(R_a) = \frac{1}{N}\sum_{i=1}^{N} u^2(R_i) \tag{5.9}$$

Using an assumption, the points on the roughness profile have identical uncertainty and then $u^2(R_1)+u^2(R_2)+u^2(R_3)+ u^2(R_N) = Nu^2(R_i)$ can be modified as shown in equation 5.10.

$$u^2(R_a) = u^2(R_i) \tag{5.10}$$

The filter applied to separate the roughness profile from the waviness profile is a phase correct filter (the so-called Gaussian filter). The weighing function of the low-pass part having the shape of a Gaussian density function is shown in Figure 4.26, and its mathematical model is described in equation 4.28. The measurement uncertainties of the roughness and waviness were obtained by calculating the propagation of the measurement uncertainty in the case of filtering process (Krystek, 2001). Given the roughness profile $R(x)$ calculated from primary profile $Z(x)$ by using Gaussian function

S(x) and convolution principle, the uncertainty of *u(R)* can be reduced by the smoothing factor

$$u(R)=\sqrt{1-\frac{\Delta x}{\alpha\lambda_c}\left(2-\frac{1}{\sqrt{2}}\right)}\cdot u(Z) \tag{5.11}$$

where Δx is the sampling interval

$$\alpha=\sqrt{\frac{\log 2}{\pi}}=0.4697 \tag{5.12}$$

λ_c is the cut-off wavelength of the filter, and *u(Z)* is the uncertainty of the primary profile, the equation 5.12 is inserted into equation 5.11

$$u^2(R)=\left[1-\frac{\Delta x}{0.4697\lambda_c}\left(2-\frac{1}{\sqrt{2}}\right)\right]\cdot u^2(Z) \tag{5.13}$$

For example, the sampling interval is 0.026 μm calculating from equation 4.25, and the cut-off wavelength for measuring the average roughness is 800 μm:

$$u^2(R)=\left[1-\frac{0.026}{0.4697\times 800}\left(2-\frac{1}{\sqrt{2}}\right)\right]\cdot u^2(Z)\approx\cdot u^2(Z) \tag{5.14}$$

The uncertainty of the arithmetical mean deviation of the assessed profile is then shown in equation 5.15:

$$u^2(R_a)=u^2(R)=u^2(Z) \tag{5.15}$$

5.5 Estimating uncertainty of the PS system for surface roughness measurement

The measurement uncertainty of the PS system for the surface roughness measurement has been evaluated following the recommended guideline (Leach, 2001), the calibration analysis follows the guide to the expression of uncertainty in measurement (JCGM 100.2008, 2008), as well as the European Accreditation Publication Expressions of the Uncertainty of Measurement in Calibration and Geometrical Product Specification

(GPS) – Surface texture (ISO 12179, 2000). The mathematical model of vertical height as determined by the PS system can be solved as

$$Z = C \cdot Z_m \tag{5.16}$$

where Z is the corrected measurement of vertical height, $Z_m$is the measured depth and C is the calibration factor defined by

$$C = \frac{d_c}{d_m} \tag{5.17}$$

where d_c is the average roughness correction as quoted from the calibration certificate and d_m is the measured value of standard surface roughness before using the calibration factor.

The Z_m depends on additive factors having effects of the PS system. The number of factors can be shown as

$$Z_m = Z_p + Z_{ind} + Z_l + Z_{ix} + Z_{mc} + Z_g + Z_n \cdot \bar{\alpha} \cdot \Delta\bar{t} \tag{5.18}$$

Equation 5.17 and 5.18 are replaced by equation 5.16. The above equation can therefore be rewritten as

$$Z = \left(\frac{d_c}{d_m}\right) \cdot \left(Z_p + Z_{ind} + Z_l + Z_{ix} + Z_{mc} + Z_g + Z_n \cdot \bar{\alpha} \cdot \Delta\bar{t}\right) \tag{5.19}$$

where Z_p : the width of a pixel of the camera in mm

Z_{ind} : the measured value of the surface roughness standard under calibration

Z_l : the intensity of light source affecting with average roughness variation

Z_{ix} : the resolution of the PS system

Z_{mc} : the correction due to mechanical effect of CMM's movement correlating with roughness average variation

Z_g : the length of actual working standard scale from calibration certificate.

Z_n : the nominal value of surface roughness standard

$\bar{\alpha}$: the thermal expansion coefficient between the material of measurand and standard

$\Delta\bar{t}$: the difference in room temperature during the measurement period.

To combine the standard uncertainty $u_c(Z)$ from equation 5.16, it is to estimate of the standard deviation of the distribution of possible values that deviate from nominal value of the depth measurement standard which is measured by the PS system (EA-4/02, 1999). The combined standard uncertainty can be found by a quadrature sum of the uncertainties $u(x_i)$ of all of the influence factors x_i :

$$u_c^2(Z) = \sum_{i=1}^{n} c_i^2 u^2(x_i) \tag{5.20}$$

where $u(x_i)$ is the standard uncertainties associated with the input estimate x_i, and the sensitivity coefficients can be evaluated as

$$c_i = \frac{\partial z}{\partial x_i} \tag{5.21}$$

Therefore, the uncertainty of depth measurement standard can be calculated as follows

$$u_c^2(Z) = \left(\frac{\partial Z}{\partial C}\right)^2 u^2(C) + \left(\frac{\partial Z}{\partial Z_m}\right)^2 u^2(Z_m) \tag{5.22}$$

$$u_c^2(Z) = \left(Z_m \frac{\partial C}{\partial C}\right)^2 u^2(C) + \left(C \frac{\partial Z_m}{\partial Z_m}\right)^2 u^2(Z_m) \tag{5.23}$$

$$u_c^2(Z) = C^2 u^2(Z_m) + Z_m{}^2 u^2(C) \tag{5.24}$$

The uncertainty of the calibration factor ($u^2(C)$) is solved as follows

$$u^2(C) = \left(\frac{\partial C}{\partial d_c}\right)^2 u^2(d_c) + \left(\frac{\partial C}{\partial d_m}\right)^2 u^2(d_m) \tag{5.25}$$

$$u^2(C) = \frac{1}{d_m^2} \cdot u^2(d_c) + \frac{d_c^2}{d_m^4} \cdot u^2(d_m) \tag{5.26}$$

The uncertainty of the measurement depth ($u^2(Z_m)$) is solved using equation 5.18. The combined standard uncertainty is expressed by the uncertainties of the input values as follows

$$u^2(Z_m) = {c_{Z_p}}^2 u^2(Z_p) + {c_{Z_{ind}}}^2 u^2(Z_{ind}) + {c_{Z_l}}^2 u^2(Z_l) + {c_{Z_{ix}}}^2 u^2(Z_{ix}) + {c_{Z_{mc}}}^2 u^2(Z_{mc}) + {c_{Z_g}}^2 u^2(Z_g) + {c_{Z_{\Delta t}}}^2 u^2(Z_{\Delta \bar{t}}) \quad (5.27)$$

where c_i represents the partial derivatives of equation (5.19):

$$c_{Z_p} = \frac{\partial Z_m}{\partial Z_p} = 1$$

$$c_{Z_{ind}} = \frac{\partial Z_m}{\partial Z_{ind}} = 1$$

$$c_{Z_l} = \frac{\partial Z_m}{\partial Z_l} = 1$$

$$c_{Z_{ix}} = \frac{\partial Z_m}{\partial Z_{ix}} = 1$$

$$c_{Z_{mc}} = \frac{\partial Z_m}{\partial Z_{mc}} = 1$$

$$c_{Z_g} = \frac{\partial Z_m}{\partial Z_g} = 1$$

$$c_{\Delta T} = \frac{\partial Z_m}{\partial \Delta \bar{t}} = Z_n \cdot \bar{\alpha}$$

The standard uncertainties of the input values are evaluated and estimated for the applied equipment and method as well as for the supposed measurement conditions.

5.5.1 Uncertainty of width of camera's pixel, Z_p

Z_p is the width of the camera's pixel in mm. The width of the camera's pixel has an effect on the results from the roughness measurement. The digital gigabit Ethernet camera with a 25× optical zoom lens was utilized to capture pictures from the PS system. The resolution of the acquired image was 512×320 pixels, with pixel sizes of 7.4 µm×7.4 µm. For our experiment, when the three images were captured from the PS system for the evaluation of surface roughness, the pixel size needed to be calibrated for the length measurement. A working standard scale was utilized to verify the conversion of the pixels to the length measurement. These conversions were performed by the

MATLAB software. The standard uncertainty of width of the camera's pixel was assessed by rectangular distribution. From the experiment, for the measuring range within 10 mm, the measurement uncertainty is 0.577 μm.

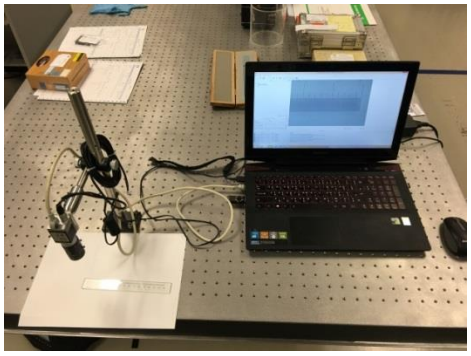

Figure 5.1 **Calibration system for the camera's pixel**

$$u(Z_p) = Z_p/\sqrt{3} \quad (5.28)$$

$$= 1/\sqrt{3}$$

$$= 0.577\ \mu m$$

5.5.2 Uncertainty of repeat measurement of the surface roughness standard under calibration, Z_{ind}

The surface roughness standard 12 lines were measured by the PS system; each line was determined five times.

Table 5.1 The measurement results of Ra determined from the PS system after using the calibration factor.

Number of measurement	Measured value, μm
1	5.39
2	5.42
3	5.41
4	5.46

5	5.51
6	5.61
7	5.68
8	5.74
9	5.86
10	6.00
11	6.06
12	5.94

The arithmetic mean of the measured value of surface roughness standard = 5.67 μm. The experimented standard deviation of the measured value of the surface roughness standard σ_{n-1}= 0.25 μm. The standard uncertainty of the repeat measurement is assessed by normal distribution. The experimented standard deviation of the mean is calculated as shown in equation 5.29.

$$u(Z_{ind}) = \sigma_{n-1}/\sqrt{n} \quad (5.29)$$

$$= 0.25\ /\sqrt{12}$$

$$= 0.07\ \mu m$$

5.5.3 Uncertainty of light intensity of the light source, Z_l

The uncertainty associated with light intensity of the light source, affecting to average roughness values on the surface, was investigated by external potentiometer intensity control of the LED diver. The voltage output, measured directly from the light source, proportionally varied with an external potentiometer, as shown in Figure 5.2.

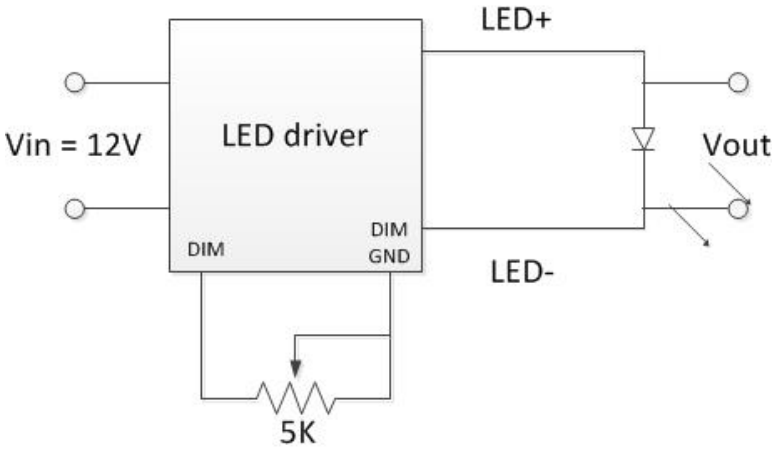

Figure 5.2 External potentiometer

The light intensity of light source can be examined by using a digital multimeter, as illustrated in Figure 5.3, for measuring the output voltage from the LED driver. When the LED driver generates a high output voltage, the light source will provide high brightness on the surface roughness standard. On the contrary, the light source will provide low brightness on the surface roughness standard when the LED driver generates a low output voltage.

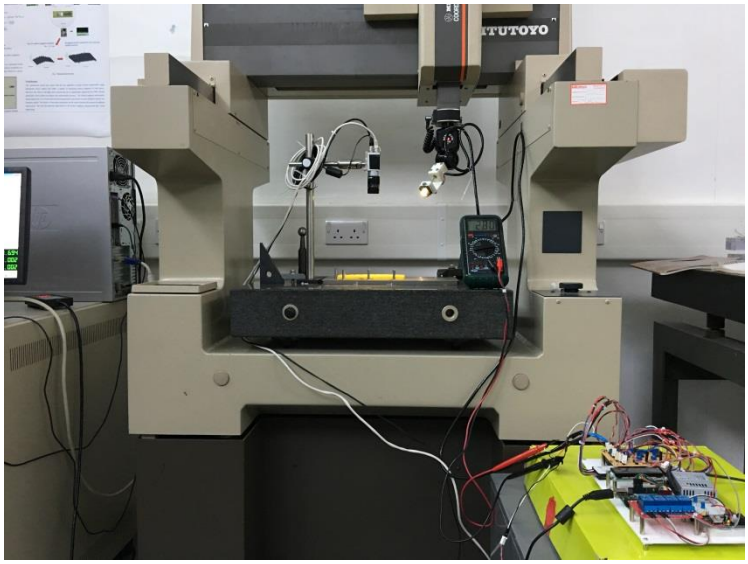

Figure 5.3 The experimental method for finding the influence of light intensity on average roughness results

The results in Table 5.2 have shown that average roughness values have a correlation with the light intensity on the surface object being measured.

Table 5.2 The measurement results of average roughness values in which the light intensity on the surface object is changed

V_{out} (V)	Ra value measured from the PS system (μm)					Average μm	Max-Min μm
	1	2	3	4	5		
2.70	5.51	5.57	5.51	5.51	5.57	5.53	0.39
2.75	5.70	5.70	5.70	5.63	5.63	5.67	
2.80	5.89	5.89	5.82	5.89	5.89	5.87	
2.85	5.89	5.89	5.95	5.95	5.95	5.95	

The standard uncertainty of light intensity, affecting with average roughness values, is assessed by rectangular distribution.

$$u(Z_l) = Z_l/\sqrt{3} \quad (5.30)$$

$$= 0.39\ /\sqrt{3}$$

$$= 0.225\ \mu m$$

5.5.4 Uncertainty of the digital resolution of the PS system, Z_{ix}

The uncertainty of the digital resolution can be expressed from the known interval in which the result is rounded up. The ability of the PS system to distinguish between closely adjacent in the profile, the resolution of PS system is 10 nm. The standard uncertainty of digital resolution is assessed by rectangular distribution.

$$u(Z_{ix}) = Z_{ix}/2\sqrt{3} \quad (5.31)$$

$$= 10\ /2\sqrt{3}$$

$$= 0.003\ \mu m$$

5.5.5 Uncertainty of the mechanical effect of the PS system for measuring surface roughness, Z_{mc}

The uncertainty of the mechanical effect of movement of the CMM's illumination angles movement has a correlation with the measurement results as the CMM was used for holding the light source in order to study the effects of the tilt and slant angles. The effects of the tilt and slant angles were investigated and corrected to give the measurement results, were shown in Table 5.3.

Table 5.3 The measurement results of average roughness values when start position is changed.

Started position of the CMM (mm)	Ra value measured from the PS system (μm)					Average μm	Max-Min μm
	1	2	3	4	5		
+3	5.70	5.70	5.70	5.76	5.76	5.72	0.04
0	5.76	5.76	5.76	5.76	5.76	5.76	
-3	5.76	5.76	5.70	5.70	5.70	5.72	

The start position of the CMM was varied by 3 mm on the plus and the minus sides, which can be observed from the CMM indicator, in each position of image capture to observe the measurement uncertainty that occurred during the CMM's movement. Since the standard uncertainty of the mechanical effect is assessed by rectangular distribution, the standard uncertainty is shown in equation 5.32.

$$u(Z_{mc}) = Z_{mc}/\sqrt{3} \tag{5.32}$$

$$= 0.04\ /\sqrt{3}$$

$$= 0.022\ \mu m$$

5.5.6 Uncertainty of the working standard scale used for calibration of the PS system, Z_g

The Z_g value is the length value quoted in the calibration certificate of working standard scale. In our experiment, the length used in the experiment is 10 mm. The equation is $\sqrt{(0.11)^2 + (4.2 \times 10^{-3} \times l)^2}$, l being the indication length of the working standard scale in mm. The expand uncertainty (k=2) is 0.18 μm. The standard uncertainty of the working standard scale is considered to be normal distribution.

$$u(Z_g) = Z_g/2 \tag{5.33}$$

$$= 0.117\ /2$$

$$= 0.058\ \mu m$$

5.5.7 Uncertainty of temperature variation occurring on measurement system in laboratory and affect with average roughness results, $\Delta\bar{t}$

The temperature was recorded every 5 minutes during 2 hours. The variation of entire measuring periods of 2 hours at the metrology laboratory of Brunel University London was calculated 24 times, and it was found that temperature variations were not more than 3 ^{o}C. Since these variations were cyclic, a U-shaped distribution was used to evaluate the standard uncertainty. The uncertainty of the difference between the temperatures on the laboratory correlates with three variables. Firstly, the difference is at room temperature during the measurement period ($\Delta\bar{t}$). The temperature of the laboratory was maintained at $20 \pm 3\ ^{o}$c. Secondly, the average linear thermal expansion is on standard and unknown materials ($\bar{\alpha}$); based on the manufacturer's data for the surface roughness standard produced by steel, the linear thermal expansion coefficient of the steel is assumed to be within the interval $(11.5 \pm 1)10^{-6}\ ^{\circ}C^{-1}$. In term of light source, it does not have linear thermal expansion. Finally, Z_n is the nominal value of the surface roughness standard. The standard uncertainty is shown in equation (5.34).

$$u(\Delta t) = Z_n \times \overline{\alpha} \times \left(\Delta\bar{t}/\sqrt{2}\right) \tag{5.34}$$

$$= 6.3 \times (11.5 \times 10^{-6}/\ ^{o}C) \times \left(3\ ^{o}C/\sqrt{2}\right)$$

$$= 0.00015\ \mu m$$

As can be seen from the result above, the standard uncertainty of the temperature variation is less than ten times that of the standard uncertainty of the digital resolution. It indicates that the variable does not affect the measurement uncertainty.

5.5.8 Uncertainty of the roughness measurement standard used for the calibration of the PS system, d_c

The d_c value is the roughness measurement standard value quoted in calibration certificate; the expanded uncertainty (k=2) is 0.07 μm, and the value of roughness average is 5.84 μm. The standard uncertainty has to be considered in normal distribution with a sensitivity coefficient $1/d_m$= 0.14.

$$u(d_c) = 1/d_m \times d_c/2 \times Z_m \quad (5.35)$$

$$= 0.14\ um^{-1} \times 0.035\ um \times Z_m$$

$$= 0.0049 Z_m$$

5.5.9 Uncertainty of the measured value of the surface roughness standard used for the calibration of the PS system, d_m

The mean value of the roughness measurement standard is 7.04 μm, and the repeatability of the measured value has to be considered in the normal distribution with a sensitivity coefficient d_c/d_m^2= 0.12. The surface roughness standard 12 lines were measured by the PS system, each line was determined five times. The measurement results are shown in Table 5.4.

Table 5.4 The measurement results of Ra determined from the PS system before using the calibration factor.

Number of measurement	Measured value, μm
1	7.00
2	6.68
3	6.72
4	6.72
5	6.81
6	6.92
7	6.95
8	7.03
9	7.35
10	7.47
11	7.41
12	7.45

Arithmetic mean of the measured value of the surface roughness standard = 7.041 μm. The experimented standard deviation of the measured value of the surface roughness standard σ_{n-1}= 0.30 μm.

$$u(d_m) = d_c/d_m^2 \times \sigma_{n-1}/\sqrt{n} \times Z_m \quad (5.36)$$

$$= 0.12 \times 0.30/\sqrt{12}\,\mu m \times Z_m$$

$$= 0.010 Z_m$$

5.6 Measurement uncertainty budget for the PS system

Table 5.5 Uncertainty budget of the PS system for measuring surface roughness average profile.

Quantity X_i	Estimate x_i	Standard Uncertainty $u(x_i)$		Probability Distribution	Effective degree of freedom	Sensitivity Coefficient c_i	Uncertainty Contribution	
		Absolute	Relative				Absolute	Relative
Z_p	0 μm	5.77E-01 μm	-	Rectangular	∞	1	5.77E-01 μm	-
Z_l	0 μm	2.26E-01 μm	-	Rectangular	∞	1	2.26E-01 μm	-
Z_{ix}	0 μm	2.89E-03 μm	-	Rectangular	∞	1	2.89E-03 μm	-
Z_{mc}	0 μm	2.19E-02 μm	-	Rectangular	∞	1	2.19E-02 μm	-
Z_g	0 μm	5.89E-02 μm	-	Rectangular	∞	1	5.89E-02 μm	-
Z_{ind}	5.67 μm	7.06E-02 μm		Normal	11	1	7.06E-02 μm	-
d_C	5.84 μm	-	0.035	Normal	∞	0.14 Z_m	-	4.97E-03 Z_m
d_m	7.04 μm	-	0.087	Normal	11	0.12 Z_m	-	1.02E-02 Z_m
$u(Z)$							0.39 μm^2	1.29E-04 Z_m^2
							0.63 μm	1.14E-02 Z_m
Z	5.67 μm			Normal	K=2		1.25 μm	2.27E-02 Z_m

5.7 Proposed validation method

The method for validating the performance of the PS system has been evaluated following the recommended guidelines; the evaluation of the performance follows the ISO Guide general requirements for proficiency testing (ISO/CASCO 17043, 2010). The standard roughness standards used in the experiment comprised R_a values from 3.2 µm to 50 µm. They were calibrated using the stylus instrument to calculate accurately the true values, and these were then measured with the PS system to acquire the average roughness values. The values from the stylus instrument and the PS system created a relation using the linear regression method. To validate the accuracy of the PS system, the specimen was precisely manufactured by a Computer Numerical Control (CNC) and measured by the PS system as illustrated in Figure 5.4.

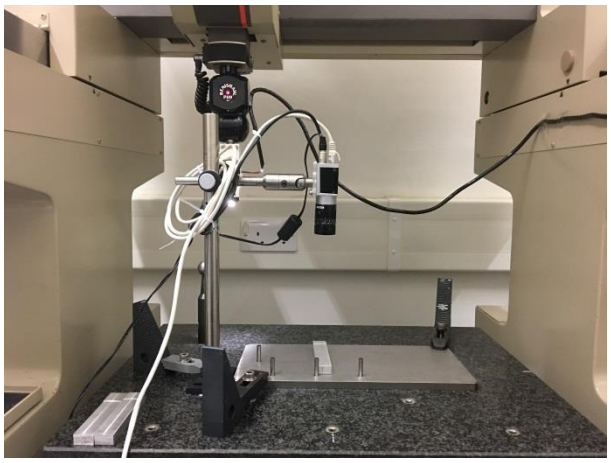

Figure 5.4 Using the PS system to measure the specimen produced by the CNC

The measurement result and measurement uncertainty obtained from the PS system were compared with the result derived from the standard contact method, using the stylus instrument. The specimen was calibrated with the commercial instrument (Surfcorder ET4000A). The degree of equivalence ratio (*En***)** is calculated by using equation 5.37 where x_{ref} is the reference value, x_i is the measured value, U_{ref} is the uncertainty from the reference instrument (Surfcorder ET4000A), and U_i is the measurement uncertainty of the PS system.

$$En = \left|x_{ref} - x_i\right| \Big/ \sqrt{U_{ref}^2 + U_i^2} \qquad (5.37)$$

The measurement results are summarized in Table 5.6. The 3D recovery profile of the surface roughness specimen using the PS system is illustrated in Figure 5.5, and the roughness average profiles are shown in Figure 5.6 whose z axis is properly scaled from the linear equation at a slant angle of 45^{o}.

Table 5.6 The result of surface roughness specimen measured from the PS method and the contact method.

Roughness specimen Nominal value	Standard Contact method		Photometric stereo method		En ratio
Ra(μm)	x_{ref} (μm)	U_{ref} (μm)	x_i (μm)	U_i (μm)	
9.0	9.05	0.04	7.46	1.26	0.13

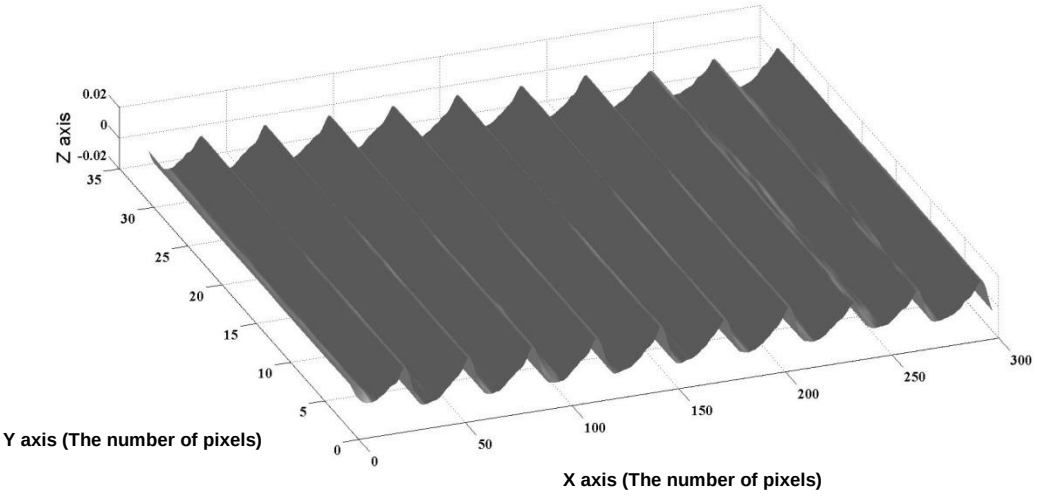

Figure 5.5 3D profile of surface roughness specimen produced by the CNC

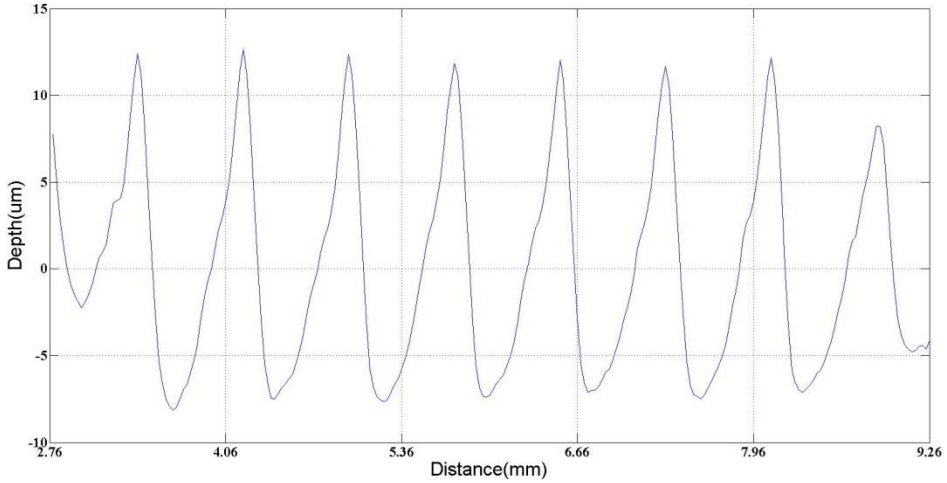

Figure 5.6 Surface roughness specimen produced by the CNC after using the linear regression model

5.8 Conclusion

Measurement uncertainty of the traditional photometric stereo method for measuring surface roughness has been built. The measurement uncertainty of the PS system for measuring surface roughness, which is shown at a 95% confidence level (k=2), is 1.26 µm at the nominal value of the roughness standard of 6.3 µm. From the uncertainty budget, the uncertainty of the width of a pixel component has a high value from the combined uncertainty, it seems that a quick way to reduce the uncertainty is to use a higher resolution camera. The smallest value of standard uncertainty is the uncertainty of temperature variation while the surface roughness standard being measured. The value is less than ten times in which comparing with the standard uncertainty of digital resolution. Therefore, the uncertainty of temperature variation does not affect the PS system. The En ratio used for the evaluation of performance on the PS system is less than 1, which shows that the system has a satisfactory performance for measuring surface roughness. To conclude, the PS technique have presented capabilities in surface roughness measurement with several advantages such as less expensive, simple and quick in operating procedure. It can be implied that the PS technique is suitable for measuring an object's surface roughness on on-line measurement within the engineering industry and this technique also can be used as a secondary option for surface roughness measurement.

Chapter 6 Form measurement using multi-source photometric stereo

6.1 Introduction

This chapter presents a multi-source photometric stereo technique using the advantages of the CMM to move the light source around an object precisely. This method is employed by using a hierarchical selection strategy to eliminate the effects of shadows and specularities for form measurement (Sun, et al., 2007). By using the proposed method, shape analysis after 3D surface reconstruction can be greatly enhanced. The object having more highlights created by a 3D printing machine is measured by the CMM as a reference value. This value is used to perform a linear regression with measurement results, which are showed as surface normal from each pixel, obtaining from the multi-source photometric stereo technique.

Several different methods have been applied for form measurement. The most common technique is the mechanical sensing of the traced specimen by a stylus. There are many disadvantages of this contact-type method. Firstly, the stylus of an instrument makes scratches on a measured surface. Secondly, the contact-type approach is possible to do changing in shape and distorting of the object caused by the probing force of the stylus.

Within the field of non-contact methods, they can be divided into ‘target-type’, where the measurement is of single, discrete, points which are features of the object (edges, lines, etc.) and ‘form-type’, where the measurement is of arbitrary points on a continuous surface such as the measurement of featureless surfaces and a body scanner.

6.2 Coordinate Measuring Machine (CMM)

An arc shape produced by a 3D printed machine was used in the experiment. It was measured by the Coordinate measuring machine (CMM) to obtain the height value. Specifications and measurement protocols for the instrument are now detailed.

All measurements reported in this experiment were performed on the CMM. It is absolutely essential that a sufficiency of air pressure should be enough for the CMM’s

movement as it is likely to damage x, y, and z axes. The arc shape used in the research is shown in Figure 6.1.

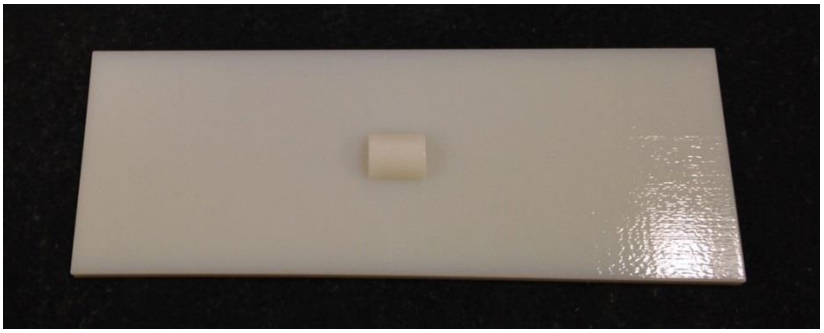

Figure 6.1 The arc shape utilized to be the specimen in the research

The arc shape shown in Figure 6.1 must be cleaned before initiation of measurement by the standard cleaning procedure described in Chapter 3. The following cleaning procedures have been applied. Firstly, the arc shape should be cleaned by using ethyl alcohol and wiped off with soft lint-free cloth or appropriate wiper. Secondly, the arc shape is stabilized at least 1 hour before measurement; the stabilization process is necessary because the geometric parameters of the object, as well as of the measuring instrument, depends on temperature and atmospheric pressure. For this reason, the calibration sample should be stored near the instrument in an environment that has been stabilized on temperature and humidity.

6.2.1 Initial setup of CMM

Below is a step-by-step protocol that was followed for the preparation and operation of the CMM, including screen shots from the related software packages. Brief comments are also included on the purpose of each of the procedures performed. The CMM specifications are as follows:

- Model: Mitutoyo CMMC-IS
- X-axis – measuring range of 500 mm, resolution of 0.001 mm
- Y-axis – measuring range of 300 mm, resolution of 0.001 mm
- Z-axis – measuring range of 270 mm, resolution of 0.001 mm, rube probe model PH9 Renishaw, tip radius of 1 mm

- The ambient temperature measured by a digital thermometer at 20 ± 3 ºC / relative humidity at 50 ± 10%.

The start-up sequence is as follows:

1) Turn on the pneumatic system for x, y, and z axes. This ensures that the air pressure is adequately supplied to avoid affecting measurement errors and damage the machine.
2) Check the air pressure from the pressure gauge under the granite table. Ensure that, the pressure gauge is between 4 kg/cm^2 and 5 kg/cm^2. This ensures that all the moving parts are able to perform reliable measurements.
3) Turn on the power of the control unit, probe head control unit, printer and personal computer in the CMM as shown in Figure 6.2 and leave it to be stabilized for least 30 minutes. The stabilization period is necessary because the electrical characteristics of the electronics are temperature-dependent and the temperature distribution takes the time to reach the equilibrium state after the system is powered on.

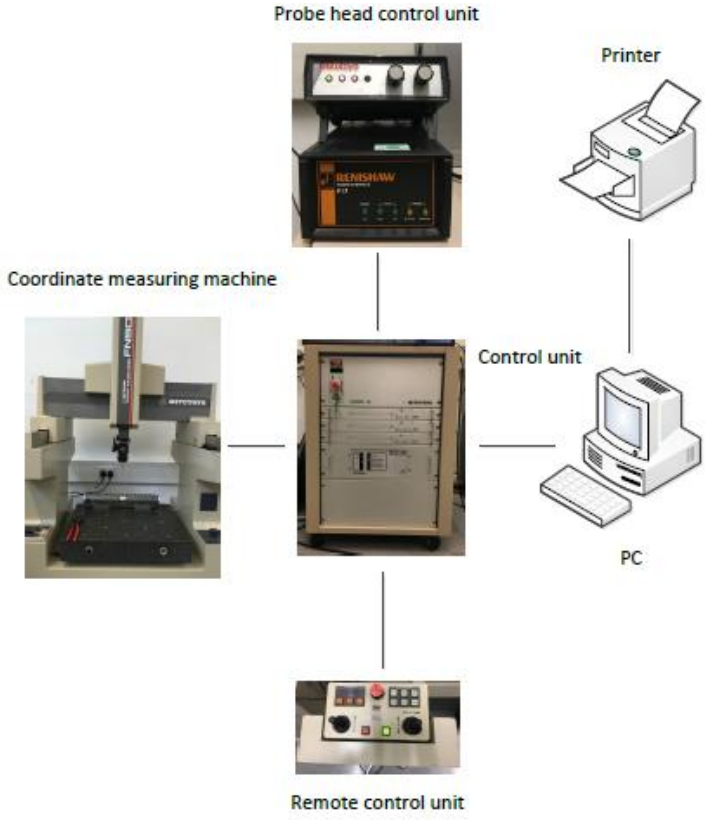

Figure 6.2 Schematic diagram of the CMM

Figure 6.3 Screenshot of the computer desktop containing the CMM software start-up icon

4) Double click the MCOSMOS v3.0 application icon on the computer desktop as illustrated in Figure 6.3 and then press the start button on the remote control unit. The instrument will initialize along x, y, and z axes. When the CMM has already finished initialization, the probe system can be moved around the arc shape.
5) Before the experiment is performed, the probe builder window has been defined as shown in Figure 6.4; each part comprised as the probe system must be added in probe builder window, and then the Swivel Length value will be automatically calculated by their chosen parts.
6) The next step is to calibrate the probe system with a CMM master ball. Each master ball is designated to a particular CMM, and the master ball should be maintained, including periodic measurements of check standards. When the probe is calibrated by master ball, the software shows the actual value of probe diameter. All the measurements performed after using probe calibration are accurate because the values evaluated from the CMM are compensated error from the true diameter of probe.

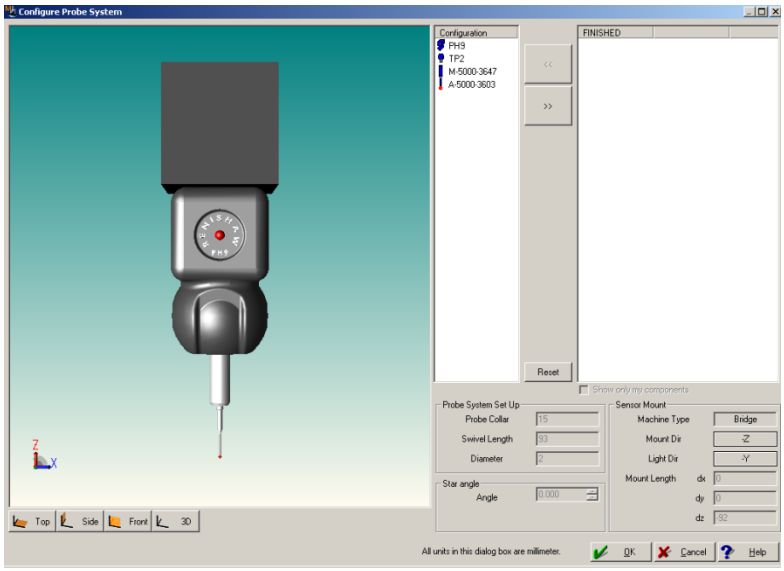

Figure 6.4 Probe builder selection window of the CMM software

The configuration selection window of the probe builder displays each item contained in the probe system. Its graphical display is shown on the left of panel display.

6.2.2 Form measurement determined by the CMM

The form measurement sequence on the CMM is as follows:

1) Put the arc shape in the middle position of the instrument table as shown in Figure 6.5.

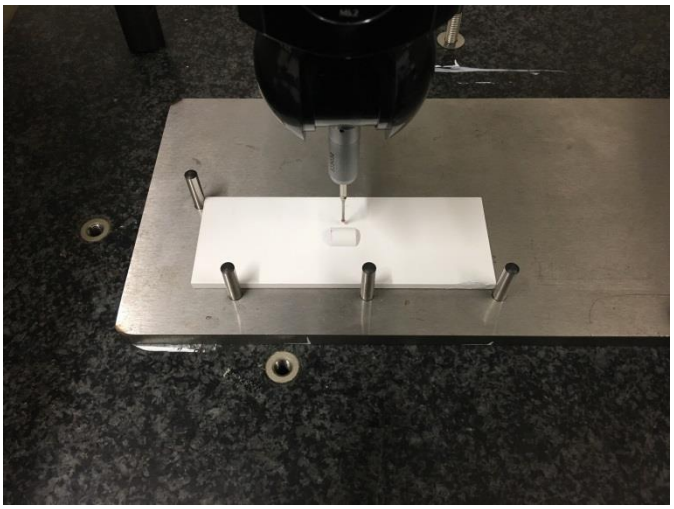

Figure 6.5 The arc shape is placed in the middle of instrument

2) Create a co-ordinate system on the arc shape.
3) By using remote control unit, the probe system is moved until the stylus is close to the surface of the arc shape.
4) Having selected a geometric element, the arc shape is based on choosing a contour function. The software will then show the measurement method on the computer screen.
5) Design the measuring distance, a number of points and geometric plane.
6) After finishing contour measurement, choose a circle function and then select a connect element to create a connection line on arc shape.
7) Save the results of measurement.
8) After finishing the measurement, move the probe from the arc shape and remove the arc shape from the table. The probe should move back to the start position of the CMM.

6.2.3 Measurement results

The measuring experiments were conducted using the CMM as shown in Figure 6.6. The measurement was set up on the table of CMM and a clamping device. The contour function on MCOSMOS V3.0 was applied for measuring the arc circle. The experimental results are shown in Table 6.1. The reported radius of the arc shape is the average of five-time measurements in fixed orientation.

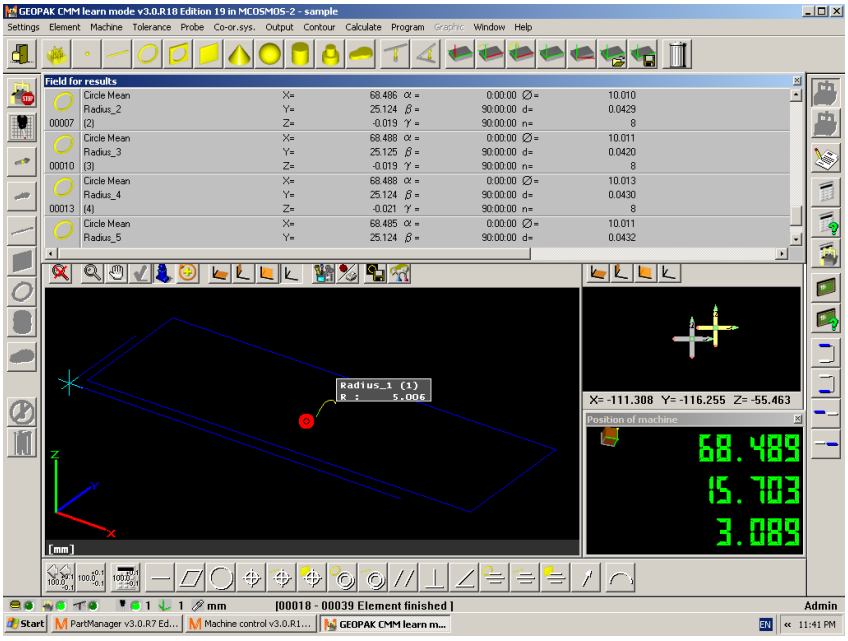

Figure 6.6 The arc shape measured by the CMM at centre position

Table 6.1 The measurement results from the arc shape determined by the CMM

Radius(mm)	Number of measurement					Average (mm)
	1	2	3	4	5	
5	5.006	5.007	5.006	5.007	5.005	5.006

6.3 Proposed Method for measuring the arc shape

The setup of the multi-source photometric stereo method on the CMM is similar to the traditional PS method, but the essential difference is that the light source positions have to perform the new calibration. As mentioned in Figure 4.3, the light source positions were calibrated at three positions, which are the minimum positions of the PS method. In this experiment, we also show 3D profiles that can recover from four and six source positions to compare 3D profile from the traditional PS method. As shown schematically in Figure 6.7(a) and (b), a collimated beam of light rays illuminates into curved specimen denoted by a hemisphere with a camera mounted perpendicular to itself. The hemisphere is represented a general case. It is found that the shadow region on the hemisphere always shifts with incident angles. As can be seen from Figure 6.7(a), the illuminated light is to cover all visible positions on the object surface when the light is incident directly on the object. If the angle of incidence approaches 90^{o} to the vertical axis, the entire visible object is to be fully illuminated. The light is then equally separated above the equatorial plane and symmetrically distributed over two sides of the object. Providing that there be three couples of such lights, every surface patch or region on the curved object is to be illuminated by three or more light sources. Traditionally, the photometric stereo method has been used three light sources. Figure 6.7(c) shows that the hemisphere placed in the center of the plane is symmetrically shined by six light sources. Interestingly, for the surface of the illuminated hemisphere, it can be separated into four region types; blank areas are illuminated by three lights, areas with one pattern are illuminated by four light sources, areas overlapped by two texture patterns are illuminated by five light sources, and regions overlapped by three patterns are illuminated by six light sources. Six light sources are the minimum positions needed to cover all visible points of the hemisphere (Hernandez, et al., 2008; Hin-Shun and Jiaya, 2008; Lee and Kuo, 1992).

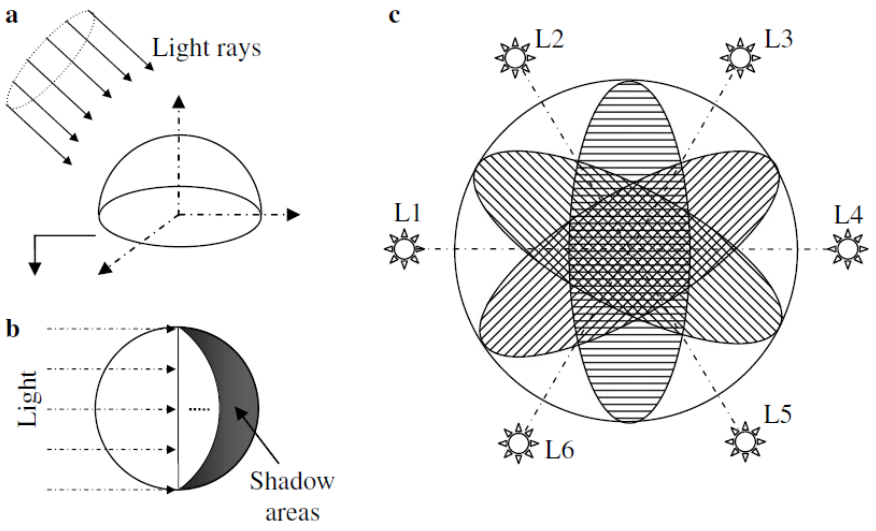

Figure 6.7(a) a convex object under a beam of collimated light, (b) projection of the light onto the object, (c) setting six distant point light sources

6.3.1 Light source position estimation

Following the concept of six light sources photometric stereo method, the positions of the light source must be calibrated. The calibration method is similar to the traditional photometric stereo. The light source is moved six positions around the hemisphere, in which it is placed in the center of CMM's table, to calculate light directions. The positions of the light source are sequentially moved as shown in Figure 6.8. As the experimental results from Table 4.5, the best slant angle is 45^{o} for our system. This angle is chosen for each tilt angle for our design.

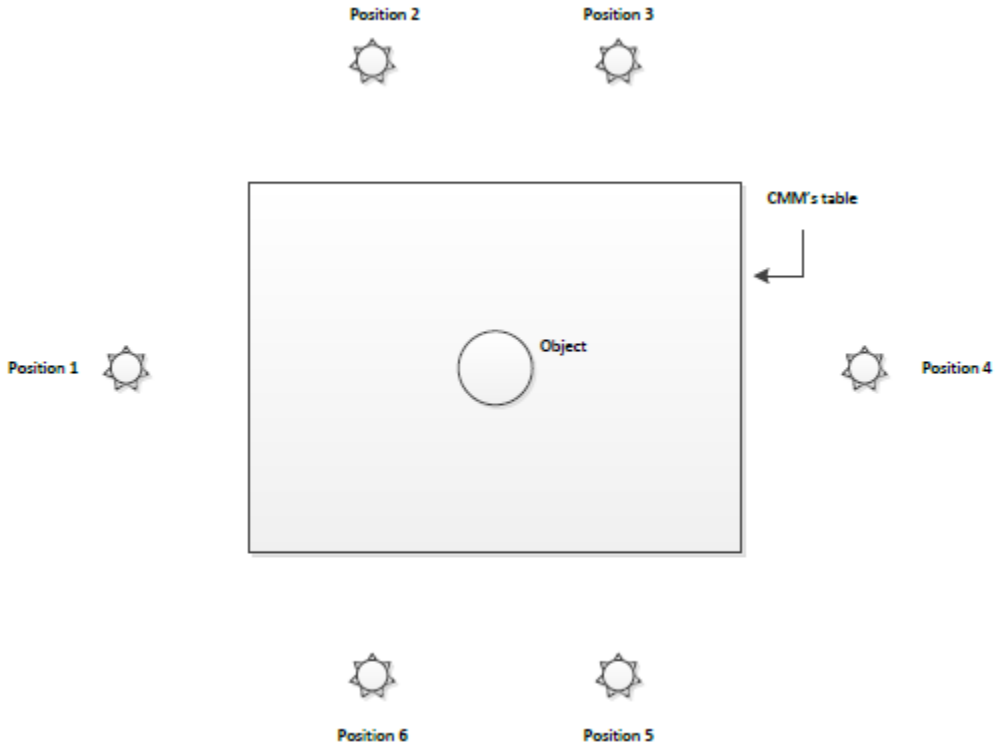

Figure 6.8 All light source positions

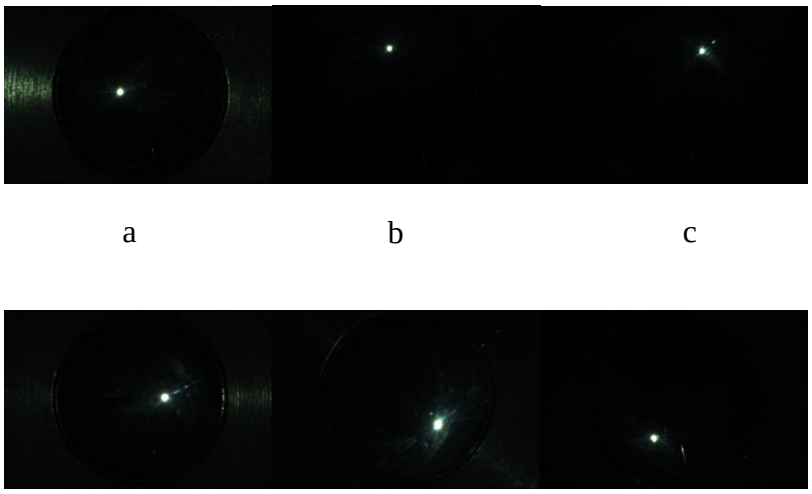

a b c

d e f

Figure 6.9 (a) light source at position 1 (b) light source at position 2 (c) light source at position 3 (d) light source at position 4 (e) light source at position 5 (e) light source at position 6

Figure 6.9(a), (b), (c), (d), (e), and (f) show the results of the real images of the hemisphere, illuminated sequentially by lighting angles.

6.3.2 Form and shape recovery system

The 3D printing machine used to produce a specimen has been installed at Brunel University London. The object was designed with an arc shape, having a radius of 5 mm. The object was placed on the CMM that its centre coincides with the image centre.

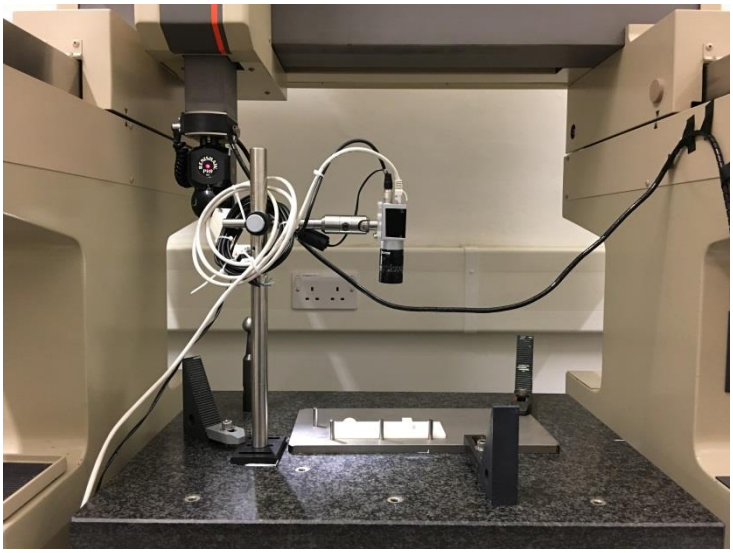

Figure 6.10 The arc shape positioned on the CMM

As shown in Figure 6.10, the object produced from the 3D printing machine has a more specular highlight. In this experiment, the multi-light photometric stereo method is utilized to eliminate the specular effect. The experimental setup used for the real pictures consist of Digital Gigabit Ethernet camera with 25× optical zoom lens. The front of the arc shape was located 194 mm from the camera lens. One spot light source, the neutral white LED was installed with the CMM's probe, which performed to move following positions as shown in Figure 6.8. It can be precisely shifted around the arc shape whose position was placed at the center of the camera. Three, four and six images then were acquired, corresponding to the different lighting conditions, each light direction active in different positions as shown in Figure 6.11, 6.12 and, 6.13 respectively.

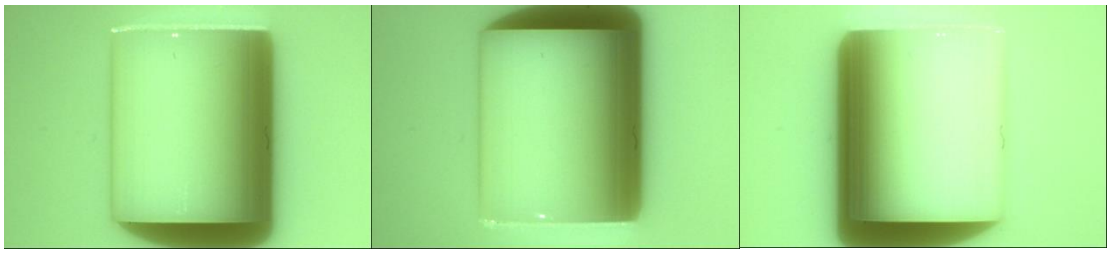

Figure 6.11 All pictures taken by 3-source photometric stereo technique

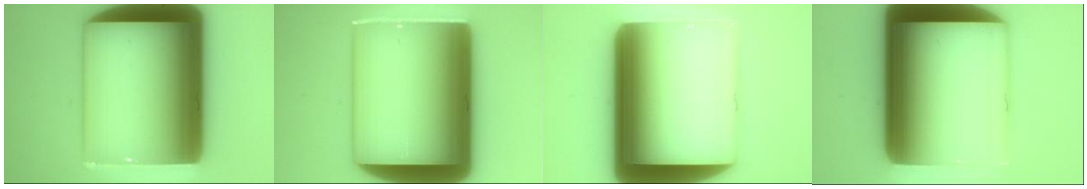

Figure 6.12 All pictures taken by 4-source photometric stereo technique

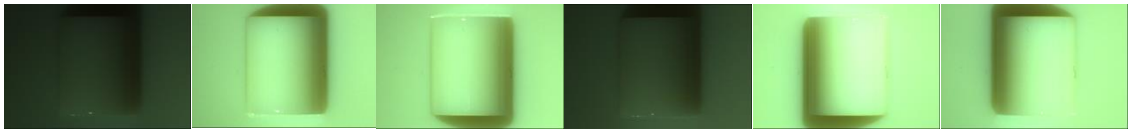

Figure 6.13 All pictures taken by 6-source photometric stereo technique

After recovery these images to 3D surface profiles, it is cropped into a 300×30 pixel sizes. The profile recovered by the traditional photometric stereo technique was assessed the efficiency of surface recovery experiments by comparing its profiles to surface recovered from 4-source and 6-source photometric stereo techniques.

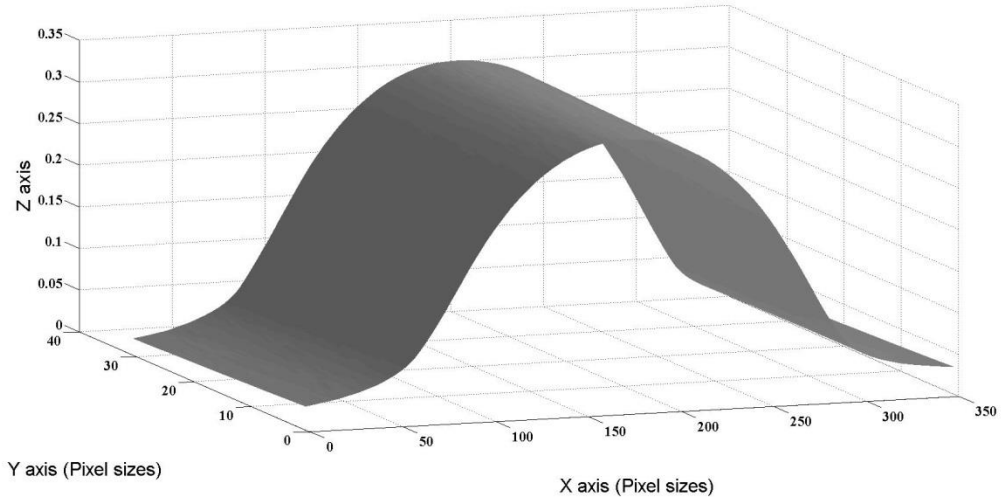

Figure 6.14 3D profile recovered by 3-source photometric stereo technique

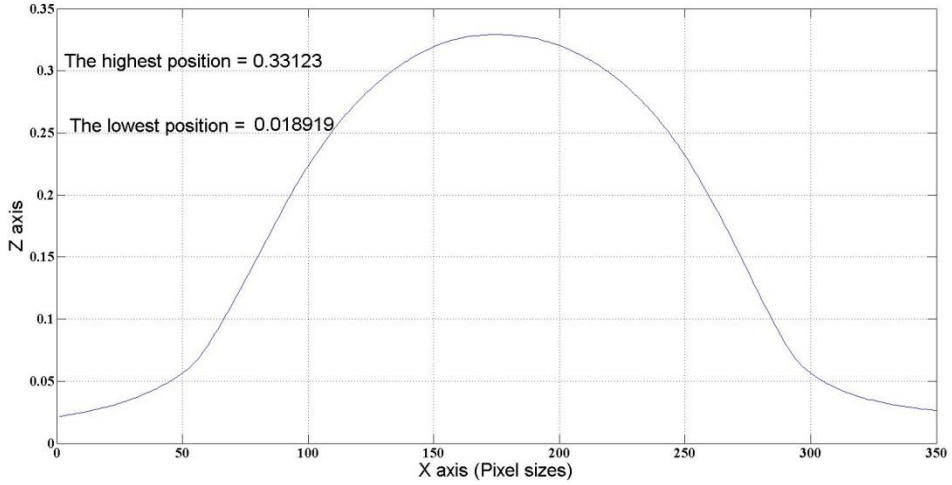

Figure 6.15 The line profile at center position recovered from 3-source photometric stereo technique

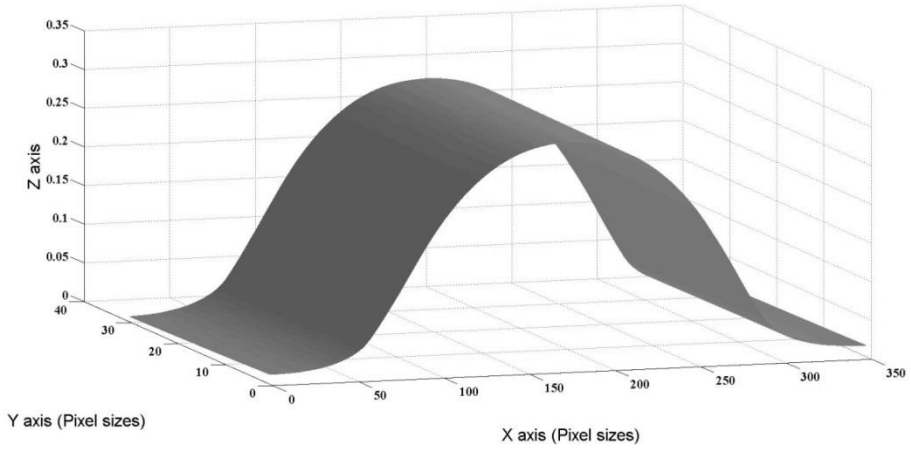

Figure 6.16 3D profile recovered by 4-source photometric stereo technique

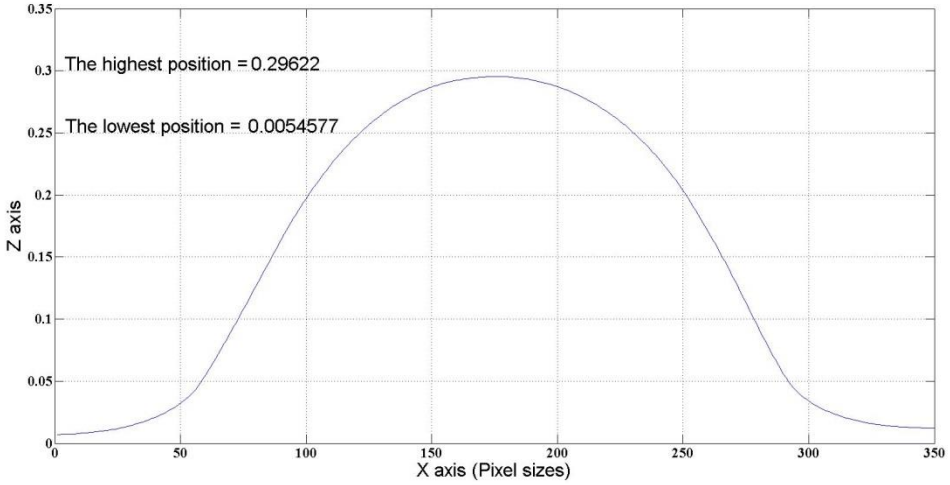

Figure 6.17 The line profile at center position recovered from 4-source photometric stereo technique

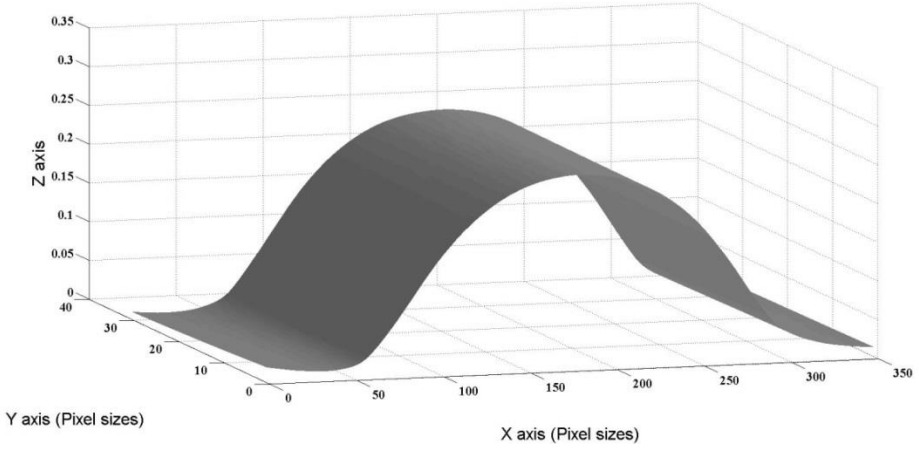

Figure 6.18 3D profile recovered by 6-source photometric stereo technique

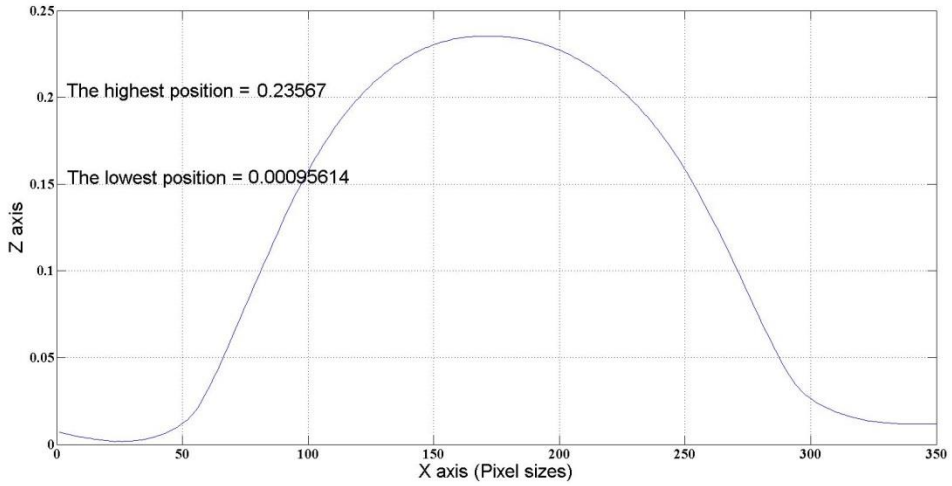

Figure 6.19 The line profile at centre position recovered from 6-source photometric stereo technique

As can be seen from the line profile from each method, the greatest recovery surface is performed by the 6-source photometric stereo technique because the arc shape is recovered symmetrically and the 2-dimensional pattern is closest to the reference plane. Although this method is more robust and accurate than the other method, regarding the time duration for the procedure of surface recovery, it requires a little more time for image processing.

The line profile from 6-source photometric stereo technique is used to compare the accuracy of our system with the line determined from the CMM. In the case of transformation pixel sizes in x-axis to length measurement, the working standard scale was utilized. In the event of transformation surface normal in z axis to length measurement, the arc shape is calibrated by the CMM to confirm the true values. The equation of a straight line graph is utilized to convert surface normals to the dimensional measurement of the z-axis. The general equation of a straight line graph is

$$y = mx + c \tag{6.1}$$

where m is the gradient of a straight line graph and c is the y-axis intercept. Using equation 6.1, the equation of our system can be written

$$y_1 = mx_1 + c \tag{6.2}$$

$$y_2 = mx_2 + c \tag{6.3}$$

y_1 and y_2 are the results measured from the CMM in Table 6.1, and x_1 and x_2 are the results recovered from the 6-source photometric stereo technique. The results from both measurements are placed on equations as shown

$$0 = 0.001m + c \tag{6.4}$$

$$5.006 = 0.236m + c \tag{6.5}$$

Equation 6.5 is subtracted from equation 6.4

$$5.006 = 0.235m \tag{6.6}$$

The gradient is 21.302 and c is -0.021. The equation for changing surface normals in z-axis from Figure 6.19 to be length measurement is shown

$$y = 21.302x - 0.021 \tag{6.7}$$

From equation 6.7, we can change the z-axis in Figure 6.19 to mm, and then the x-axis is transformed to mm by pixel calibration from equation 4.17. Figured 6.19 can be modified to new scales in x and y axes as illustrated in Figure 6.20.

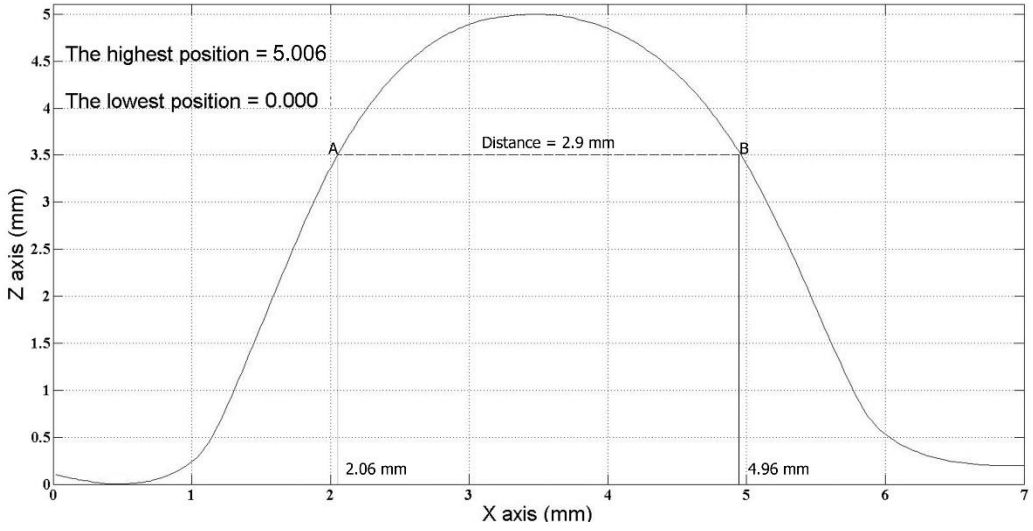

Figure 6.20 The line profile after changing the scales

The next step of our research, the distance between positions A and B from Figure 6.20 evaluated from proposed method will be compared measurement result with the CMM. Both points have an interval 2.9 mm. This result is to be compared with the result

determined by the CMM whose each value is positioned and acquired results at matching position.

6.3.3 Measurement results

The following experiments are designed to verify the accuracy of the 6-source photometric stereo imaging system and the performance for shape and form measurements. A commercial CMM are being employed as a reference for comparing results. To quantify the error of distance between position A and B obtained from the 6-source photometric stereo, comparing it with the distance determined from the CMM having higher accuracy. The result in Table 6.2 shows the measurement results from the 6-source photometric stereo and Table 6.3 shows the measurement results from the CMM.

Table 6.2 Measurement results of positions A and B by the 6-source photometric stereo technique

Distance between A and B (mm)	Results measured by the 6-source photometric stereo technique					Average (mm)
	1	2	3	4	5	
2.90	2.901	2.900	2.901	2.902	2.898	2.900

Table 6.3 Measurement results of positions A and B by CMM

Distance between A and B (mm)	Results measured by the CMM					Average (mm)
	1	2	3	4	5	
2.90	3.029	3.030	3.029	3.031	3.032	3.030

As shown the average value from table 6.2 and 6.3, the measurement error can be calculated from the following expression:

$$\text{Error} = \text{unknown} - \text{standard} \tag{6.8}$$

$$= 2.90 - 3.03$$

$$= -0.13 \text{ mm}$$

Unknown is averaged value of positions A and B determined by the 6-source photometric stereo technique, and standard value is averaged value of positions A and B determined by the CMM. The percent error can be evaluated as follows:

$$\%error = |(unknown - standard)/standard| \cdot 100 \quad (6.9)$$

$$= 4.29$$

6.4 Conclusion

This chapter has presented the multi-source photometric stereo system for recovering surface shape and improving 3D surface reconstruction performance, using the movement of CMM's probing. The arc shape manufactured by 3D printing machine were used as a standard form measurement in the research. The 3D profile, measured by multi-source photometric stereo, provided a symmetrical shape more than the 3D profile recovering from traditional PS method. Moreover, the arc shape manufactured by shiny material, the multi-source PS system system was utilised to improve both specular reflections and shadowing contributions with a shiny object. In addition, full recovery of the arc shape in the three-dimensional surface was used to present more detail of surface characteristics than contact method. The measuring points between A and B after surface recovering were made a comparison measurement with the CMM. The measurement error is -0.13 mm. In summary, the PS technique can be used to measure arc shape's width and the results have shown less error compared to the results measured by CMM. However, this technique is not suitable to measure an object having a shape edge because the light cannot be shined cover in that area, affecting loss reconstructed surface.

Chapter 7 Conclusion and recommendation for future work

7.1 Conclusions

In order to accomplish the aim and objectives of the research approach, the experimental and simulation results are implemented, analysed, compared, and discussed in previous chapters. The distinctive conclusions can be summarised in this chapter

1) The surface roughness standards are calibrated by stylus instrument to establish the reference values of average roughness. Thus, its values are utilised as the standard values of average roughness measured by the PS method. The surface normals from the PS method can be changed as the unit length using least square technique. The accuracy values of surface roughness standards and measurement uncertainty have an affect with the PS method because its values are used as the reference values.
2) The accuracy values of surface roughness standards and measurement uncertainty can be minimised and reduced by using the high precision roughness instrument because the standard uncertainty type A is calculated in terms of repeatability. The high precision roughness instrument is to provide good repeatability and high accuracy. Moreover, the surface roughness standards shall also be sent to accredited calibration laboratory for reduction measurement uncertainty and increased confidence in measurement results.
3) The three-dimensional surface recovery method is proposed for average surface roughness investigation based on the photometric stereo method at the five values surface roughness standards can work extremely well for obtaining the completely surface characteristics. Its surface characteristics depend on light source direction. Each surface specimen has a differential reflection, relating directly to recovering surface. In the traditional PS method, four-different slant angles of the light source holding with CMM's probe system were experimentally done, and the best slant angle was suitable for recovery surface roughness standard profiles as 45^{o}, evaluated by the coefficient of determination. The coefficient of determination, denoted by R^2, of slant angle at 45^{o} was 0.99.

4) In order to separate the roughness component from waviness and form components, a filter being the most common filter in surface metrology is the Gaussian filter. It is used for mean-line creation using a digital low-pass filter and then calculating the deviation of the profile from the mean line. The original profile from the PS method convoluted by the mean line from the standard Gaussian Filter is separated only surface roughness profile departing waviness and form profiles. Roughness average (R_a) can be then evaluated by equation (4.35), and (4.36), created from surface normals along pixels.
5) As results with specified uncertainties in the PS system from measuring *Ra*, the measurements results will be traceable to the SI. The measurement uncertainty of the PS system for measuring surface roughness, which is shown at 95% confidence level (k=2), is 1.26 μm at the nominal value of roughness standard 6.3 μm. The En ratio used for evaluation of performance on our system is less than 1, which is shown that the system has satisfactory performance for measuring surface roughness.
6) The six-source PS technique is stronger than traditional PS technique as the 3D profile of the arc shape, measured by six-source PS technique, has more symmetrical than the 3D profile from traditional PS technique.

7.2 Recommendations for future work

The future work is recommended into two parts. Firstly, it is the ideas which can directly improve the surface roughness measurement using the PS method with the CMM. Secondly, some ideas are suggested for further work to be considered as future research lines. Thus, the suggestions for future action are recommended as the following areas:

Further work which can directly improve:

1) On the surface roughness standard, the specimen using for measurement system should have surface varieties or surface occurring from many methods to produce it such as grinding, milling, turning, and finishing.
2) The specular component of surface roughness measurement is not concerned. Some points on surface reconstruction may show the effect of shadows. The best way to improve them is to apply four-source PS method which eliminates the effect of

shadows and surface recovering results will provide more accurate three-dimensional surface texture properties (Rushmeier, et al., 1997).

3) The most value of combined uncertainty coming from the “Pixel of camera” component, it seems that a quick way to reduce the uncertainty is to use a higher resolution camera.
4) The images are captured under different positions of the light source, six positions shifted by CMM’s probing, for reducing the highlight spots which show on the surface object. It is likely to increase the number of images of a surface illuminated from different lighting positions; it is possible to increase the chance to acquire high-quality surface reconstruction.

Further work along this research line

1) A hybrid scanner system is to include the advantages of PS method and stereo triangulation to combine information about the geometry in the form of three-dimensional positions and normal information. In this method, one class integrates normals to yield a surface and then merges the resulting mesh with the measured position as the final step.

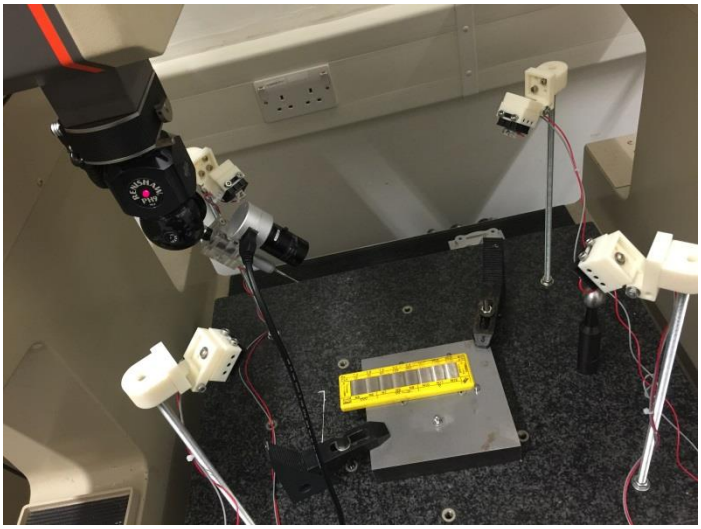

Figure 7.1 Hybrid scanner design on CMM

2) This work investigates Ra of three-dimensional surface texture using the PS technique. Surface gradient and albedo information can be recovered by using each picture of photometric images in which the light source direction is known. In the industrial manufacturing and real world, the illumination directions shining into

object's surface are unknown because the measured object normally determines in normal environmental condition. The position of illumination sources is extremely difficult to calibrate the directions of light source precisely. This will be led the investigation of non-calibrated photometric stereo.

References

Ababasa, F., Roussel, D. and Mallem, M. (2003) “Photometric aspects: a new approach for 3D free form object recognition using a single luminance image”, *Seventh International Symposium on Signal Processing and Its Applications.* , pp. 423-426.

Ahmad, J., Sun, J., Smith, L. and Smith, M. (2014) “An improved photometric stereo through distance estimation and light vector optimization from diffused maxima region”, *Pattern Recognition Letters,* 50, pp. 15-22.

Alberto Tomita, J. and Ishii, R. (1996) “Determining the orientation of a person's hand by using the photometric stereo method”, *IEEE IECON 22nd International Conference on Industrial Electronics, Control, and Instrumentation,* Taipei: IEEE, pp. 303-308.

ASME B46.1 (2002), *Surface Texture (Surface Roughness, Waviness and Lay),* The American Society of Mechanical Engineers, New York, USA.

Atkinson, G.A., Hansen, M.F., Smith, M.L. and Smith, L.N. (2010) “A efficient and practical 3D face scanner using near infrared and visible photometric stereo”, *Procedia Computer Science,* 2(0), pp. 11-19.

Barakat, N.A., Elbestawi, M.A. and Spence, A.D. (2000) “Kinematic and geometric error compensation of a coordinate measuring machine”, *International Journal of Machine Tools and Manufacture,* 40(6), pp. 833-850.

Barnard, S.T. and Fishler, M.A. (1982) “Computational stereo”, *ACM Computing Survey,* 14(4), pp. 553-572.

Barsky, S. and Petrou, M. (2003) “The 4-source photometric stereo technique for three-dimensional surfaces in the presence of highlights and shadows”, *IEEE Transactions on Pattern Analysis and Machine Intelligence,* 25(10), pp. 1239-1252.

Bell, S. (2001) “A Beginner's Guide to Uncertainty of measurement”, UK: NPL.

Bhushan, B. (2001) “Modern Tribology handbook”, CRC Press.

Coleman, J.E. and Jain, R. (1982) “Obtaining 3-dimensional shape of textured and specular surfaces using four-source photometry”, *Computer graphics and image processing,* 18(4), pp. 309-328.

Davidson, M., Kaufman, K., Mazor, I. and Cohen, F. (1987) “An Application of Interference Microscopy to Intergrated Circuit Inspection and Metrology”, *SPIE,* pp. 233-240.

Dietrich, C.F. (1991) “Uncertainty, Calibration and Probability”, 2nd ed. UK: Adam Hilger.

Drbohlav, O. and Chantler, M. (2005) “On optimal light configurations in photometric stereo”, *Tenth IEEE International Conference on Computer Vision,* pp. 1707-1712.

EA-4/02 (1999) “Expression of the Uncertainty of Measurement in Calibration”.

EAL-G17 (1995) “Coordinate Measuring Machine Calibration”.

Favaro, P. and Papadhimitri, T. (2012) “A closed-form solution to uncalibrated photometric stereo via diffuse maxima”, *2012 IEEE Conference on Computer Vision and Pattern Recognition (CVPR),* pp. 821-828.

Forbes, A.B. (2012) “Approaches to evaluating measurement uncertainty”, *International Journal of Metrology and Quality Engineering,* 3(2), pp. 71-77.

Gregory, J.W. (1992) “Measuring and modeling anisotropic reflection”, *Proceedings of the 19th annual conference on Computer graphics and interactive techniques,* New York, USA., pp. 265-272.

GUM (1993) “Guide the Expression of Uncertainty in Meaurement”, International Organisation for Standardisation.

Hansen, M.F. and Atkinson, G.A. (2010) “Biologically inspired 3D face recognition from surface normal”, *Procedia Computer Science,* 2(0), pp. 26-34.

Hariharan, P. (2003) “Optical Interferometry” 2nd ed. UK: Elsevier Science.

Harker, M. and O’Leary, P. (2013) “Direct regularized surface reconstruction from gradients for Industrial Photometric Stereo”, *Computers in Industry,* 64(9), pp. 1221-1228.

Hayakawa, H. (1994) “Photometric stereo under a light source with arbitrary motion”, *JOSA A,* 11(11), pp. 3079-3089.

Healey, G. and Binford, T.O. (1988) “Local shape from specularity”, *Computer Vision, Graphics, and Image Processing,* 42(1), pp. 62-86.

Hernandez, C., Vogiatzis, G. and Cipolla, R. (2008) “Multiview Photometric Stereo”, *IEEE Transactions on Pattern Analysis and Machine Intelligence,* 30(3), pp. 548-554.

Hin-Shun, C. and Jiaya, J. (2008) “Efficient photometric stereo on glossy surfaces with wide specular lobes”, *IEEE Conference on Computer Vision and Pattern Recognition, 2008,* pp. 1-8.

Ho, Y.X., Landy, M.S. and Maloney, L.T. (2006) “How direction of illumination affects visually perceived surface roughness”, *Journal of vision,* 6(5), pp. 634-648.

Horn, B.K.P. (1989) “Shape from shading”, UK: MIT Press.

Horn, B.K.P. (1986) “Robot vision”, UK: MIT Press.

Horn, B.K.P. (1975) “Obtaining shape from shading information” US: P.H. Winston.

Horn, B.K.P., Woodham, R.J. and Silverwilliam, M. (1978) “Determining shape and reflectance using multiple images”.

Horovitz, I. and Kiryati, N. (2004) “Depth from gradient fields and control points: bias correction in photometric stereo”, *Image and Vision Computing,* 22(9), pp. 681-694.

Ikehata, S., Wipf, D., Matsushita, Y. and Aizawa, K. (2014) “Photometric Stereo Using Sparse Bayesian Regression for General Diffuse Surfaces”, *IEEE Transactions on Pattern Analysis and Machine Intelligence,* 36(9), pp. 1816-1831.

Ikeuchi, K. (1987) “Determining a Depth Map Using a Dual Photometric Stereo”, *The International Journal of Robotics,* 6(1), pp. 15-31.

Ikeuchi, K. (1981) “Determining Surface Orientations of Specular Surfaces by Using the Photometric Stereo Method”, *IEEE Transactions on Pattern Analysis and Machine Intelligence,* 3(6), pp. 661-669.

Ikeuchi, K. and Horn, B.K.P. (1981) “Numerical shape from shading and occluding boundaries”, *Artificial Intelligence,* 17(3), pp. 141-184.

ISO 10360-2: (2009) Geometrical product specifications (GPS) - Acceptance and reverification tests for coordinate measuring machines (CMM) – Part 2: CMMs used for measuring size. International Organization for Standardization.

ISO 11562: (1996) Geometrical Product Specification (GPS) - Surface Texture: Profile Method - Metrological Characteristic of Phase Correct Filters. International Organization for Standardization.

ISO 12179 (2000) Geometrical Product Specifications (GPS)-Surface texture: Profile method - Calibration of Contact (Stylus) instruments. International Organization for Standardization.

ISO 13360-1 (2001) Geometrical Product Specifications (GPS) - Acceptance and reverification tests for coordinate measuring machines (CMM). International Organization for Standardization.

ISO 16610-21 (2012) Geometrical product specifications (GPS) - Filtration. International Organization for Standardization.

ISO 16610-61 (2015) Geometrical Product Specifications (GPS) – Filtration Part61: Linear areal filters – Gaussian filters ISO /CASCO 17043:2010, Conformity assessment – General requirements for proficiency testing. International Organization for Standardization.

ISO 3274 (1998) Geometric Product Specifications (GPS) - Surface texture: Profile method - Nominal characteristics of contact (stylus) instruments. International Organization for Standardization.

ISO 4287 (1998) Geometrical product specification (GPS) - Surface texture: Profile method - Terms, definitions and surface texture parameters. International Organization for Standardization.

ISO 4288 (1998) Geometric Product Specification (GPS) - Surface texture - Profile method: Rules and procedures for the assessment of surface texture. International Organization for Standardization.

ISO 5436 (2000) Geometrical Product Specification(GPS) - Surface texture: Profile method; Part 1: Material measures. International Organization for Standardization.

ISO/CASCO 17043 (2010) Conformity assessment – General requirements for proficiency testing. International Organization for Standardization.

JCGM 100.2008 (2008) Evaluation of measurement data - Guide to the expression of uncertainty in measurement(GUM).

Karris, S.T. (2007) "Numerical Analysis Using MATLAB and Excel", 3rd ed. US: Orchard Publications.

Kee, S.C., Lee, K.M. and Lee, S.U. (2000) "Illumination invariant face recognition using photometric stereo", *Machine Vision and Applications*, 3(7).

Kim, B. and Burger, P. (1988) "Calculation of surface position and orientation using the photometric stereo method", *Computer Society Conference on Computer Vision and Pattern Recognition,* pp. 492-497.

Kolagani, N. and Blidberg, D.R. (1992) "Photometric stereo using point light sources", *IEEE International Conference on Robotics and Automation*, pp. 1759 - 1764.

Kumar, R., Kulashekar, P., Dhanasekar, B. and Ramamoorthy, B. (2005) "Application of digital image magnification for surface roughness evaluation using machine vision", *International Journal of Machine Tools and Manufacture*, 45(2), pp. 228-234.

Krystek, M. (2001) "Measurement uncertainty propagation in the case of filtering in roughness measurement", *Measurement Science and Technology*, 12(1), pp. 63.

Leach, R. (2011) "Optical Measurement of Surface topography", UK: Springer.

Leach, R. (2010) "Funamental Principles of Engineering Nanometrology", 1st ed. USA: Elsevier Inc.

Leach, R. (2001) "Measurement Good Practice Guide NO.37, The Measurement of Surface Texture using Stylus Instruments", UK: NPL.

Leach, R., Brown, L. and Jiang, X. (2008) "Guide for the Measurement of Smooth Surface Topography using Coherence Scanning Interferometry", UK: NPL.

Leclerc, Y.G. and Bobick, A.F. (1991) "The direct computation of height from shading", *IEEE Computer Society Conference on Computer Vision and Pattern Recognition,* pp. 552-558.

Lee, B.S. and Strand, T.C. (1990) "Profilometry with a coherence scanning microscope", *Applied Optics*, 29(26), pp. 3784-3788.

Lee, C.H. and Rosenfeld, A. (1985) “Improved methods of estimating shape from shading using the light source coordinate system”, *Artificial Intelligence,* 26(2), pp. 125-143.

Lee, K.M. and Kuo, C.C.J. (1992) “Shape reconstruction from photometric stereo”, *IEEE Computer Society Conference on Computer Vision and Pattern Recognition*, pp. 479-484.

Lee, K.M. and Kuo, C.J. (1993) “Surface reconstruction from photometric stereo images”, *JOSA A,* 10(5), pp. 855-868.

Lee, B.Y. and Tarng, Y.S. (2001) “Surface roughness inspection by computer vision in turning operations”, *International Journal of Machine Tools and Manufacture,* 41(9), pp. 1251-1263.

Lina, B., Zhan, S. and Linmin, X. (2014) “A novel LCD based photometric stereo method”, *2014 4th IEEE International Conference on Information Science and Technology (ICIST)*, pp. 611-614.

Liu, T.Y., Hsu, W.H. and Chen, Y.H. (1992) “Shape description via shading images”, *Image and Vision Computing,* 10(1), pp. 46-54.

Lv, H., Cai, Y. and Guo, S. (2012) “3D reconstruction of tongue surface based on photometric stereo”, *2012 IEEE 11th International Conference on Signal Processing,* pp. 1668-1671.

Maria, E.A. and Maria, P. (2014) “Evaluating the effect of diffuse light on photometric stereo reconstruction”, *Machine Vision and Applications,* 25(1), pp. 199-210.

Mears, L., Roth, J.T., Djurdjanovic, D., Yang, X. and Kurfess, T. (2009) “Quality and inspection of machining operations: CMM integration to the machine tool”, *Journal of manufacturing science and engineering,* 131(5).

MINAMITANI, H. (1993) “A new photometric method using 3 point light sources”, *IEICE Transactions on Information and Systems,* 76(8), pp. 898-904.

Nayar, S.K., Ikeuchi, K. and Kanade, T. (1989) “Determining shape and reflectance of Lambertian, specular, and hybrid surfaces using extended sources”, *International Workshop on Industrial Applications of Machine Intelligence and Vision, 1989,* IEEE, pp. 169-175.

Nayar, S.K., Sanderson, A.C., Weiss, L.E. and Simon, D.A. (1990) “Specular surface inspection using structured highlight and Gaussian images”, *IEEE Transactions on Robotics and Automation,* 6(2), pp. 208-218.

Nevatia, R. (1976) “Depth measurement by motion stereo”, *Computer Graphics and Image Processing,* 5(2), pp. 203-214.

Okatani, T. and Deguchi, K. (2012) “Optimal integration of photometric and geometric surface measurements using inaccurate reflectance/illumination knowledge”, *2012 IEEE Conference on Computer Vision and Pattern Recognition (CVPR)*, pp. 254-261.

Onn, R. and Bruckstein, A. (1990) “Integrability disambiguates surface recovery in two-image photometric stereo”, *International Journal of Computer Vision*, 5(1), pp. 105-113.

Palm, W.J. (2005) “Introduction to Matlab 7 for Engineers”, US: McGraw-Hill.

Ping-Sing, T. and Shah, M. (1994) “Shape from shading using linear approximation”, *Image and Vision Computing*, 12(8), pp. 487-498.

Radler, B., Harker, M., O'Leary, P. and Lucyshyn, T. (2016) “Non-contact measurement of circular surfaces via photometric stereo in polar coordinates”, *2016 IEEE International Instrumentation and Measurement Technology Conference Proceedings*, pp. 1-6.

Raja, J., Muralikrishnan, B. and Fu, S. (2002) “Recent advances in separation of roughness, waviness and form”, *Precision Engineering*, 26(2), pp. 222-235.

Ray, R., Birk, J. and Kelley, R.B. (1983) “Error Analysis of Surface Normals Determined by Radiometry”, *IEEE Transactions on Pattern Analysis and Machine Intelligence*, 5(6), pp. 631-645.

Rea, N.P., Wilson, T. and Juskaitis, R. (1996) “Semiconductor laser confocal and interference microscopy”, *Optics Communications*, 125(3), pp. 158-167.

Rhee, H., Lee, Y., Lee, I. and Vorburger, T. (2006) “Roughness Measurement Performance Obtained with Optical Interferometry and Stylus Method”, *Journal of the Optical Society of Korea*, 10(1), pp. 48-54.

Rushmeier, H. and Bernardini, F. (1999) “Computing consistent normals and colors from photometric data”, *International Conference on 3D Digital Imaging and Modeling*. Ottawa, Canada: IEEE Computer Society.

Rushmeier, H., Taubin, G. and Gueziec, A. (1997) “Applying Shape from Lighting Variation to Bump Map Capture”, *Rendering Techniques*, pp. 35-44.

Sakane, S., Sato, T. and Kakikura, M. (1990) “Automatic planning of light source placement for an active photometric stereo system”, *IEEE International Workshop on Intelligent Robots and Systems*, pp. 559-566 vol.2.

Sakarya, U. and Erkmen, l. (2003) “An improved method of photometric stereo using local shape from shading”, *Image and Vision Computing*, 21(11), pp. 941-954.

Sakarya, U., Leloğlu, U.M. and Tunalı, E. (2008) “Three-dimensional surface reconstruction for cartridge cases using photometric stereo”, *Forensic science international*, 175(2–3), pp. 209-217.

Sanderson, A.C., Weiss, L.E. and Nayar, S.K. (1988) “Structured highlight inspection of specular surfaces”, *IEEE Transactions on Pattern Analysis and Machine Intelligence*, 10(1), pp. 44-55.

Sandler, N. (2011) 'Photometric imaging in particle size measurement and surface visualization', *International journal of pharmaceutics,* 417(1–2), pp. 227-234.

Schwenke, H., Siebert, B.R.L., Wäldele, F. and Kunzmann, H. (2000) "Assessment of Uncertainties in Dimensional Metrology by Monte Carlo Simulation: Proposal of a Modular and Visual Software", *CIRP Annals - Manufacturing Technology*, 49(1), pp. 395-398.

Sherrington, I. and Smith, E.H. (1988) "Modern measurement techniques in surface metrology: part II; optical instruments".

Shi, B., Matsushita, Y., Wei, Y., Xu, C. and Tan, P. (2010) "Self-calibrating photometric stereo", *2010 IEEE Conference on Computer Vision and Pattern Recognition (CVPR),* pp. 1118-1125.

Smith, G.T. (2002) "Industrial Metrology Surfaces and Roundness", UK: Springer-Verlag London Limited.

Smith, M.L. (1999) "The analysis of surface texture using photometric stereo acquisition and gradient space domain mapping", *Image and Vision Computing,* 17(14), pp. 1009-1019.

Smith, M.L., Hill, T. and Smith, G. (1997) "Surface texture analysis based upon the visually acquired perturbation of surface normal", *Image and Vision Computing,* 15(12), pp. 949-955.

Smith, M.L., Smith, G. and Hill, T. (1999) "Gradient space analysis of surface defects using a photometric stereo derived bump map", *Image and Vision Computing,* 17(3–4), pp. 321-332.

Smith, M.L. and Smith, L.N. (2005) "Dynamic photometric stereo—a new technique for moving surface analysis", *Image and Vision Computing,* 23(9), pp. 841-852.

Solomon, F. and Ikeuchi, K. (1996) "Extracting the shape and roughness of specular lobe objects using four light photometric stereo", *IEEE Transactions on Pattern Analysis and Machine Intelligence,* 18(4), pp. 449-454.

Son, S., Park, H. and Lee, K.H. (2002) "Automated laser scanning system for reverse engineering and inspection", *International Journal of Machine Tools and Manufacture,* 42(8), pp. 889-897.

Spence, A. and Chantler, M. (2003) "Optimal illumination for three-image photometric stereo acquisition of texture", *Proceedings of the 3rd International Workshop on Texture Analysis and Synthesis,* pp. 89-94.

Spence, A.D. and Chantler, M.J. (2006) "Optimal illumination for three-image photometric stereo using sensitivity analysis", *Vision, Image and Signal Processing,* 153(2), pp. 149-159.

Sun, J., Smith, M., Smith, L. and Farooq, A. (2007) “Examining the uncertainty of the recovered surface normal in three light photometric stereo”, *Image and Vision Computing*, 25(7), pp. 1073-1079.

Sun, J., Smith, M., Smith, L., Midha, S. and Bamber, J. (2007) “Object surface recovery using a multi-light photometric stereo technique for non-Lambertian surfaces subject to shadows and specularities”, *Image and Vision Computing*, 25(7), pp. 1050-1057.

Sun, Y., Xu, W., Zhu, L., Du, H. and Zhang, Y. (2009) “Estimation of uncertainty in form error CMM measurement according to new GPS standard system”, *International Technology and Innovation Conference 2009 (ITIC 2009)*, pp. 1-4.

Tagare, H.D. and Defigueiredo, R.J. (1991) “A theory of photometric stereo for a class of diffuse non-Lambertian surfaces”, *IEEE Transactions on Pattern Analysis and Machine Intelligence*, 13(2), pp. 133-152.

Taylor, R.J. (1997) “An Introduction to Error Analysis”, 2nd ed. US: University Science Books.

Torrance, K.E. and Sparrow, E.M. (1967) “Theory for off-specular reflection from roughened surfaces”, *JOSA*, 57(9), pp. 1105-1112.

Tsai, D.M. and Huang, T.Y. (2003) “Automated surface inspection for statistical textures”, *Image and Vision Computing*, 21(4), pp. 307-323.

Um, D. (2014) “Multiple Intensity Differentiation-Based 3-D Surface Reconstruction With Photometric Stereo Compensation”, *Sensors Journal, IEEE*, 14(5), pp. 1453-1458.

Vogiatzis, G., Hernandez, C. and Cipolla, R. (2006) 'Reconstruction in the Round Using Photometric Normals and Silhouettes.', *2006 IEEE Computer Society Conference on Computer Vision and Pattern Recognition*, pp. 1847-1854.

Vorburger, T.V., Rhee, H.G., Renegar, T.B., Song, J.F. and Zheng, A. (2007) “Comparison of optical and stylus methods for measurement of surface texture”, *The International Journal of Advanced Manufacturing Technology*, 33(1), pp. 110-118.

Vorburger, T.V., Song, J.F., Giauque, C.H.W., Renegar, T.B., Whitenton, E.P. and Croarkin, M.C. (1996) “Stylus-laser surface calibration system”.

Webb, R. (1996) 'Confocal optical microscopy', *Reports on Progress in Physics*, 59(3), pp. 427.

Wei, T. and Klette, R. (2002) “Height from Gradient Using Surface Curvature and Area Constraints”, *ICVGIP*.

Whitehouse, D. (2002) “Surface and their Measurement”, UK: Hermes Penton.

Whitehouse, D. (1997) “Surface metrology”, *Measurement Science and Technology*, pp. 955-972.

Woodham, R.J. (1989) “Determining Surface Curvature with Photometric Stereo”, *IEEE International Conference on Robotics and Automation,* USA: IEEE, pp. 36.

Woodham, R.J. (1980) “Photometric method for determining surface orientation from multiple images”, *Optical engineering*, 19(1).

Xiao, G.Q., Corle, R. and Kino, G.S. (1988) “Real-time confocal scanning optical microscope”, *Applied Physics Letters*, 53(8), pp. 716-718.

Yang, Q. and Ahuja, N. (2012) “Surface reflectance and normal estimation from photometric stereo”, *Computer Vision and Image Understanding*, 116(7), pp. 793-802.

Yoichi, S., Mark, D.W. and Ikeuchi, K. (1997) “Oject shape and reflectance modeling from observation”, *Computer graphics and interactive techniques*, New York, USA: ACM Press/Addison-Wesley Publishing, pp. 379-387.

Yuan, Y.B., Qiang, X.F., Song, J.F. and Vorburger, T.V. (2000) “A fast algorithm for determining the Gaussian filtered mean line in surface metrology 1”, *Precision Engineering*, 24(1), pp. 62-69.

Zafeiriou, S., Hansen, M.F., Atkinson, G.A., Petrou, M. and Smith, M.L. (2010) “Baseline face recognition using photometric stereo data”, *Procedia Computer Science*, 2(0), pp. 20-25.

Zhengzhen, L. and Tianding, C. (2009) “Distance Measurement System Based on Binocular Stereo Vision”, *International Joint Conference on Artificial Intelligence*, Hainan Island: IEEE, pp. 456 - 459.

Appendices

Appendix 1:

List of Publications Arising from the Research

1) Thammarat Somthong and Qingping Yang "Average Surface Roughness Measurement using Photometric Stereo Method", *the 3rd Asia-Pacific Conference on Life Science and Engineering*, 18-20th November 2015, Chiang Mai, Thailand

2) Thammarat Somthong and Qingping Yang "Surface Roughness Measurement using Photometric Stereo Method with Coordinate Measuring Machine", *2016 IEEE International Instrumentation and Measurement Technology Conference(I^2MTC)*, 23rd-26th May 2016, Taipei, Taiwan

3) Thammarat Somthong and Qingping Yang "Average Surface Roughness Measurement using Photometric Stereo Method", *Universal Journal of Electrical and Electronic Engineering*, Vol.4(3), pp.73-79, 2016 (Published)

4) Thammarat Somthong and Qingping Yang "Average surface roughness evaluation using 3-source photometric stereo technique", *International Journal of Metrology and Quality Engineering*, Vol.7(4), pp.406, 2016 (Published)

5) Thammarat Somthong and Qingping Yang "Uncertainty Estimation and Validation Method of Surface Roughness Measurement on Coordinate Measuring Machine using Photometric Stereo Method", *Journal of the International Societies for Precision Engineering and Nanotechnology*, 2016 (Submitted)

Appendix 2:

Summary of Facilities in the Research

Facilities	Performance Specifications	Calibration Equipment
CMM	Range: XYZ X-axis: Measuring range: 500 mm Y-axis: Measuring range: 300 mm Z-axis: Measuring range: 270 mm Resolution : 0.001 mm	MFR. : Mitutoyo Model : - S/N : -
Roughness measuring instrument	X-axis: Measuring range: 100 mm Resolution : 0.01 μm Z-axis: Measuring range: 32μm Resolution : 1 nm	MFR. :Kosaka Laboratory Model : ET4000AK S/N : MB 00536
Surface roughness standard	Uncertainty(k=2) $R_a \sqrt{(10)^2 + (12 \cdot Z_m)^2}$ nm Z_m is measured value of roughness standard in μm	MFR. : Rubert Model : 100 S/N : 1

Working standard scale	Uncertainty(k=2) $\sqrt{(0.11)^2 + (4.2 \times 10^{-3} \times l)^2}$ l is the indication length of the working standard scale in mm	MFR. : Mitutoyo Model : HL1-150 S/N : 182-513
Digital thermometer	Uncertainty(k=2) 0.02^{O}C, 1.1%RH	MFR. : Almemo Model : 2390-8 S/N : H06100184

Appendix 3:

Technical Specification of Light source and Lens

1. Light source

SP-05 SinkPAD-II™ Rebel 10mm Square LED Assembly

lead-free RoHS compliant

Assembly Specifications

Parameter	Value
Base Type	0.8mm SinkPAD-II™ Aluminum
Thermal Performance $R\theta_{C-B}$ See the thermal model on page 8	0.4 °C/W
Pad Finish	Lead Free HASL
Solder Mask Color	White
Solder Paste	AIM NC-258 No-Clean, Lead-Free
Max Operating Temperature (Aluminum Base)[1]	120°C
Overall Dimensions (mm)	9.9L x 9.9H x 2.87H
Weight	0.4g

1. For maximum life, the aluminum board temperature must be kept below this value.
For LED specifications, please refer to the Philips Lumileds Rebel LED datasheet.

Eliminating the dielectric layer between the LED thermal pad and the aluminum base means that the SinkPAD-II™ can easily outperform even the best MCPCB boards available.

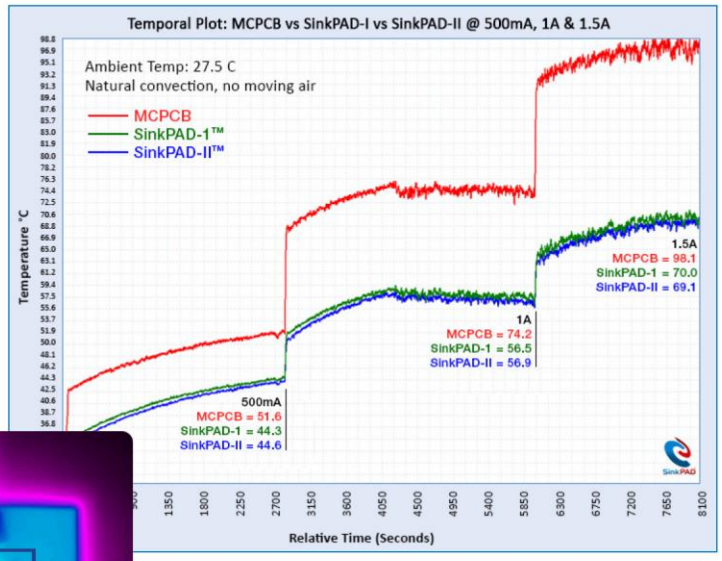

Image 1

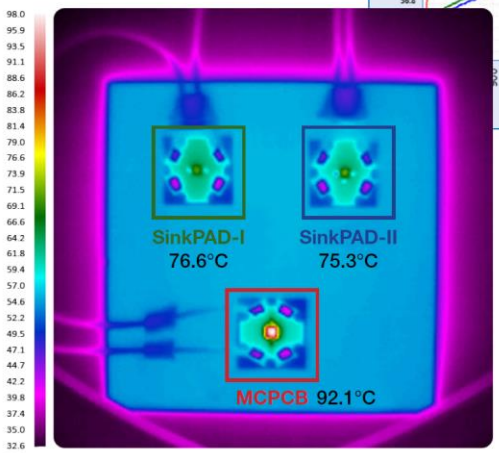

Image 2

HB LEDs radiate minimal heat around the LED. Instead all generated heat must be conducted away from the LED through the thermal pad on the bottom. By soldering the LED thermal pad directly to the aluminum base, a **Direct Thermal Path** is established that efficiently conducts the heat to the cooling surface.

2. Lens

Opticselect
www.carclo-optics.com

10.0MM LENS FRONT NARROW TIR

Status	Production
Part no.	10417
Drawing no.	60553
Product type	Optic
Type	TIR
Pieces	1
Diameter	10.0
Height	6.00
Beam	Lens Front Narrow
Flange	Yes
Files	Customer drawing (PDF) Customer 3D model (.igs)

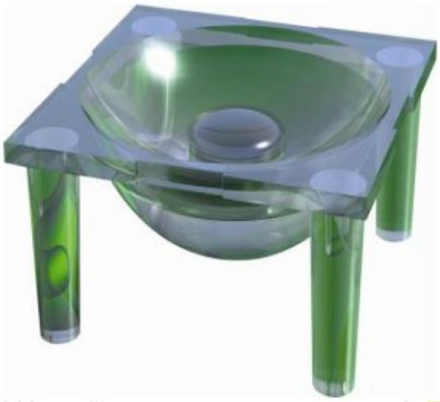

LEDs & Performances	Eff.	FWHM	Cd/lm	Spot	Cross-section	Files
Lumileds Rebel Cool White	84.5%	17.7	6.9			10417_Rebel_White_250408.ies
Lumileds Rebel Neutral White	86.0%	18.3	7.4			10417_Rebel_Neutral_White_250408.ies
Lumileds Rebel Warm White	86.3%	15.7	10.7		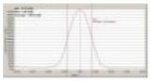	10417_Rebel_Warm_White_250408.ies
Cree XP-E XLamp® White	88.7%	16.4	9.8			10417_cree_xpe_white_250408.ies
Cree XP-G XLamp® White	87.3%	24	4.9		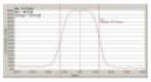	10417_cree_xpg_white_250408.ies
Osram Oslon SSL Oslon Ultra White	85.5%	18.5	8.6			10417_Oslon_wht_250408.ies 10417_Oslon_wht_250408.ldt
Nichia NCSL 119-H3 Top Emitting Warm White	82.6%	16.7	7.7		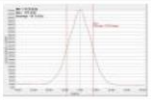	10417_Nichia_119_Warm_White_250408.ies
SSC Z5 Pure White	84.8%	15.8	12.8		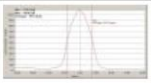	10417_Seoul_Z5_white_250408.ies
Everlight Shuen Warm White	85.0%	21.1	5.2		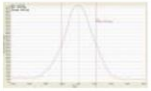	10417_Shuen_wwht_250408.ies
Everlight Shuen Cool White	84.9%	20.6	5.1		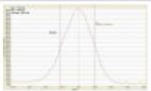	10417_Shuen_cwht_250408.ies

Appendix 4:

Technical Specification of Camera and Lens

1) Camera

TECHNICAL DETAILS

Specifications

Basler ace	Resolution (H x V pixels)	Sensor	Sensor Technology	Sensor Size (optical)	Pixel Size (µm)	Frame Rate	Power Consumption (PoE/AUX)	Weight (typical)
acA640-90gm/gc	659 x 494	Sony ICX424	Progressive Scan CCD	1/3"	7.4 x 7.4	90	3.1 W/2.7 W	<90g
acA640-100gm/gc	659 x 494	Sony ICX618	Progressive Scan CCD	1/4"	5.6 x 5.6	100	2.3 W/2.0 W	<90 g
acA645-100gm/gc	659 x 494	Sony ICX414	Progressive Scan CCD	1/2"	9.9 x 9.9	100	3.6 W/3.3 W	<90g
acA750-30gm/gc	752 x 580	Sony ICX409	Interlaced Scan CCD	1/3"	6.5 x 6.25	30	2.5 W/2.3 W	<90 g
acA780-75gm/gc	782 x 582	Sony ICX415	Progressive Scan CCD	1/2"	8.3 x 8.3	75	3.6 W/3.3 W	<90g
acA1300-30gm/gc	1296 x 966	Sony ICX445	Progressive Scan CCD	1/3"	3.75 x 3.75	30	2.5 W/2.2 W	<90 g
NEW acA1300-60gm/gc*	1280 x 1024	EV76C560	CMOS, global shutter	1/1.8"	5.3 x 5.3	60	<3.0W	<90 g
NEW acA1300-60gm NIR*	1280 x 1024	EV76C661	CMOS, global shutter	1/1.8"	5.3 x 5.3	60	<3.0W	<90 g
acA1600-20gm/gc	1628 x 1236	Sony ICX274	Progressive Scan CCD	1/1.8"	4.4 x 4.4	20	3.4 W/2.9 W	<90 g
NEW acA1600-60gm/gc*	1600 x 1200	EV76C570	CMOS, global shutter	1/1.8"	4.5 x 4.5	60	<3.0W	<90 g
acA2000-50gm/gc	2048 x 1088	CMOSIS CMV2000	CMOS, global shutter	2/3"	5.5 x 5.5	50	3.4 W/2.9 W	<90 g
acA2000-50gm NIR	2048 x 1088	CMOSIS CMV2000 NIR-enhanced	CMOS, global shutter	2/3"	5.5 x 5.5	50	3.4 W/2.9 W	<90 g
acA2040-25gm/gc	2048 x 2048	CMOSIS CMV4000	CMOS, global shutter	1"	5.5 x 5.5	25	3.4 W/2.9 W	<90 g
acA2040-25gm NIR	2048 x 2048	CMOSIS CMV4000	CMOS, global shutter	1"	5.5 x 5.5	25	3.4 W/2.9 W	<90 g
acA2500-14gm/gc	2592 x 1944	Aptina MT9P	CMOS, rolling shutter	1/2.5"	2.2 x 2.2	14	2.5 W/2.2 W	<90 g

*Available Q2/2013

Specifications Applicable For All ace GigE Models:

Mono / Color	Mono / Color (NIR models: Mono only)
Interface	Fast Ethernet (100 Mbit/s) or Gigabit Ethernet (1000 Mbit/s)
Video Output Format	Mono 8, Mono 12, Mono 12 Packed, YUV 4:2:2 Packed, YUV 4:2:2 (YUYV) Packed, Bayer BG 8, Bayer BG 12, Bayer BG 12 Packed / in addition: Bayer GB (Aptina), Bayer GR (CMOSIS)
	acA750-30gc: Mono 8, YUV 4:2:2 Packed, YUV 4:2:2 (YUYV) Packed only
Synchronization	Via external trigger, via the Ethernet connection or free run
Exposure Control	Via external trigger or programmable via the camera API
Housing Size (L x W x H)	42 mm x 29 mm x 29 mm
Housing Temperature	Up to 50 °C
Lens Mount	C-mount, CS-mount (except models with CMOSIS or e2v sensors)
Digital I/O	1 opto-isolated input / 1 opto-isolated output
Power Requirements	Via Power over Ethernet (802.3af) or + 12VDC (±10%) via the camera´s 6-pin Hirose connector
Conformity	CE, FCC, IP30, RoHS, PoE (802.3af), UL, GigE Vision, GenICam
Driver	Basler pylon driver package
Operating System	Windows, Linux - 32 bit and 64 bit

2) Lens

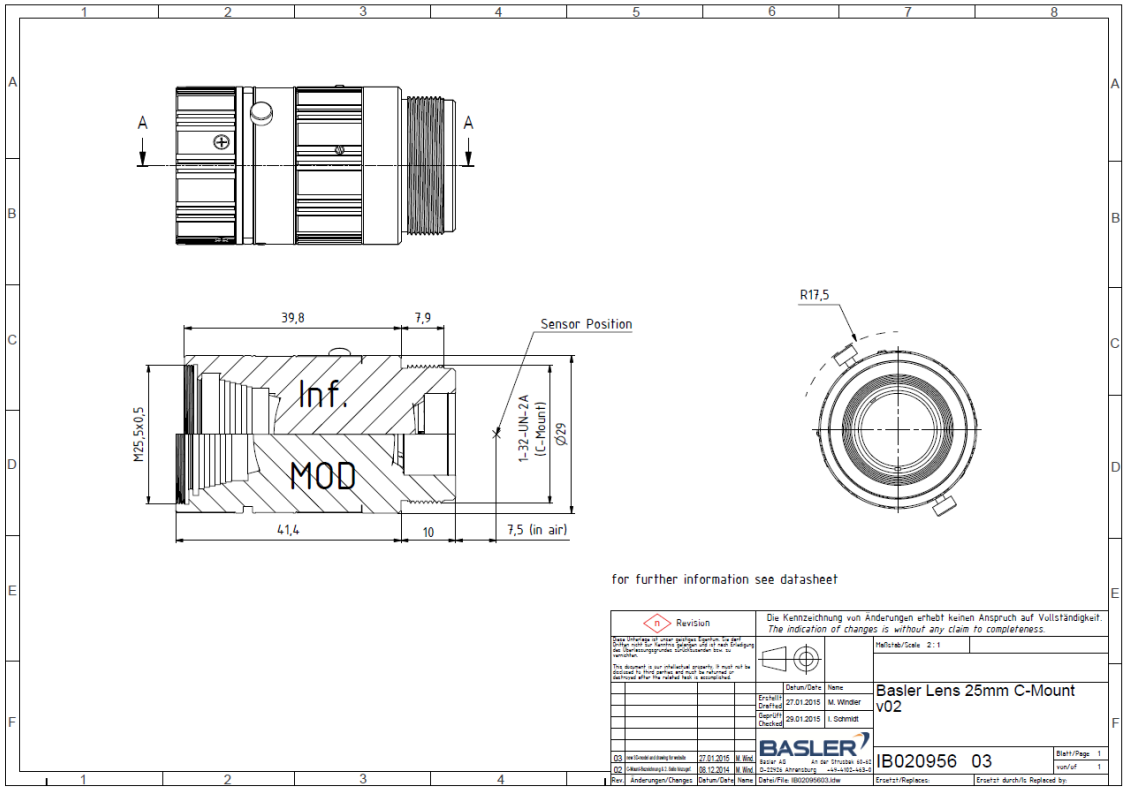
A
A
39,8
7,9
Sensor Position
Inf.
MOD
M25,5x0,5
1-32-UN-2A
(C-Mount)
Ø29
41,4
10
7,5 (in air)
R17,5
for further information see datasheet
Basler Lens 25mm C-Mount
v02
IB020956 03

Appendix 5:

Technical Specification of Electrical Circuit

1) LED driver

LUXdrive™ by LEDdynamics

A009 BuckBlock™

High Output Wide Range LED Power Module

DATA SHEET Page 1 of 9

Product Overview

The A009 BuckBlock™ High Output Wide Range LED Power Modules are a line of true current regulated drivers for powering LEDs. The LUXdrive BuckBlock™ line of LED drivers are the ideal choice for powering all types of high-brightness and high-power LED Packages and arrays.

BuckBlock™ LED drivers provide high efficiency and require no external current limiting resistors. A fast response current-sensing circuit makes the BuckBlock™ ideal for applications where flashing or strobe operation of the LED(s) is required.

A dimming input, compatible with many commercially available 0-10V low voltage dimming controls, provides a convenient method to control the brightness of the LEDs. The standard units are potted in an extremely small, low profile package* and come with 6" 18AWG colored leads.

Features

- DC input voltage up to 32V
- 1.0A, 1.4A, or 2.1A constant current output*
- Extremely small form factor* (2.0"x1.2"x0.38")
- 18 AWG wires for easy electrical connections
- External analog/digital intensity control
- External potentiometer intensity control (0-100%)
- Continuous output short circuit protection
- Continuous output open circuit protection
- Input reverse polarity protection with Polarifet™ Technology
- Pulse and strobe capable (dim input)
- 0-10V Dimming compatible with many available controls

Typical Applications

- Solar & Landscape Lighting
- Architectural Lighting
- Track Lighting
- Automotive & Marine Lighting
- Portable Lighting & Flashlights
- Point of Purchase Lighting
- Desk & Reading Lamps
- Signal & marker Lighting
- Flashing & Strobe Lighting
- Cabinet & Display Case Lighting
- Sign & Channel Letters
- Much More...

Appendix 6:

The mechanical parts

1) Mechanical design for holding light source with probe system

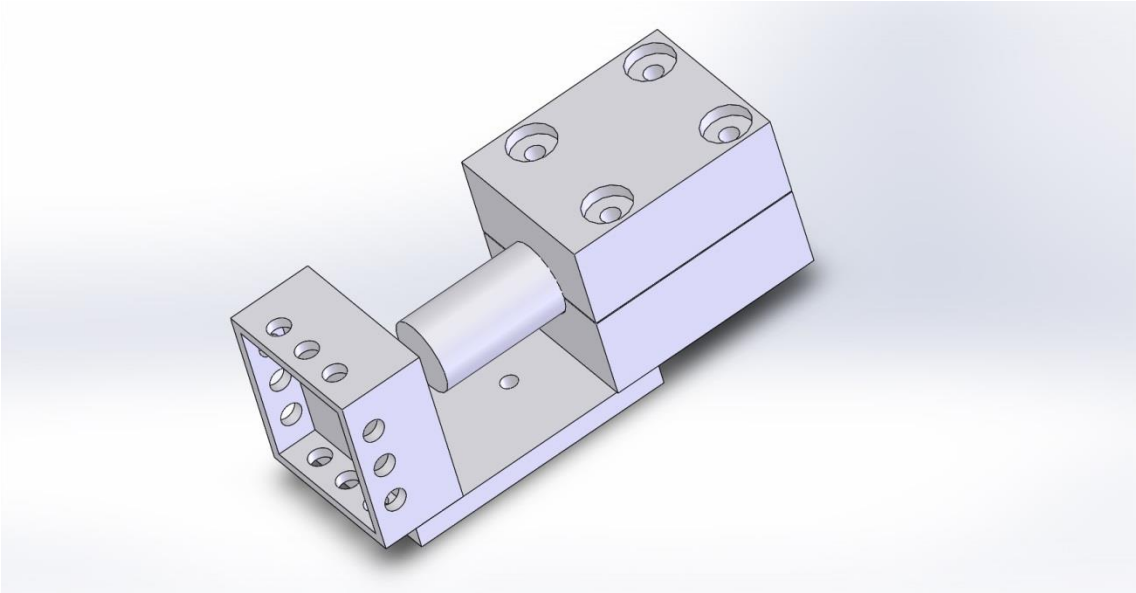

2) Jig fixture for measuring standard surface roughness

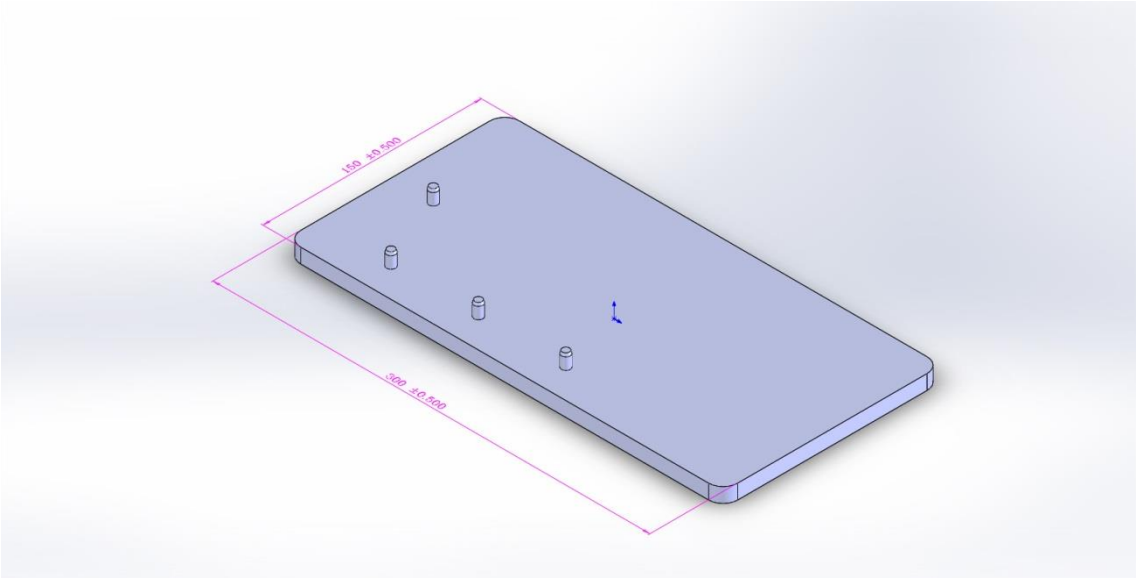

3) The specimen manufactured by 3D printing machine

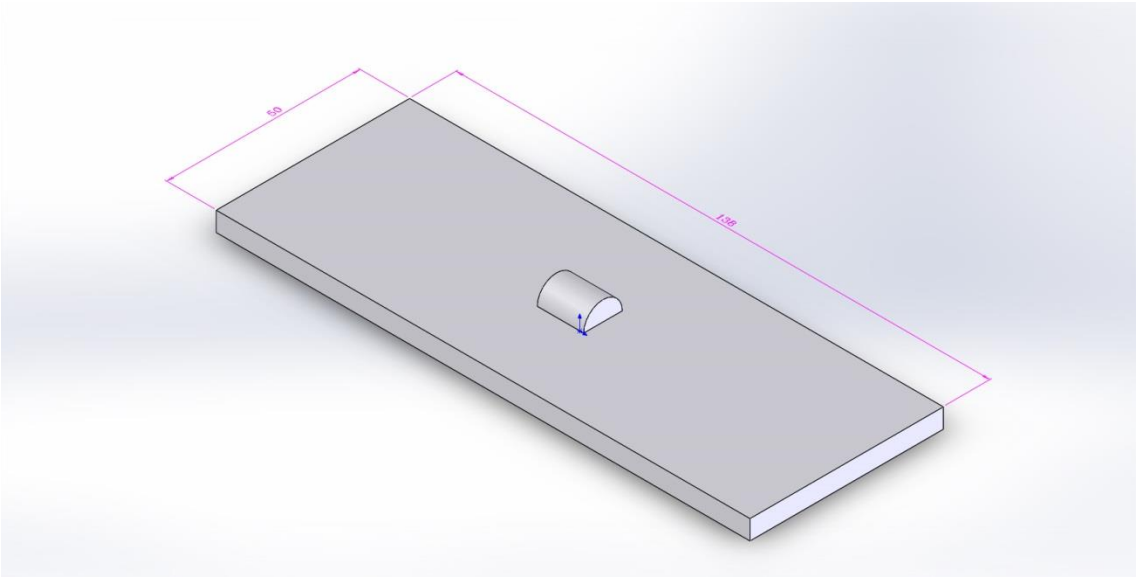

Appendix 7:

Part of LabView Programming

1) This programming has been used to acquire images from the PS technique sequentially and control the light source.

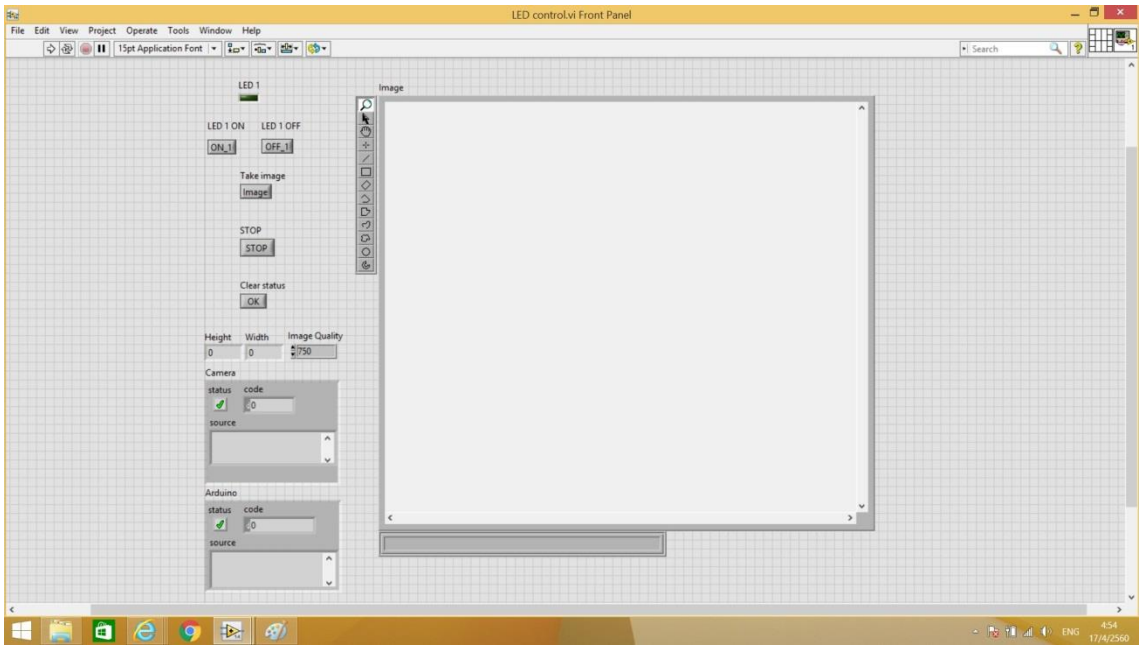

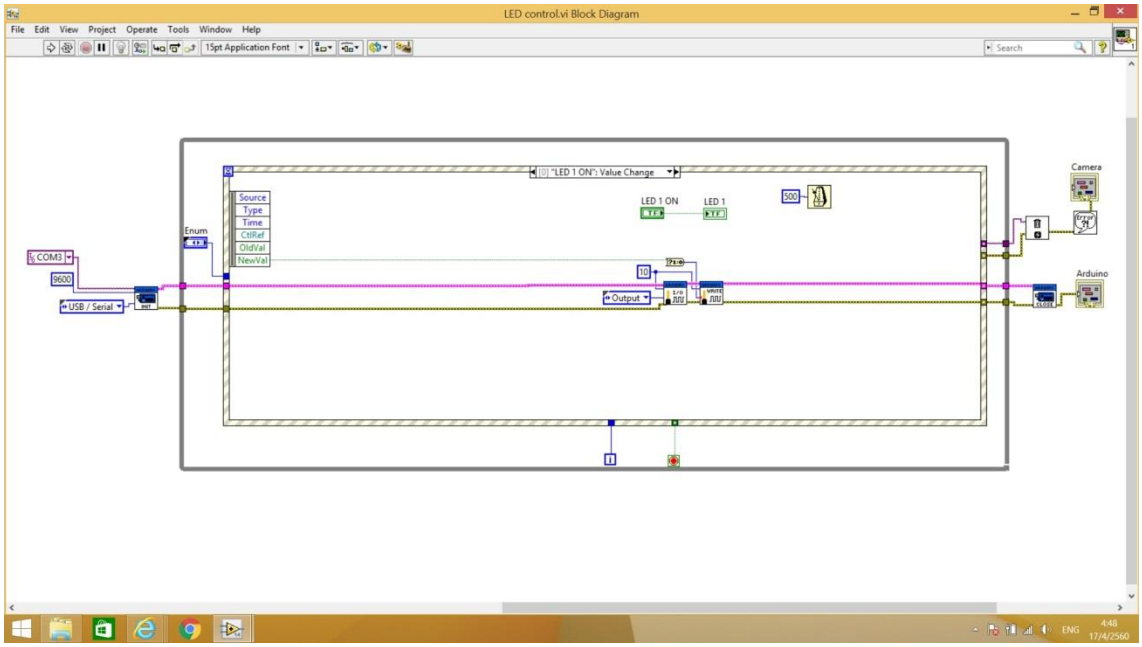

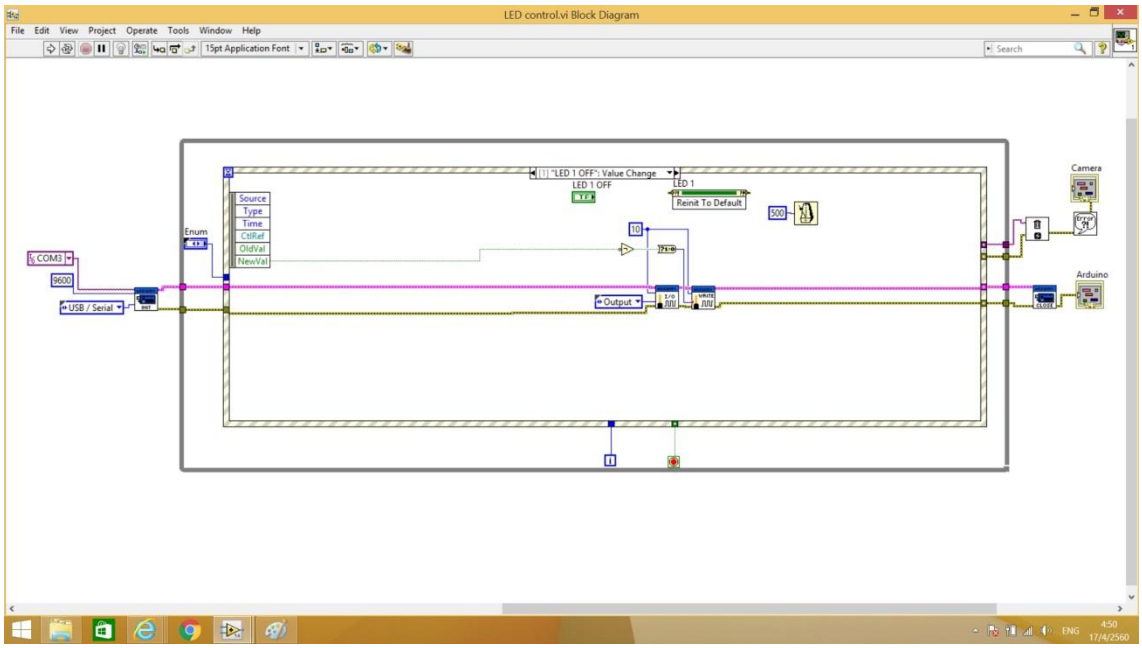
LED control.vi Block Diagram
File Edit View Project Operate Tools Window Help
15pt Application Font
Search
[1] "LED 1 OFF": Value Change
LED 1 OFF
LED 1
Reinit To Default
500
10
Source
Type
Time
CtlRef
OldVal
NewVal
Enum
COM3
9600
USB / Serial
Output
Camera
Arduino
ENG
4:50
17/4/2560

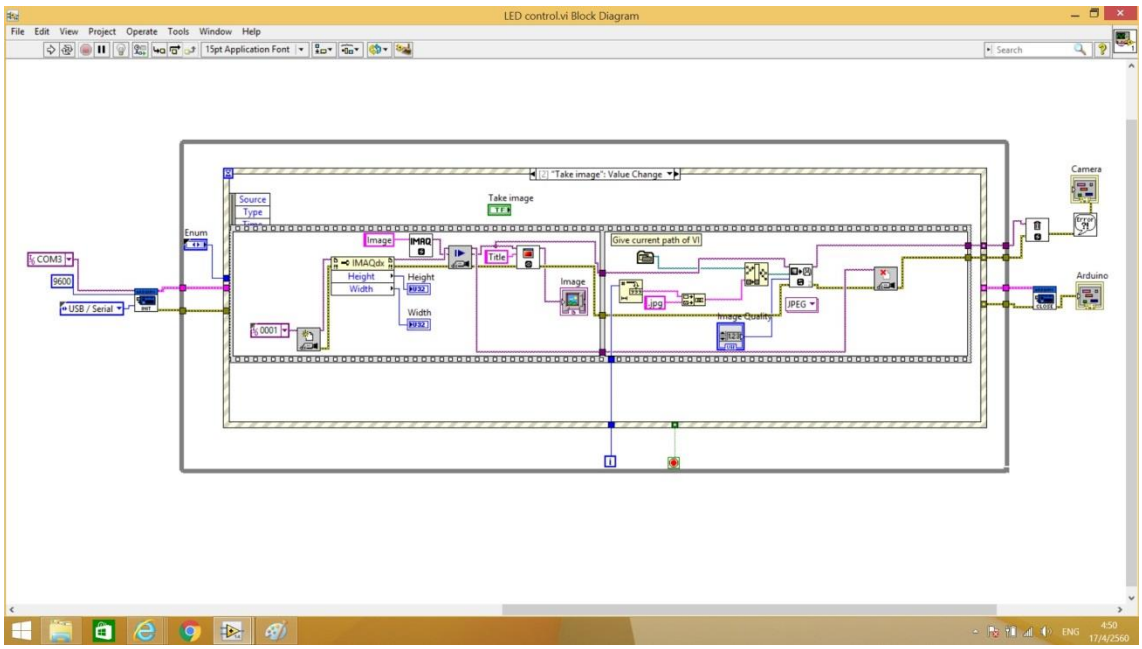
LED control.vi Block Diagram
File Edit View Project Operate Tools Window Help
15pt Application Font
Search
[2] "Take image": Value Change
Take image
Source
Type
Enum
COM3
9600
USB / Serial
Image
IMAQ
IMAQdx
Height
Width
Title
Image
Give current path of VI
jpg
JPEG
Image Quality
0001
Camera
Arduino
ENG
4:50
17/4/2560

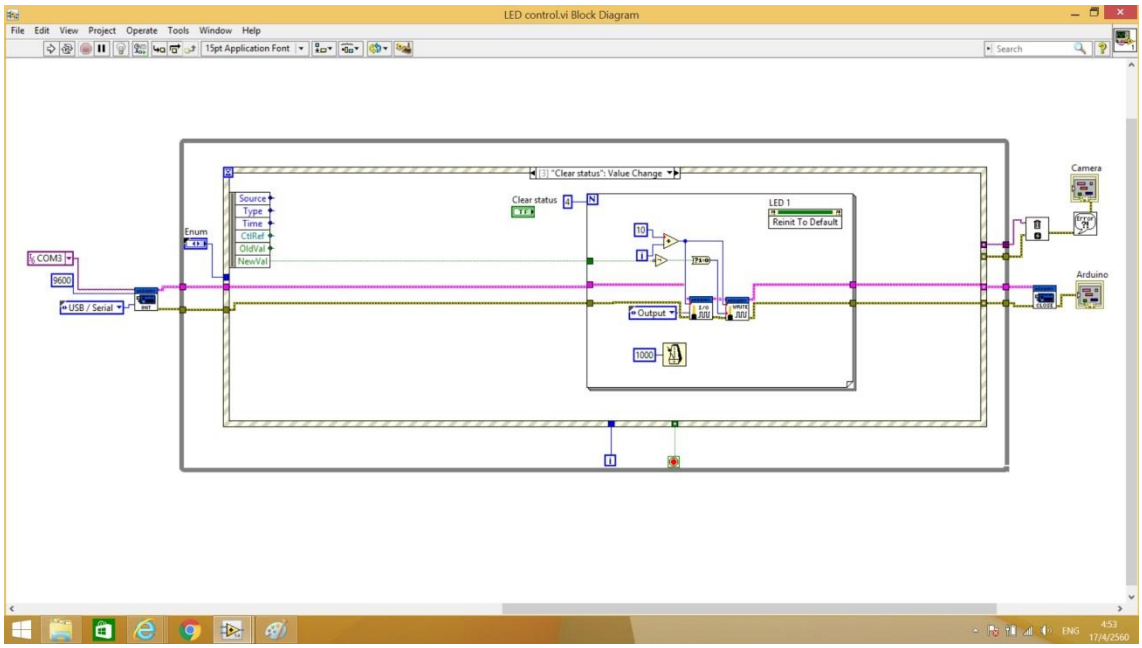
LED control.vi Block Diagram
File Edit View Project Operate Tools Window Help
15pt Application Font
Search
[3] "Clear status": Value Change
Source
Type
Time
CtlRef
OldVal
NewVal
Clear status
LED 1
Reinit To Default
Enum
COM3
9600
USB / Serial
Output
1000
Camera
Arduino

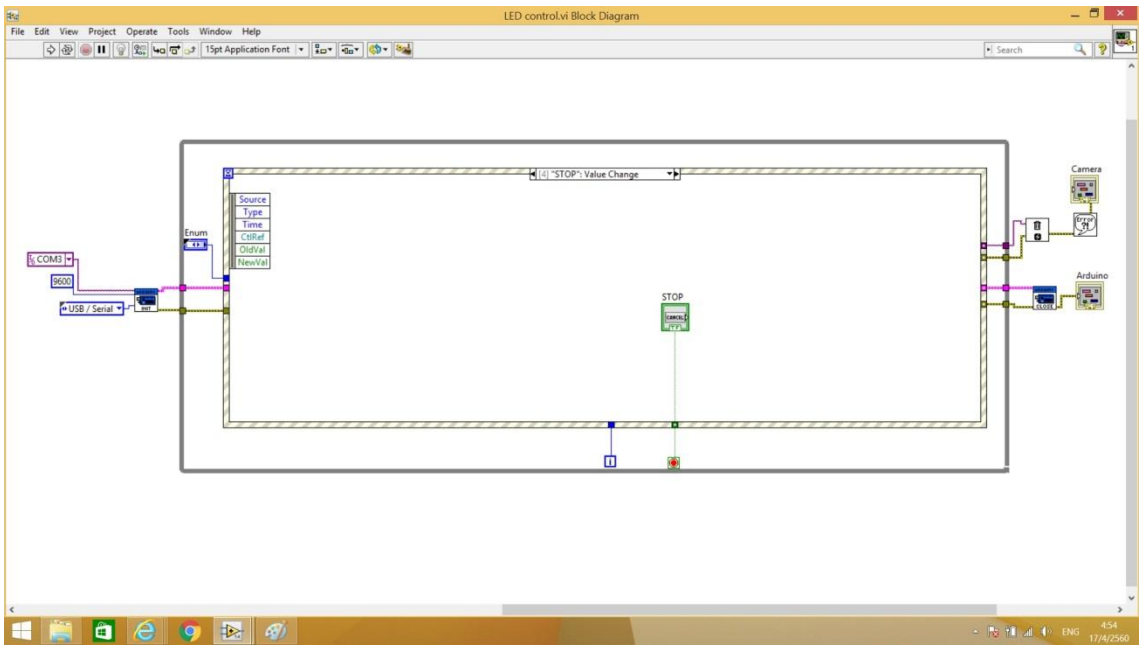
LED control.vi Block Diagram
File Edit View Project Operate Tools Window Help
15pt Application Font
Search
[4] "STOP": Value Change
Source
Type
Time
CtlRef
OldVal
NewVal
Enum
COM3
9600
USB / Serial
STOP
Camera
Arduino

Appendix 8:

Part of MATLAB Programming

This programming has been used to recover surface normals from the PS technique and to calculate both average roughness and shape from their profiles.

1) Light source calibration

```
% Light source calibration %
clc;
clear;
if 'D:\code matlab\matlab photometric\psmImages\chrome' ~= '/'
    filename = ['D:\code matlab\matlab photometric\psmImages\chrome' '/'];
end
filename = [filename 'chrome.'];
maskfilename = [filename 'mask.png'];
circle = imread(maskfilename);
circle = rgb2gray(circle);

% Calculate the center of the chrome ball.
  maxval = max( max( circle ) );
  [circleRow circleCol] = find(circle == maxval);
  maxRow = max(circleRow);
  minRow = min(circleRow);
  maxCol = max(circleCol);
  minCol = min(circleCol);
  xc     = double((maxCol + minCol)/2);
  yc     = double((maxRow + minRow)/2);
  center = [xc, yc]
  radius = double((maxRow - minRow)/2)

% R: The reflection direction.
  R = [0 0 1.0];
  L = [];

  for i = 1:3
      imgFileName = strcat('D:\code matlab\matlab
photometric\psmImages\chrome\chrome.',num2str(i),'.png');
      image = imread(imgFileName);
      image = rgb2gray(image);
      maxval = max( max( image ) );
      [pointRow, pointCol] = find(image == maxval);
      nSize  = size( pointRow, 1);
      px     = sum(pointCol)/double(nSize);
      py     = sum(pointRow)/double(nSize);
      Nx     =   px - xc;
```

```
      Ny     = -(py - yc);
      Nz     = sqrt( radius^2 - Nx^2 - Ny^2 );
      normal = [Nx, Ny, Nz];
      normal = normal/radius;
      NR     = normal(1)*R(1) + normal(2)*R(2) + normal(3)*R(3);
      L(i,:) = 2*NR*normal - R;
  end

% Write the new lighting direction into a test file.
  fid = fopen('calibratedLight.txt', 'w');
  fprintf( fid, '%d \n', 3);
  for row = 1:3
      fprintf(fid, ' %10.5f %10.5f %10.5f \n', L(row,1), L(row,2), L(row,3) );
  end
  fclose(fid);
```

2) Three-dimensional surface recovered by the PS technique

```
%   ********************************************************************
%   Read the lights and directions:
%   ********************************************************************
clc;
clear;
    fid = fopen('D:\code matlab\calibratedLight.txt','r');
    numLights = 3;
    numLights = fscanf(fid, '%d \n', [1]);

    LightMatrix = [];
    for i = 1:numLights
        lightDir = fscanf(fid, '%f %f %f \n', [3]);
    lightDir = lightDir/norm(lightDir);
    lightMatrix(i,:) = lightDir;
    end

%   ********************************************************************
%   Read the mask file and threshold the values
%   ********************************************************************

    crop_image = imread('D:\code matlab\matlab
photometric\psmImages\rough\rough.mask.png');

    %crop_image = rgb2gray(crop_image); %increase
    number_rows  = size(crop_image,1);
    number_cols  = size(crop_image,2);
```

```
    maxval = max(max(crop_image));

    for i = 1:number_rows
    for j = 1:number_cols
       if( crop_image(i,j) == maxval)
           crop_image(i,j) = 1;
       else
           crop_image(i,j) = 0;
       end
    end
    end

%
**************************************************************************
%   Read all the images .,, ( In RGB Format...
%
**************************************************************************
    accumImage = zeros(number_rows, number_cols, 3);
%   Read all the images..
    for im = 1:3
        id = num2str(im-1);
        filename = strcat( 'D:\code matlab\matlab
photometric\psmImages\rough', '\','rough', '.', id, '.png');
        newImage = imread(filename);
    if( size(newImage,1) ~= number_rows)
        fprintf( ' mask image and source image size do not match ');
        return;
        end
    if( size(newImage,2) ~= number_cols)
        fprintf( ' mask image and source image size do not match ');
        return;
    end
          for i = 1:number_rows
        for j = 1:number_cols
            accumImage(i,j,1) = accumImage(i,j,1) + double(newImage(i,j,1));
            accumImage(i,j,2) = accumImage(i,j,2) + double(newImage(i,j,2));
            accumImage(i,j,3) = accumImage(i,j,3) + double(newImage(i,j,3));
        end
        end

    images(:,:,:,im) = newImage;
    grayImageSet(:,:,im) = rgb2gray(newImage);
    end
     for i = 1:number_rows
    for j = 1:number_cols
        r = accumImage(i,j,1);
```

```
    g = accumImage(i,j,2);
    b = accumImage(i,j,3);
   if( r  < 5.0 || g < 5.0 || b < 5.0 )
       crop_image(i,j) = 0;
   end
end
end

  whichChannel = 0
  nms = [];

number_rows     = size(images,1);
number_cols     = size(images,2);
numColors = size(images,3);
numImages = size(images,4);

for i = 1:number_rows
for j = 1:number_cols
    nms(i,j,1) = 0.0;
    nms(i,j,2) = 0.0;
    nms(i,j,3) = 1.0;
    albedo(i,j)        = 0.0;
end
end

%L = lightDir, nms = surfacenormals;
%%%%%%%
 if( whichChannel == 0)
    for im = 1:numImages
    grayimages(:,:,im) = rgb2gray(images(:,:,:,im));
    end

    for i = 1:number_rows
    for j = 1:number_cols
        if( crop_image(i,j) )
        L = lightMatrix;
        I = 0;
        LT = 0;
        for im = 1:numImages
            I(im) = double(grayimages(i,j,im));
        end

          I  = I';
          LT = L';
          A  = LT*L;
          b  = LT*I;
```

```
                g  = inv(A)*b;
                R  = norm(g);
                N  = g/R;

              nms(i,j,1) =  N(1);
              nms(i,j,2) =  N(2);
              nms(i,j,3) =  N(3);
              albedo(i,j)        = R;

              end
          end
          end
      end

 %OPR = ObjectPixelRow, OPC = ObjectPixelCol, OP = ObjectPixels;
 z = [];
 number_rows = size(crop_image, 1)
 number_cols = size(crop_image, 2)
  [OPR OPC] = find(crop_image);
   OP = [OPR OPC];

  index = zeros(number_rows, number_cols);

  numPixels =  size(OP, 1);

  for d = 1:numPixels
      Pixel_R = OP(d, 1);
      Pixel_C = OP(d, 2);
      index(Pixel_R, Pixel_C) = d;
  end
  index_2 = zeros(size(index,1));
  index  = horzcat(index,index_2);

  M = sparse(2*numPixels, numPixels);
  b = zeros(2*numPixels, 1);
  z =[];

for d = 1: numPixels
      Pixel_R = OP(d, 1);
      Pixel_C = OP(d, 2);
      if (Pixel_C >= 0) && (Pixel_C <=512)
      nx = nms(Pixel_R, Pixel_C, 1);
      ny = nms(Pixel_R, Pixel_C, 2);
      nz = nms(Pixel_R, Pixel_C, 3);
      elseif (Pixel_C >= 513) && (Pixel_C <=1024)
      nx = nms(Pixel_R, Pixel_C-512, 1);
```

```
ny = nms(Pixel_R, Pixel_C-512, 2);
nz = nms(Pixel_R, Pixel_C-512, 3);
else Pixel_C > 1024
nx = nms(Pixel_R, Pixel_C-1024, 1);
ny = nms(Pixel_R, Pixel_C-1024, 2);
nz = nms(Pixel_R, Pixel_C-1024, 3);
end

if (index(Pixel_R, Pixel_C+1) > 0) && (index(Pixel_R-1, Pixel_C) > 0);
    M(2*d-1, index(Pixel_R, Pixel_C))   = 1;
    M(2*d-1, index(Pixel_R, Pixel_C+1)) = -1;   % (X+1, Y)
    b(2*d-1, 1) = nx / nz;

    M(2*d, index(Pixel_R, Pixel_C))     = 1;
    M(2*d, index(Pixel_R-1, Pixel_C))   = -1;     % (X, Y+1)
    b(2*d, 1) = ny / nz;

elseif (index(Pixel_R-1, Pixel_C) > 0);
    f = -1;
    if (index(Pixel_R, Pixel_C+f) > 0);
        M(2*d-1, index(Pixel_R, Pixel_C)) = 1;
        M(2*d-1, index(Pixel_R, Pixel_C+f)) = -1;   % (X+f, Y)
        b(2*d-1, 1) = f*nx / nz;
    end
    M(2*d, index(Pixel_R, Pixel_C)) = 1;
    M(2*d, index(Pixel_R-1, Pixel_C)) = -1;     % (X, Y+1)
    b(2*d, 1) = ny / nz;

elseif (index(Pixel_R, Pixel_C+1) > 0);
    f = -1;
    if (index(Pixel_R-f, Pixel_C) > 0);
        M(2*d, index(Pixel_R, Pixel_C)) = 1;
        M(2*d, index(Pixel_R-f, Pixel_C)) = -1;     % (X, Y+f)
        b(2*d, 1) = nx / nz;
    end
    M(2*d-1, index(Pixel_R, Pixel_C)) = 1;
    M(2*d-1, index(Pixel_R, Pixel_C+1)) = -1;   % (X+1, Y)
    b(2*d-1, 1) = f*ny / nz;

else
    f = -1;
    if (index(Pixel_R, Pixel_C+f) > 0);
        M(2*d-1, index(Pixel_R, Pixel_C)) = 1;
        M(2*d-1, index(Pixel_R, Pixel_C+f)) = -1;   % (X+f, Y)
        b(2*d-1, 1) = f*nx / nz;
    end
```

```
            f = -1;
            if (index(Pixel_R-f, Pixel_C) > 0);
                M(2*d, index(Pixel_R, Pixel_C)) = 1;
                M(2*d, index(Pixel_R-f, Pixel_C)) = -1;      % (X, Y+f)
                b(2*d, 1) = f*ny / nz;
            end
        end
    end

    x = M \ b;
    x = x - min(x);

    tempShape = zeros(number_rows, number_cols);
    for d = 1:numPixels
        Pixel_R = OP(d, 1);
        Pixel_C = OP(d, 2);
        tempShape(Pixel_R, Pixel_C) = x(d, 1);
    end

    z  = zeros( number_rows, number_cols);
    for i = 1:number_rows
        for j = 1:number_cols
            z(i, j) = tempShape(number_rows-i+1, j);
        end
    end


    z = mat2gray(z);
    figure(1); surfl(z); shading interp; colormap gray; rotate3d;
    save z.mat z
```

3) Average roughness profile

```
% Average roughness profile calculation %
clc;
clc;
clear;
load z.mat
figure(1); surfl(z); shading interp; colormap gray; rotate3d;
[r_crop,c_crop,v_crop] = find(z);
r_inloop = r_crop(1,1)-1
R_Crop = max(r_crop)-min(r_crop)
C_Crop = max(c_crop)-min(c_crop)

[number_rows number_cols] = size(z);
```

```
P = 1:C_Crop+1; %column of profile; take a look on Z...follwing from area of
interest
xscale = [];
for i = 1:R_Crop
xscale(i,:) = z(i+r_inloop,min(c_crop):max(c_crop));
r = fit(P',xscale(i,:)','poly1');
cof = coeffvalues(r);

    xa = (cof(1,1)*P)+cof(1,2);
    X(i,:) = xscale(i,:)- xa;
end
%X = X*-1;
figure(2); surfl(X); shading interp; colormap gray; rotate3d; xlabel('X axis
(Pixel sizes)','FontSize',24); ylabel('Y axis (Pixel sizes)','FontSize',24);
zlabel('Z axis (Intensities)','FontSize',24);
X1 = X(5:35,50:350); % Decreasing the image resolution.
figure(3); surfl(X1(:,1:300)); shading interp; colormap gray; rotate3d;
xlabel('X axis (Pixel sizes)','FontSize',28); ylabel('Y axis (Pixel
sizes)','FontSize',28); zlabel('Z axis','FontSize',28);
X2 = X1(20,:);
X3 = X2';
save X3.txt X3 -ASCII


[m_data1 n_data1] = size(X1);
center_x = floor(n_data1/2);
center_y = floor(m_data1/2);
y_gau_minus = (-m_data1)+1;
y_gau_plus = (m_data1*2)-2;
x_gau_minus = (-n_data1)+1;
x_gau_plus = (n_data1*2)-2;
alpha = 0.4697;
cutoff = 50;
x_axis = (x_gau_minus:1:x_gau_plus);
y_axis = (y_gau_minus:1:y_gau_plus);
[x_axis,y_axis] = meshgrid(x_axis,y_axis);
Gau = ((1/(alpha^2*cutoff.^2))*exp(-((pi()/alpha.^2))*(((x_axis-
150).^2+(y_axis-15).^2)/(cutoff.^2))));

figure(4); surf(Gau(:,400:500)); axis([0 100 0 90 0 0.1]); rotate3d; xlabel('X
axis'); ylabel('Y axis') ;zlabel('Z axis');

% Weighting function for the phase correct profile filter

alpha = 0.4697; %sqrt((ln(2)/pi()))
cutoff = 70; %the position in relation to the centre of the weighting funtion
```

```
number = 1:1:300;
[rn,cn] = size(number)
x =(cn/2);
for i = 1:cn
weif(1,i) = 1/(alpha*cutoff)*exp(-pi()*(((number(i)-150)/(alpha*cutoff))^2));

end

[a b c] = find(weif);
figure(5),plot(number,weif);grid on;%axis([138 162 0 1.2]);

g_vau = cutoff/2;
[m_data n_data] = size(a);
wa = [];
%High pass filter

for ii = 1:31
    for ij = 1:g_vau
        for ik = 1:g_vau

a = X1(ii,1:300);
a_lower(ij) = a(1,n_data+1-ij);
a_lower = fliplr(a_lower);
a_upper(ik) = a(1,ik);
a_data = [a_lower a a_upper];
k = conv(a_data,c); %convolution


if (length(k) >= 300) %the picture to be shown at 0-300 pixels
    k_after_1 = length(k)-299;
end
    % Process to eliminate exceed data from Gaussian filter
k_after_2 = k_after_1/2;
k_after_3 = length(k)-k_after_2;
k_after_4 = k(k_after_2:k_after_3);
k_after = length(a_data)+length(c)-1;

%LP_L = True roughness before moving data
LP_L(ii,:) = a-k(k_after_2:k_after_3);
LP_W(ii,:) = k(k_after_2:k_after_3);
        end
    end
end
%change Z to um by linear regression
[mz1 nz1] = size(LP_L);
for ji = 1:mz1
```

```
    for jj = 1:nz1
        LP_LL(ji,jj) = (761.4*LP_L(ji,jj))+3.98;
    end
end

figure(6);surfl(LP_L); shading interp; colormap gray; rotate3d; xlabel('X axis
(Pixel sizes)','FontSize',24); ylabel('Y axis (Pixel sizes)','FontSize',24);
zlabel('Z axis','FontSize',24);
figure(7);surfl(LP_W); shading interp; colormap gray; rotate3d; xlabel('X axis
(Pixel sizes)','FontSize',24); ylabel('Y axis (Pixel sizes)','FontSize',24);
zlabel('Z axis','FontSize',24);
%Changed axis to be millimetre
figure(8);surfl(LP_LL); shading interp; colormap gray; rotate3d;
xlabel('Distance(mm)','FontSize',24); ylabel('Distance(mm)','FontSize',24);
zlabel('Depth(um)','FontSize',24);
figure(9);plot(LP_LL(16,1:250)),xlabel('Distance(mm)','FontSize',24);
ylabel('Depth(um)','FontSize',24),grid on,set(gca,'XTickLabel',[2.76 4.06 5.36
6.66 7.96 9.26 10.56] );
gm = mean(LP_LL(16,:));

for i = 1:300
    LP_LLL(1,i) = LP_LL(16,i)-gm;
end
figure(10);plot(LP_LLL(1,1:250)),xlabel('Distance(mm)','FontSize',24);
ylabel('Depth(um)','FontSize',24),grid on,set(gca,'XTickLabel',[2.76 4.06 5.36
6.66 7.96 9.26 10.56] );%True roughness2d,move to 0

for i = 1:300
    LP_LLL(1,i) = abs(LP_LL(16,i)-gm);
end
true_rough = mean(LP_LLL)
```

4) Least square technique

```
clc;
clear;
n = input('The number of values  = ');
for i = 1:n
    number = num2str(i);
    fname =  strcat('x',number,'=');
    x(i) = input(fname);
end
    start_plot_x = x(1);
    end_plot_x = x(end);
for i = 1:n
    number = num2str(i);
```

```
    fname =  strcat('y',number,'=');
    y(i) = input(fname);
end
    start_plot_y = y(1);
    end_plot_y = y(end);

x = x';y = y';onemetric = ones(n,1);
Matric_A = horzcat(x,onemetric)
Matric_B = y;
X = Matric_A\Matric_B;
% M value
M = X(1,1)
B = X(2,1)
C = fprintf('Linear Equation Y = %.4fX + %.4f\n',M,B);
% Return M to the linear function
XT = start_plot_x:0.0001:end_plot_x;
Yall = zeros(size(XT));
for i = 1:length(XT)
    Yall(i)= M*XT(i)+B;
end
YT = start_plot_y:0.1:end_plot_y;
subplot(4,1,1);
plot(XT,Yall,'k',x,y,'r+','MarkerSize',10);
grid on;legend('Slant angle at 30');
%%%%%%%%%%%%%%%%%%1%%%%%%%%%%%%%%%
clear all;
n = input('The number of values  = ');
for i = 1:n
    number = num2str(i);
    fname =  strcat('x',number,'=');
    x(i) = input(fname);
end
    start_plot_x = x(1);
    end_plot_x = x(end);
for i = 1:n
    number = num2str(i);
    fname =  strcat('y',number,'=');
    y(i) = input(fname);
end
    start_plot_y = y(1);
    end_plot_y = y(end);

x = x';y = y';onemetric = ones(n,1);
Matric_A = horzcat(x,onemetric)
Matric_B = y;
X = Matric_A\Matric_B;
```

```
% M value
M = X(1,1)
B = X(2,1)
C = fprintf('Linear Equation Y = %.4fX + %.4f\n',M,B);
% Return M to the linear function
XT = start_plot_x:0.0001:end_plot_x;
Yall = zeros(size(XT));
for i = 1:length(XT)
    Yall(i)= M*XT(i)+B;
end
YT = start_plot_y:0.1:end_plot_y;
subplot(4,1,2);
plot(XT,Yall,'k',x,y,'r+','MarkerSize',10);
ylabel('Rastd (um)','FontSize',20);
grid on;legend('Slant angle at 37.5');
%%%%%%%%%%%%%%%%%%%2%%%%%%%%%%%%%%%%%%%
clear all;
n = input('The number of values  = ');
for i = 1:n
    number = num2str(i);
    fname =  strcat('x',number,'=');
    x(i) = input(fname);
end
    start_plot_x = x(1);
    end_plot_x = x(end);
for i = 1:n
    number = num2str(i);
    fname =  strcat('y',number,'=');
    y(i) = input(fname);
end
    start_plot_y = y(1);
    end_plot_y = y(end);

x = x';y = y';onemetric = ones(n,1);
Matric_A = horzcat(x,onemetric)
Matric_B = y;
X = Matric_A\Matric_B;
% M value
M = X(1,1)
B = X(2,1)
C = fprintf('Linear Equation Y = %.4fX + %.4f\n',M,B);
% Return M to the linear function
XT = start_plot_x:0.0001:end_plot_x;
Yall = zeros(size(XT));
for i = 1:length(XT)
    Yall(i)= M*XT(i)+B;
```

```
end
YT = start_plot_y:0.1:end_plot_y;
subplot(4,1,3);
plot(XT,Yall,'k',x,y,'r+','MarkerSize',10);
grid on;legend('Slant angle at 45');
%%%%%%%%%%%%%%%%%%%3%%%%%%%%%%%%%%%%%%
clear all;
n = input('The number of values  = ');
for i = 1:n
    number = num2str(i);
    fname =  strcat('x',number,'=');
    x(i) = input(fname);
end
    start_plot_x = x(1);
    end_plot_x = x(end);
for i = 1:n
    number = num2str(i);
    fname =  strcat('y',number,'=');
    y(i) = input(fname);
end
    start_plot_y = y(1);
    end_plot_y = y(end);

x = x';y = y';onemetric = ones(n,1);
Matric_A = horzcat(x,onemetric)
Matric_B = y;
X = Matric_A\Matric_B;
% M value
M = X(1,1)
B = X(2,1)
C = fprintf('Linear Equation Y = %.4fX + %.4f\n',M,B);
% Return M to the linear function
XT = start_plot_x:0.0001:end_plot_x;
Yall = zeros(size(XT));
for i = 1:length(XT)
    Yall(i)= M*XT(i)+B;
end
YT = start_plot_y:0.1:end_plot_y;
subplot(4,1,4);
plot(XT,Yall,'k',x,y,'r+','MarkerSize',10);xlabel('Raps
(intensities)','FontSize',20);
grid on;legend('Slant angle at 52.5');
%%%%%%%%%%%%%%%%%%%4%%%%%%%%%%%%%%%%%%
```

5) Three-dimensional surface shape

```
clc;
clear;
load z.mat
[r_crop,c_crop,v_crop] = find(z);
r_inloop = r_crop(1,1)-1
R_Crop = max(r_crop)-min(r_crop)
C_Crop = max(c_crop)-min(c_crop)

[number_rows number_cols] = size(z);
P = 1:C_Crop+1; %column of profile; take a look on Z...follwing from
area of interest
xscale = [];
for i = 1:R_Crop
xscale(i,:) = z(i+r_inloop,min(c_crop):max(c_crop));
r = fit(P',xscale(i,:)','poly1');
cof = coeffvalues(r);

    xa = (cof(1,1)*P)+cof(1,2);
    X(i,:) = xscale(i,:)- xa;
end
%X = X*-1;
X1 = abs(min(min(X)));
X2 = X1+X;
figure(1); surfl(X2); shading interp; colormap gray; rotate3d;
xlabel('X axis (Pixel sizes)','FontSize',24); ylabel('Y axis (Pixel
sizes)','FontSize',24); zlabel('Z axis','FontSize',24);
X3 = X2(5:35,50:400); % Decreasing the image resolution.
figure(2); surfl(X3(:,1:350)); shading interp; colormap gray;
rotate3d; xlabel('X axis (Pixel sizes)','FontSize',24); ylabel('Y axis
(Pixel sizes)','FontSize',24); zlabel('Z axis','FontSize',24);
Height_1 = max(max(X3))
Base_1 = min(min(X3))
Height_1 = num2str(Height_1)
Base_1 = min(min(X3))
Base_1 = num2str(Base_1)
figure(3); plot(X3(20,1:350));xlabel('X axis (Pixel
sizes)','FontSize',24);ylabel('Z axis','FontSize',24);grid on;
gtext({'The highest position =';Height_1},'FontSize',24)
gtext({'The lowest position =';Base_1},'FontSize',24)
y_new = (21.30*(X3(30,1 :350)))-0.02;
xc = 1:1:350;
```

```
x_new = xc*0.020;
Height_1 = max(max(y_new))
Base_1 = min(min(y_new))
Height_1 = num2str(Height_1)
Base_1 = min(min(y_new))
Base_1 = num2str(Base_1)
figure(4),plot(x_new,y_new);xlabel('X axis
(mm)','FontSize',24);ylabel('Z axis (mm)','FontSize',24);grid
on;axis([0 7 0 5.1]);
gtext({'The highest position =';Height_1},'FontSize',24)
gtext({'The lowest position =';Base_1},'FontSize',24)
```

6) Changing from pixel sizes to length measurement

```
clc
clear
format long
I = imread('D:\my research\results\glass scale\1.bmp');
IM = im2double(I);
xscale=IM(110,1:512);
P=1:512;
r = fit(P',xscale','poly1');
cof = coeffvalues(r);

    xa = (cof(1,1)*P)+cof(1,2);
    X = xscale - xa;

plot(P,X);xlabel('X axis (Pixel sizes)','FontSize',24);ylabel('Y axis
(Intensities)','FontSize',24);axis([0 512 -0.1 0.04]);
grid on;

[a1,b1]=ginput(3);
am1=mean(a1);
[a2,b2]=ginput(3);
am2=mean(a2);
dam=am2-am1;
ls=input('Enter true value of scale in mm : ');
pxs=ls/dam
```